Christian-Albrechts-Universität zu Kiel
Institut für Theoretische Physik und Astrophysik Department of Physics
University of Florida

Quantum Fluid Description of Dense Plasmas

Dissertation

zur Erlangung des Doktorgrades
der Mathematisch-Naturwissenschaftlichen Fakultät
der Christian-Albrechts-Universität zu Kiel

vorgelegt von

Zhandos Moldabekov

Kiel, October 24, 2018

Printed and/or published with the support of the German Academic Exchange Service

Erster Gutachter:	Prof. Dr. Michael Bonitz Institut für Theoretische Physik und Astrophysik, Christian-Albrechts-Universität zu Kiel, Leibnizstraße 15, 24098 Kiel, Deutschland
Zweiter Gutachter:	Prof. Dr. James W. Dufty Department of Physics, University of Florida, PO Box 11840, Gainesville, FL 32611-8440, United States
Tag der mündlichen Prüfung:	October 24, 2018

Zum Druck genehmigt:

gez.

_____

Dekan

Kel, balalar, oqylyq,
Oqyǵandy kónilge
Yqylaspen toqylyq...

Ibrahim Altynsarin[*]
(1841–1889)

[*]With these words, Ibrahim Altynsarin invited the nomadic children to start studying and do it diligently. IA was the most prominent Kazakh educator of the late 19th century.

This thesis is based on the results published in the following papers*:

I Zh. Moldabekov, M. Bonitz, and T. Ramazanov. *Theoretical foundations of quantum hydrodynamics for plasmas.* Physics of Plasmas, vol. 25, page 031903, 2018.

II Zh. Moldabekov, S. Groth, T. Dornheim, H. Kählert, M. Bonitz and T. Ramazanov. *Structural characteristics of strongly coupled ions in a dense quantum plasma.* Physical Review E, vol. 98, page 023207, 2018.

III Zh. Moldabekov, M. Bonitz and T. Ramazanov. *Gradient correction and Bohm potential for two- and one-dimensional electron gases at a finite temperature.* Contributions to Plasma Physics, vol. 57, pages 499-505, 2017.

IV Zh. Moldabekov, S. Groth, T. Dornheim, M. Bonitz and T. Ramazanov. *Ion potential in non-ideal dense quantum plasmas.* Contributions to Plasma Physics, vol. 57, pages 532-538, 2017.

The results of this thesis were presented at the following conferences:

i Zh. Moldabekov, M. Bonitz, T. Ramazanov, Fluid description of dense quantum plasmas: the quantum hydrodynamic approach, 38th International Workshop on High Energy Density Physics with Intense Ion and Laser Beams, Hirschegg, January 29- February 2, 2018.

ii Zh. Moldabekov, and M. Bonitz, Theoretical foundations of quantum hydrodynamics for plasmas, DPG-Frühjahrstagung der Sektion Materie, Kosmos und Plasmaphysik, Bremen, 13. - 17. März 2017 (P 12.2, Verhandlungen der DPG).

iii Zh. Moldabekov and M. Bonitz, Quantum hydrodynamic approach for quantum plasmas, The 44th European Physical Society Conference on Plasma Physics Belfast, UK, June 26-30, 2017 (P1.401)

*A complete list of publications is given in Appendix F.

iv Zh. Moldabekov, M. Bonitz, T. Ramazanov, Foundations of quantum hydrodynamics for dense plasmas, The 44th International Conference on Plasma Science (ICOPS 2017), Atlantic City, New Jersey, USA May 21-25, 2017 (identification number 1452).

v Zh. Moldabekov, M. Bonitz, T. Ramazanov, Fluid description of dense quantum plasmas in RPA and beyond, Strongly Coupled Coulomb Systems (SCCS), Kiel, July 29- August 4, 2017.

vi Zh. Moldabekov, T. Dornheim, S. Groth, P. Ludwig, M. Bonitz, and T. Ramazanov, Screening of ion potential in quantum non-ideal dense plasmas, Strongly Coupled Coulomb Systems (SCCS), Kiel, July 29-August 4, 2017.

vii Zh. Moldabekov, M. Bonitz, T. Ramazanov, Quantum fluid description of dense plasmas, Scientific-Coordination Session on "Non-Ideal Plasma Physics", Moscow, November 29-30, 2017.

Abstract: Two-component dense quantum plasmas are created in various experimental facilities by means of compression of matter by charged particles or laser beams. These experiments are motivated by the problem of inertial confinement fusion and the investigation of the physics of massive astrophysical objects. The simultaneous importance of thermal excitations and electronic quantum and correlation effects makes a theoretical study of dense quantum plasmas challenging. *Ab initio* methods such as Quantum Monte Carlo and Kohn-Sham density functional theory are, currently, not able to serve as a tool for the large scale simulation of dense quantum plasmas due to the large computational effort. Therefore, quantum hydrodynamics (QHD) has gained attention as a possible method to circumvent this restriction and, thus, to carry out large scale simulations. However, it appeared that QHD suffers from a lack of a reliable theoretical foundation and has not yet been generalized to finite temperatures. With the aforementioned shortcomings, we have to consider QHD as a unreliable method to simulate high-energy-density plasmas. Therefore, the thesis at hand presents the first consistent derivation of finite temperature QHD for fermions and the first unifying picture to the various previously used versions of the QHD. Moreover, linking with the linear response theory, the results presented in this thesis go beyond all previous considerations by providing a consistent derivation of the fully non-local potentials taking into account the electronic exchange-correlation effects for both low frequency and high frequency phenomena. Further, in order to verify the importance of the electronic quantum non-locality and correlations, different existing approximations describing the electronic density response function have been implemented to study the structural properties of strongly coupled ions. As a result, the applicability ranges of the involved approximations are determined and the plasma parameters at which the electronic quantum non-locality and correlations cannot be neglected are found. The latter allows to allocate the range of the plasma parameters where the presented QHD equations with non-local potentials are appropriate for the investigation of a dense plasma.

Keywords: Quantum hydrodynamics at finite temperature, dense plasmas, strongly coupled plasmas, Thomas-Fermi model with gradient corrections, Bohm potential, Screening, Structural properties.

Zusammenfassung: Zweikomponentige, dichte Quantenplasmen werden in verschiedenen Versuchsanlagen erzeugt. Dabei wird Materie durch Laser oder hochenergetische Bündel geladener Teilchen komprimiert. Motiviert sind diese Experimente durch Arbeiten an der Trägheitsfusion und der Untersuchung der physikalischen Eigenschaften massereicher astrophysikalischer Objekte. Die gleichzeitige Bedeutung von thermischen Anregungen und elektronischen Quanten- und Korrelationseffekten macht eine theoretische Untersuchung von dichten Quantenplasmen äußerst schwierig. Ab initio-Methoden wie Quantum Monte Carlo und die Kohn-Sham-Dichtefunktionaltheorie sind derzeit aufgrund des hohen erforderlichen Rechenaufwands nicht in der Lage, als Werkzeug für großskalige Simulation von dichten Quantenplasmen zu dienen. Daher hat die Quantenhydrodynamik (QHD) als mögliche Methode zur Umgehung dieser Einschränkungen und damit zur Durchführung von großskaligen Computersimulationen an Bedeutung gewonnen. Es zeigt sich jedoch, dass es der QHD an verlässlichen theoretischen Grundlagen mangelt und sie noch nicht auf endliche Temperaturen verallgemeinert wurde. Deshalb muss die QHD als unzuverlässige Methode zur Simulation von hochenergetischen Plasmen angesehen werden. Dadurch motiviert, gibt die vorliegende Arbeit eine erste konsequente Ableitung der fermionischen QHD für endliche Temperaturen und die erste Vereinheitlichung verschiedener zuvor verwendeter Versionen der QHD. Weiterhin gehen die Ergebnisse dieser Arbeit, durch die Verknüpfung mit der Linear-Response-Theorie sowie eine konsequente Ableitung vollständig nicht-lokaler Potenziale unter Berücksichtigung der elektronischen Austausch-Korrelations-Effekte für niederfrequente und hochfrequente Phänomene, über alle bisherigen Arbeiten hinaus. Um den Einfluss von elektronischer Quanten-Nichtlokalität und von Korrelationen zu überprüfen, werden verschiedene bestehende Approximationen zur Beschreibung der elektronischen Dichte-Antwort-Funktion für die Untersuchung der strukturellen Eigenschaften von stark gekoppelten Ionen implementiert. Dadurch werden die Anwendungsbereiche der beteiligten Approximationen ermittelt und die Plasmaparameter bestimmt, bei denen die elektronische Quanten-Nichtlokalität und Korrelationen nicht vernachlässigt werden können. Letzteres erlaubt es, den Bereich der Plasmaparameter zu bestimmen, in dem die dargestellten

QHD-Gleichungen mit nicht-lokalen Potentialen für die Untersuchung eines dichten Plasmas geeignet sind.

Schlüsselwörter: Quantenhydrodynamik bei endlicher Temperatur, dichte Plasmen, stark gekoppelte Plasmen, Thomas-Fermi-Modell mit Gradientenkorrekturen, Bohm-Potential, Screening, Struktureigenschaften.

Contents

Acronyms

QHD	Quantum hydrodynamics
HNC	Hypernetted chain approximation
STLS	Singwi-Tosi-Land-Sjölander
RPDF	Radial pair distribution function
SSF	Static structure factor
DFT	Density functional theory
OF-DFT	Orbital-free density functional theory
TDDFT	Time-dependent density functional theory
QMC	Quantum Monte Carlo
ICF	Inertial confinement fusion

Chapter 1

Introduction

A quantum plasma can be characterized as a system consisting of free electrons and of positively charged ions, where the Fermi energy of the electrons is comparable with or larger than the thermal energy of the electrons. In this thesis, the quantum plasma is considered in the context of high-energy-density plasma physics. The subject of high-energy-density plasmas is the state of matter with extraordinarily high energy densities [Fortov 2016] such as dense plasmas, warm dense matter, hot dense matter etc., [Graziani 2014a]. From now on, under a *quantum plasma*, I will be referring to a *dense plasma with partially or totally degenerate electrons*. In this way, the subject matter of this thesis is presented in the frame of—the well defined field—dense plasmas. More precisely, I consider two-component dense plasmas consisting of quantum electrons and strongly correlated ions.

Experimentally, a plasma with quantum electrons is realized by compressing matter until a high degree of ionization is achieved at temperatures comparable with the electronic Fermi energy. Recent examples include the experiments on inertial confinement fusion (ICF) [Zastrau 2014, Hurricane 2014, Cuneo 2012, Gomez 2014], and the compression of a target by lasers or intense charged particle beams [Sharkov 2016, Kawata 2016]. In particular, plasmas generated at the OMEGA Laser System and at the National Ignition Facility enter the regime of a quantum plasma with strongly coupled ions [Hu 2010]. Additionally to ICF, the aforementioned experiments are motivated by the interest in understanding physics of astrophysical objects like the giant planets of the Solar System, exoplanets, brown and white dwarfs, neutron stars etc., [Fortov 2016, Graziani 2014a].

The ability to simulate dynamical properties is crucial due to the out-of-equilibrium state of the experimentally generated dense plasmas (warm dense matter). For example, the simulation of such processes as the relaxation from the non-isothermal state with cold ions and hot electrons (or vice versa) to a thermal equilibrium, the energy loss of an ion, and the dynam-

ics of the system under impact of external fields are of importance for the realization of the ICF [Graziani 2012]. Arguably, at the moment the most advanced and reliable theoretical method for the description of high-energy-density plasmas at finite temperature is based on free-energy (finite temperature) Kohn-Sham DFT (e.g., see Refs. [Eschrig 2010, Pribram-Jones 2016]). This method is already computationally costly at relatively low temperatures ($T \lesssim 10^3$ K), with a computation time proportional to the cube of the number of electrons (N_e^3), and at more extreme parameters ($T \gtrsim 10^4$ K) has its computational bottleneck. In the latter case, a severe limitation of the application of Kohn-Sham DFT is caused by the additional N_b^3 scaling of the calculation cost [Karasiev 2014], where N_b is the number of the occupied levels (basis functions) due to thermal excitations. Time-dependent Kohn-Sham DFT at relevant temperatures and densities suffers from the same (or even worse) computational bottlenecks as the aforementioned static version. As the result, the large scale (with at least $N_e \sim 10^3$) simulation of the dynamics of a quantum plasma as well as warm dense matter at $T \gtrsim 10^4$ K by Kohn-Sham DFT based methods is not feasible [Karasiev 2014].

Other *ab initio* methods for the simulation of non-ideal dense quantum two-component plasmas at finite temperature like quantum Monte Carlo methods [McMahon 2012, Dornheim 2018] and non-equilibrium Green functions [Bonitz 2016] are in the stage of development and computationally even more challenging than the finite temperature Kohn-Sham DFT. It should be remarked that another important method is based on the use of so called quantum potentials [Filinov 2003, Filinov 2004] in a molecular dynamics simulation (MD). The advantage of this approach is that electrons and ions are treated on an equal footing, i.e., without involving an adiabatic approximation. However, this method has the unsolved problem of defining the so-called electron-ion temperature [Seuferling 1989, Bredow 2003, Shaffer 2017]. Additionally, the applicability of this method is restricted to classical and semi-classical plasmas. Besides, the classical mapping approach is promising; the main idea of which is the introduction of a set of modified parameters, like an effective temperature [Dharma-wardana 2000, Liu 2014], in order that classical methods can be used for the prediction of the properties of the quantum system of interest [Dufty 2013, Dutta 2013]. However, this method has not been applied yet to a two-component quantum plasma.

To find a workaround to the problem of the unfeasibility of large scale *ab initio* Kohn-Sham DFT simulations of quantum plasmas and warm dense matter, intensive development of orbital-free DFT (OF-DFT) has been performed in the recent years [Sjostrom 2015, Sjostrom 2014a, Karasiev 2012, Sjostrom 2013a, Sjostrom 2014b, White 2013]. The outcome of these studies is that OF-DFT is now able to describe the thermodynamic properties of dense plasmas with the same accuracy as finite temperature Kohn-Sham DFT (at the parameters relevant to the warm dense matter regime with $T \gtrsim 10^4$ K). In the OF-DFT one only needs to solve a single Euler-Lagrange problem using a proper free energy functional, instead of the multidimensional Kohn-Sham eigenvalue problem in Kohn-Sham DFT. As a result, the power-law scaling of the computation time of Kohn-Sham DFT is replaced by a behavior that is almost invariant under temperature variations [Sjostrom 2014a, Karasiev 2014]. Obviously, the OF-DFT, determining the electronic density distribution at given ionic configuration, is not able to describe the dynamical density distribution of electrons, which is needed, e.g., to compute important quantities like the stopping power, for the simulation of the system under the impact of the alternating external field, and for the case of a dense plasma with a stream of heavy particles relative to the electrons [Graziani 2012, Ludwig 2010]. Therefore, a method which allows for the large scale simulation of electronic dynamics taking into account important quantum and non-ideality effects is crucial for high-energy-density plasma physics. To this end, the development of a quantum fluid description of dense plasmas, which can be the basis for the needed large scale simulation of a two component plasma, is the primary goal of this thesis. Accordingly, the electronic subsystem is treated via continuous variables within the quantum fluid model taking into account electronic correlations. The ions are described by using the method of integral equations and molecular dynamics simulations.

The quantum fluid description of electrons is considered on the basis of the so called *quantum hydrodynamics* (QHD). Below, the terms "quantum fluid description" and "quantum hydrodynamics" are used as synonyms. Here, the term "quantum hydrodynamics" is introduced with a note of caution in order to avoid any confusion related to the meaning and assumptions that are embedded in the word "hydrodynamics" in classical physics, where this usually means the consideration of macroscopic phenomena at a scale much larger than both the mean interparticle distance and the char-

acteristic de Broglie wave length of an electron. In contrast, the quantum hydrodynamics—which is the focus of this work—is formulated in the spirit of DFT and based on the dynamical quantum response function at a finite wavenumber, and, therefore, is not restricted by the length and time scales of the hydrodynamics in the classical meaning of this word.

Since the works by Manfredi and Haas at the beginning of the new millennium [Manfredi 2001], the quantum hydrodynamics of fermions has gained popularity as a "simplified, but not simplistic approach" [Haas 2011] for quantum plasmas. Manfredi and Haas used the formulation of quantum hydrodynamics with the quantum non-locality taken into account as the first order gradient correction to the Fermi pressure, which is referred to as the Bohm potential due to its similarity to the namesake in the famous Bohmian mechanics [Bohm 1952a, Bohm 1952b, Bohm 1954]. Based on such a formulation of the QHD, for the sake of finding agreement with the results of the random phase approximation (RPA) for the plasmon dispersion, the Fermi pressure and the Bohm potential were "corrected" by introducing constant pre-factors [Halevi 1995, Yan 2015, Akbari-Moghanjoughi 2015]. Further, an approximate static exchange correlation potential had been implemented for the study of dynamical processes [Crouseilles 2008, Yan 2015]. In this form, the QHD has often been chosen as the tool for approximate research well beyond its applicability range and, sometimes, with explicitly incorrect expressions. This has led to unphysical predictions and, thereby, to justified strong criticisms [Khan 2014, Krishnaswami 2015, Bonitz 2013a, Bonitz 2013b]. As the result, it was revealed that the QHD model suffered from the lack of consistency in the closure relation for the involved potentials (or equivalently for the force field) and in the generalization to the finite temperature case [Khan 2014].

Another important aspect of a self-consistent description of a quantum plasma with strongly coupled ions is that an accurate analysis of the effects due to ionic non-ideality is required. In addition, in experiments with the ionic temperature being much less than that of the electrons [Ma 2013, Glenzer 2007, Lee 2009], the ions can be highly sensitive to the choice of the approximation for the electronic correlations [Clérouin 2015b, Harbour 2016, Plagemann 2015]. Both circumstances were ignored in earlier considerations on the basis of the QHD.

Taking into account the described state of affairs and the requirement of a reliable quantum fluid model for high-energy-density plasma science,

within the thesis, the following objectives were set and achieved:

- Provide a consistent derivation of the QHD equations at finite temperature, that recovers the OF-DFT model in the static limit so that the recent achievements in OF-DFT can be employed for the computation of the static electronic density distribution.
- Derive the closure relation for the QHD equations on the basis of a known electronic density response function taking into account the quantum non-locality and exchange-correlation effects (without introducing uncontrolled approximations via empirical pre-factors).
- Define the applicability and limitations of widely used models of the electronic density response function applied to the quantum plasma with strongly coupled ions.

Thesis outline

Chapter 2 constitutes a bird's-eye view. In this chapter the general theoretical description of a two-component plasma with quantum electrons and classical ions is introduced using a multi-scale approach. In addition, to avoid any inconsistency inherited from the previous formulations of the QHD model, the reasons for the revision of the foundations of quantum hydrodynamics are discussed in more detail. The following chapters 3 and 4 constitute the core of the thesis. In chapter 3, the QHD equations are derived for finite temperatures and a fully non-local quantum Bohm potential is presented. The latter is derived linking the RPA polarization function to the second-order functional derivative of the non-interacting free energy density. This approach has allowed to systematically derive the equation for the exchange-correlation potential of the QHD model, which is also discussed in chapter 3. In chapter 4, the effect of the electronic degeneracy and non-ideality (correlations) on the structural properties of strongly coupled ions is analyzed using models with different levels of sophistication. This analysis sheds light on the applicability and limitations of some widely used models of the electronic density response function in the context of a non-isothermal plasma with strongly coupled ions and quantum electrons. Each of chapters 3 and 4 ends with a brief summary. Finally, I draw conclusions and give some perspectives in chapter 5.

Chapter 2

Two-component quantum plasmas

Contents

In this chapter, an extended presentation of the considered plasma state using standard dimensionless parameters is given. The theoretical consideration of two component quantum plasmas based on a multiscale approach using a fluid description of the quantum electrons is discussed. Additionally, more details about inconsistencies and limitations of the QHD potentials used in previous works are reviewed. Thereby, a clear picture about motivations for the development of an improved quantum fluid model is provided.

2.1 Dimensionless parameters

A fully ionized plasma state consisting of electrons and of a certain type of ions is specified by the number density of electrons, n, the temperature of electrons, T_e, and of ions, T_i*.

The energy scales of a two-component dense quantum plasma are defined by the thermal energy (per particle), of both electrons and ions, $E_e^{\text{th}} \sim k_B T_e$

*For given temperature and density values, ionization state can be calculated by using, e.g., Saha models or average atom models.

and $E_i^{\rm th} \sim k_B T_i$, the electron Fermi energy $E_F = \hbar^2 k_F^2/(2m_e)$, where k_F is the Fermi wave number, and the plasmon energy, $\hbar\omega_p$, with the plasma frequency $\omega_p = (4\pi n e^2/m_e)^{1/2}$ (m_e is the electron mass). The latter also characterizes the potential energy of free electrons. The time scales of the electronic and ionic subsystems are determined by the inverse plasma frequency, $\tau_e \sim \omega_p^{-1}$, and the inverse ionic plasma frequency , $\tau_i \sim \omega_{\rm pi}^{-1}$, respectively. Here, the ionic plasma frequency is $\omega_{\rm pi} = (m_e/m_i)^{1/2}\omega_p$, where m_i is the ion mass. The mean distance between adjacent electrons (ions), a_e (a), and the Bohr radius, a_B, are the length scales which are of relevance.

In what follows, the number density is in units of cm^{-3}, temperature in K, and energies in Hartree (Ha), which is related to the binding energy of a ground-state hydrogen atom by $E_R = 13.6$ eV = Ha/2. For the plasma frequency, one can find $\omega_p = 5.6 \times 10^4\ n^{1/2}$ [s^{-1}]. Additionally, the symbol "e" is used for the elementary charge equal to the absolute value of the electron charge.

The following dimensionless parameters are used to describe the plasma state:

- the electron degeneracy parameter, $\theta = k_B T_e/E_F$,
- the density parameter (Brueckner parameter) $r_s = a_e/a_B$ (with $a_e = (\frac{3}{4\pi n})^{1/3}$), which is also used as the quantum coupling parameter of electrons,
- the coupling parameter of the ions, $\Gamma = Q_i^2/(a k_B T_i)$, where the ion charge is $Q_i = Ze$.

Accordingly, knowing the plasma temperature and density, one can find the degeneracy (θ) and density (r_s) parameters characterizing the electronic subsystem, and the coupling parameter (Γ) describing the ionic component of a plasma.

It is handy to have the following formulas to easily evaluate the temperature (thermal energy per particle) and density knowing the dimensionless parameters: $T_e \simeq \frac{\theta}{r_s^2}\ 0.58 \times 10^6$ [K], $k_B T_e \simeq \frac{\theta}{r_s^2} \times 50.12$ [eV] $\simeq \frac{\theta}{r_s^2} \times 1.84$ [Ha], and $n \simeq 1.6127 \times 10^{24} \cdot r_s^{-3}$. The relation for the ionic coupling parameter $\Gamma \simeq (Z^{5/3}/1.84)(r_s/\theta)(T_e/T_i)$ is also convenient to have at hand. For example, with the choice $Z = 1$, at $r_s = 1.5$ and $\Gamma \lesssim 50$, the degeneracy parameters $\theta = 0.5$ ($\theta = 0.1$) lead to $T_e/T_i \lesssim 30$ ($T_e/T_i \lesssim 6$).

2.2 Plasma parameters under consideration

Earlier, a plasma has been identified as a quantum plasma if the electronic thermal energy is less than or comparable to the Fermi energy. Therefore, a plasma with the electronic degeneracy parameter $\theta = k_B T/E_F \lesssim 1$ is considered in this work. Further, the thermal energy of an electron must be sufficiently high so that it is able to overcome the atomic binding energy and, as the result, the state of the complete or high degree of ionization can be achieved. On the other hand, the plasma micro-fields can significantly diminish the ionization energy. This effect is known as the pressure ionization or Mott effect. At $\theta \ll 1$, the condition for the appearance of the Mott effect in experiments on quantum plasmas can be obtained approximately by requiring that the Fermi energy exceeds the characteristic attractive potential energy of an electron to an ion, i.e., $r_s = a_e/a_B < 2$ [Chabrier 1990]. This evaluation is supported by first-principles path-integral Monte Carlo simulations of the hydrogen plasma, which indicate that at $r_s \sim 1.2$ bound states break up [Bonitz 2005]. Therefore, the focus of this work is on plasmas with densities $n_e > 10^{23}$ cm^{-3} and electronic temperatures $T_e \gtrsim 10^4$ K.

Dense plasmas have been the subject of experimental investigations since the mid-1950s due to the nuclear defense projects in several countries and later due to the national ignition campaign in the US [Moses 2010a, Moses 2010b]. Nowadays, additionally to the realization of inertial confinement fusion, the scientific activity in the physics of dense plasmas is fueled by the interest in astrophysical objects as mentioned in the introduction. Experimental techniques for high-energy-density plasma research include shock-compression driven by lasers, explosions, and charged-particle beams; and, in addition, using devices like diamond anvil cells, high-current Z-pinches, and multistage light-gas guns [Fortov 2016]. In these experiments, plasmas can be realized at a broad range of parameters, with temperatures in the range from $\sim 10^3$ K up to $\sim 10^8$ K and with densities in the range from $\sim 10^{18}$ cm^{-3} up to 10^{28} cm^{-3} [Fortov 2016]. Therefore, for present purposes, some experiments where two-component dense plasmas with quantum electrons and strongly coupled ions were realized are compiled in Table 2.1. From these data, it can be concluded that the aforementioned theoretical consideration about thermal and pressure ionization, at the plasma parameters at hand, is supported by recent experiments.

Table 2.1: Examples for experiments where two component quantum plasmas with strongly coupled ions were realized. From reference [Moldabekov 2018b].

References	Plasma parameters			
	n [10^{23} cm^{-3}]	T_e & T_i [10^3 K]	θ & r_s	Γ
Cryogenic DT implosion on OMEGA [Boehly 1997, Hu 2010]	$2 \lesssim n \lesssim 10$	$23 \lesssim T_e \lesssim 230$ $T_i = T_e$	$0.2 \lesssim \theta \lesssim 0.8$ $1.17 \lesssim r_s \lesssim 2$	$1 \lesssim \Gamma \lesssim 6$
Direct-drive ignition at the NIF [Paisner 1994, Hu 2010]	$2.5 \lesssim n \lesssim 3$	$69 \lesssim T_e \lesssim 464$ $T_i = T_e$	$0.2 \lesssim \theta \lesssim 0.8$ $1.75 \lesssim r_s \lesssim 1.86$	$0.5 \lesssim \Gamma \lesssim 3$
Solid Be heated by 4-5 keV pump photons [Landen 2001]	$2 \lesssim n \lesssim 4$	$11 \lesssim T_e \lesssim 110$ $T_i = T_e$	$0.07 \lesssim \theta \lesssim 1.15$ $1.6 \lesssim r_s \lesssim 2$	$2 \lesssim \Gamma \lesssim 10$
* Laser-driven shock-compressed aluminum [Ma 2013]	$n \simeq 5.46$	$T_e \simeq 100$ $T_e/T_i \simeq 5$	$\theta \simeq 0.5$ $r_s = 1.435$	$\Gamma \simeq 50$
† Laser-driven shock-compressed Be sample [Glenzer 2007]	$n \simeq 2.28$	$T_e \simeq 139$ $2 \lesssim T_e/T_i \lesssim 20$	$\theta \simeq 0.88$ $r_s = 1.92$	$7.5 \lesssim \Gamma \lesssim 75$
‡ Laser-driven shock-compressed Be sample [Lee 2009]	$n \simeq 6.7$	$T_e \simeq 150$ $1.8 \lesssim T_e/T_i \lesssim 6.5$	$\theta \simeq 0.95$ $r_s = 1.34$	$4 \lesssim \Gamma \lesssim 16$

*T_e/T_i was evaluated in Refs. [Clérouin 2015b, Harbour 2016]
†T_e/T_i was evaluated in Ref. [Harbour 2016]
‡T_e/T_i was evaluated in Refs. [Plagemann 2015, Harbour 2016]

In addition, the ions are strongly coupled and the coupling parameter is considered to be $1 \leqslant \Gamma \leqslant 50$. For completeness, I mention that relativistic effects will not be considered in this work. Therefore, a lower bound to the density parameter is identified as $r_s \gg 0.014$, which follows from the condition $v_F \ll c$ (with $v_F = \hbar k_F/m_e$), which means that the characteristic velocity of the electrons is significantly smaller than the speed of light.

2.3 Multi-scale approach

The complete information about the considered system is contained in the full electron-nuclear wave function. However, it is conventionally assumed that a plasma of electrons and ions can be considered as a combination of two subsystems: electrons moving in the field of inert ions, and ions moving in the electronic medium. This is usually referred to as the multi-scale approach [Ludwig 2010]. Based on the fact that the mass of an ion is much larger than that of an electron, such a picture is justified by the following physical reasons:

- The characteristic time scales of electrons and of ions differs drastically because $\tau_e/\tau_i \sim \sqrt{m_e/m_i}$.
- The ions are considered to be classical due to their large mass.
- When an electron collides with an ion, the momentum transfer to the ion is negligible compared to that of due to ion-ion collision, and the ion interacting with other ions can be considered as moving in a polarizeable medium of electrons.

The multi-scale approach has long been widely used since it is intuitively clear. In spite of this, a rigorous separation of the electronic and ionic motion by an exact factorization of the full electron-ionic wave function was performed only recently in Ref. [Abedi 2010]. This exact splitting of the degrees of freedom of ions and electrons is a proper starting point for the systematic derivation of the mixed quantum-classical picture. Therefore, in what follows, a brief discussion of the road from the full quantum picture to the mixed quantum-classical one is outlined, from which the main approximations inherent to the multi-scale approach become more evident.

* The Schrödinger equation for the complete electron-ionic wave function reads

$$\hat{\mathcal{H}}\Psi\left(\underline{\underline{\mathbf{r}}},\underline{\underline{\mathbf{R}}},t\right)=i\hbar\partial_t\Psi\left(\underline{\underline{\mathbf{r}}},\underline{\underline{\mathbf{R}}},t\right), \tag{2.1}$$

with the Hamiltonian taking into account interparticle interactions and the impact of an external time-dependent potential

$$\hat{\mathcal{H}}=\hat{\mathcal{T}}_e+\hat{\mathcal{T}}_i+\hat{\mathcal{W}}_{ee}+\hat{\mathcal{W}}_{ii}+\hat{\mathcal{W}}_{ei}+\hat{\mathcal{V}}^e_{\text{ext}}+\hat{\mathcal{V}}^i_{\text{ext}}, \tag{2.2}$$

where $\hat{\mathcal{T}}_e$ ($\hat{\mathcal{T}}_i$) is the electronic (ionic) kinetic energy operator, $\hat{\mathcal{W}}_{ee}$ ($\hat{\mathcal{W}}_{ii}$) is the electron-electron (ion-ion) interaction, $\hat{\mathcal{W}}_{ei}$ is the electron-ion interaction, $\hat{\mathcal{V}}^e_{\text{ext}}$ ($\hat{\mathcal{V}}^i_{\text{ext}}$) is the potential energy of electrons (ions) due to an external potential, $\underline{\underline{\mathbf{r}}}=(\mathbf{r}_1,...,\mathbf{r}_{N_e})$ and $\underline{\underline{\mathbf{R}}}=(\mathbf{R}_1,...,\mathbf{R}_{N_i})$ denote the coordinates of the electrons (with the total number N_e) and ions (with the total number N_i), respectively. The pair interaction between particles is given by the Coulomb potential.

Following Refs. [Abedi 2010, Bao 2016], the *exact* solution of the Schrödinger equation for the complete electron-ionic wave function can be written as

$$\Psi\left(\underline{\underline{\mathbf{r}}},\underline{\underline{\mathbf{R}}},t\right)=\psi_{\underline{\underline{\mathbf{R}}}}\left(\underline{\underline{\mathbf{r}}},t\right)\chi\left(\underline{\underline{\mathbf{R}}},t\right)\exp\left[\frac{i}{\hbar}\int_{t_0}^{t}\left\langle\hat{\mathcal{H}}_e(\tau)\right\rangle_{\underline{\underline{\mathbf{R}}}}\mathrm{d}\tau\right], \tag{2.3}$$

where $\langle...\rangle_{\underline{\underline{\mathbf{R}}}}$ is the expectation value, at a given ionic configuration $\underline{\underline{\mathbf{R}}}$, of the operator

$$\hat{\mathcal{H}}_e=\hat{\mathcal{T}}_e+\hat{\mathcal{W}}_{ee}+\hat{\mathcal{W}}_{ii}+\hat{\mathcal{W}}_{ei}+\hat{\mathcal{V}}^e_{\text{ext}}+\hat{\mathcal{Q}}, \tag{2.4}$$

and

$$\hat{\mathcal{Q}}=\sum_{\nu=1}^{N_\nu}\frac{m_e}{m_i}\left[\frac{\left(-i\hbar\nabla_\nu+e\mathbf{A}_\nu\left(\underline{\underline{\mathbf{R}}},t\right)\right)^2}{2m_e}\right.$$
$$\left.+\frac{1}{m_e}\left(\frac{-i\hbar\nabla_\nu\chi}{\chi}-e\mathbf{A}_\nu\left(\underline{\underline{\mathbf{R}}},t\right)\right)\left(-i\hbar\nabla_\nu+e\mathbf{A}_\nu\left(\underline{\underline{\mathbf{R}}},t\right)\right)\right], \tag{2.5}$$

with $\mathbf{A}_\nu\left(\underline{\underline{\mathbf{R}}},t\right)=i\hbar/e\left\langle\Phi_{\underline{\underline{\mathbf{R}}}}\left(\underline{\underline{\mathbf{r}}},t\right)\middle|\nabla_\nu\Phi_{\underline{\underline{\mathbf{R}}}}\left(\underline{\underline{\mathbf{r}}},t\right)\right\rangle$ representing the so-called Berry connection (vector potential) [Berry 1984, Xiao 2010, Resta 2000],

*The main results of this thesis (chapters 3 and 4) are independent from the presented discussion of the splitting of the ionic and electronic degrees of freedom. The latter is given to illustrate the place of the QHD in the broader context of many-body physics.

and the notation $\Phi_{\underline{\underline{\mathbf{R}}}}\left(\underline{\mathbf{r}},t\right) = \psi_{\underline{\underline{\mathbf{R}}}}\left(\underline{\mathbf{r}},t\right)\exp\left[\frac{i}{\hbar}\int_{t_0}^{t}\left\langle\hat{\mathcal{H}}_e(\tau)\right\rangle_{\underline{\underline{\mathbf{R}}}}\mathrm{d}\tau\right]$ $(t > t_0)$. In the considered case, using an analogy to the relation of the vector potential and its curl from electromagnetism, $\nabla\times\mathbf{A}_\nu\left(\underline{\underline{\mathbf{R}}},t\right)$ can be described as the microscopic magnetic field induced by ion motions [Abedi 2010].

Making use of the ansatz (2.3) gives the following differential equations for the electronic, $\psi_{\underline{\underline{\mathbf{R}}}}\left(\underline{\mathbf{r}},t\right)$, and ionic, $\chi\left(\underline{\underline{\mathbf{R}}},t\right)$, wave functions [Abedi 2010, Bao 2016]:

$$\hat{\mathcal{H}}_e\psi_{\underline{\underline{\mathbf{R}}}}\left(\underline{\mathbf{r}},t\right) = i\hbar\partial_t\psi_{\underline{\underline{\mathbf{R}}}}\left(\underline{\mathbf{r}},t\right), \tag{2.6}$$

$$\left(\hat{\mathcal{T}}_i + \hat{\mathcal{V}}^i_{\mathrm{ext}} + \left\langle\hat{\mathcal{H}}_e\right\rangle_{\underline{\underline{\mathbf{R}}}}\right)\chi\left(\underline{\underline{\mathbf{R}}},t\right) = i\hbar\partial_t\chi\left(\underline{\underline{\mathbf{R}}},t\right). \tag{2.7}$$

Eqs. (2.6) and (2.7) represent the time-dependent Schrödinger equation for the two component coupled electron-ion system. Apart from $\hat{\mathcal{W}}_{ei}$, the electronic subsystem is coupled to the ions due to the presence of the terms $\hat{\mathcal{W}}_{ii}$ and $\hat{\mathcal{Q}}$ in the equation for the electronic wave function (2.6) via Hamiltonian (2.4), and the ionic subsystem is coupled to the electrons due to the term $\left\langle\hat{\mathcal{H}}_e\right\rangle_{\underline{\underline{\mathbf{R}}}}$ in Eq. (2.7). These connections are due to the fact that the location and motion of the ions depend on the state of the electrons, which, in turn, parametrically depends on the ionic coordinates. The solution of Eqs. (2.6) and (2.7) provides the formally exact wave function of the system, but is computationally highly challenging.

To facilitate the description, we can introduce a set of reasonable approximations based on the fact that $m_i \gg m_e$:

(i) Taking the limit $m_e/m_i \to 0$, it is assumed that $\hat{\mathcal{Q}} = 0$. This limit is commonly referred to as the Born-Oppenheimer approximation in the literature [Cederbaum 2008]. Therefore, the parametric dependence of the electronic wave function on the location of the ions is only due to scalar potentials.

(ii) Electronic dynamics are considered with fixed (immobile) ions, meaning that $\hat{\mathcal{W}}_{ii}$ in Eq. (2.4) is time independent when it is used in Eq. (2.6). Therefore, $\hat{\mathcal{W}}_{ii}$ is neglected in Eq. (2.6), since, in this case, $\hat{\mathcal{W}}_{ii} = \mathcal{W}_{ii}(\underline{\underline{\mathbf{R}}})$ is a constant and shifts the eigenvalues only by a finite constant.

(iii) The ions are treated classically. Therefore, the Wentzel-Kramers-Brillouin approximation [Landau 1965, Brown 1972] can be used to generate classical equations of motion of the ions on the basis of Eq. (2.7).

Approximations (i) – (iii) form the basis of the multi-scale approach to the two-component plasmas considered in this work. From Eq. (2.6), assumptions (i) and (ii) lead to the following equation for the electrons:

$$i\hbar\partial_t \psi_{\underline{\underline{\mathbf{R}}}}\left(\underline{\mathbf{r}},t\right) = \left(\hat{\mathcal{T}}_e + \hat{\mathcal{W}}_{ee} + \hat{\mathcal{W}}_{ei} + \hat{\mathcal{V}}^e_{\text{ext}}\right)\psi_{\underline{\underline{\mathbf{R}}}}\left(\underline{\mathbf{r}},t\right). \tag{2.8}$$

The many-particle Schrödinger equation (2.8) describes the electrons moving in the field of the fixed ions. Further simplification is achieved by description of the dynamics of the quantum electrons in terms of the electron density $n(\mathbf{r},t)$ and the electron current density $\mathbf{j}(\mathbf{r},t)$. The possibility of the description in terms of the continuum variables is guaranteed by the Hohenberg-Kohn-Mermin theorem of DFT [Hohenberg 1964, Kohn 1965, Mermin 1965] and the Runge-Gross theorem of time-dependent (or current) DFT [Runge 1984, Pribram-Jones 2016])*. Additionally, from assumption (iii), the classical equations of motion for ions follow. Thereby, the electronic dynamics are described by the continuity and momentum equations [Giuliani 2008], while the ions are driven classically† [Ullrich 2014]:

$$\frac{\partial}{\partial t} n\left(\mathbf{r},t\right) + \nabla\cdot\left[\mathbf{j}\left(\mathbf{r},t\right)\right] = 0, \tag{2.9}$$

$$m_e \frac{\partial}{\partial t}\mathbf{j}\left(\mathbf{r},t\right) - n\left(\mathbf{r},t\right) e\mathbf{E}(\mathbf{r},t) = -\nabla\cdot\boldsymbol{\Sigma}(\mathbf{r},t), \tag{2.10}$$

$$-\nabla_{\underline{\underline{\mathbf{R}}}}\left[\mathcal{W}_{ii} + \mathcal{V}^i_{\text{ext}} + \int \mathrm{d}\mathbf{r}\, n(\mathbf{r})\mathcal{W}_{ei}([n(\mathbf{r})];\underline{\underline{\mathbf{R}}})\right] = m_i \frac{\partial^2}{\partial t^2}\underline{\underline{\mathbf{R}}}(t). \tag{2.11}$$

where $\boldsymbol{\Sigma}$ denotes a tensor—the exact form of which is not known—that contains all many-particle and quantum effects [Tokatly 2007, Gao 2010] (including correlations and dissipation), and $\mathbf{E}$ is the strength of the electric field.

Eqs. (2.9)-(2.11) constitute the general form of the quantum fluid theory of dense plasmas within the multi-scale approach. If the microscopic

*The discussion of the electronic density and current within TD-DFT at finite temperature can be found in Ref. [Pribram-Jones 2014].

†Here, to avoid unnecessary complication of the discussions, the terms due to a magnetic field are dropped. The relevant discussion of the case with non-zero magnetic field is provided in chapter 3.

consideration of ionic dynamics is replaced by the hydrodynamic one, the description is simplified to the two-fluid model, which, e.g, is widely used for the investigation of laser plasmas [Mulser 2010]. The consistent derivation of $\mathbf{\Sigma}$—introduced in Eq. (2.10)—at finite temperature in a proper approximation for the description of quantum electrons at the considered plasma parameters is the content of chapter 3 and the investigation of the structural properties of the ions in the medium consisting the quantum electrons—in accord with Eq. (2.11)—is the subject of chapter 4.

2.4 Motivations for the revision of the foundations of QHD

Methods involving an accurate self-consistent quantum kinetic treatment of non-ideal dense quantum plasmas are challenging both theoretically and computationally. Consequently, as a simplified model for the study of quantum plasmas, the QHD has been adopted and widely used in recent years. A commonly used QHD model is based on Eqs. (2.9) and (2.10) with $\mathbf{\Sigma}$ that takes into account the pressure of ideal electrons, P, and the Bohm potential, V_B, i.e.,

$$-\nabla\cdot\mathbf{\Sigma}(\mathbf{r},t)=-\nabla P[n(\mathbf{r},t)]-n\,(\mathbf{r},t)\,\nabla V_B[n(\mathbf{r},t)]. \tag{2.12}$$

In Eq. (2.12), P and V_B were used with some ad hoc fitting parameters, which are discussed in more detail below.

In the ground state, $\theta \ll 1$, the QHD closure (2.12) was derived by different authors using different approaches. Here, the two most general and representative of them are discussed. The interested readers are refereed to Ref. [Khan 2014] for the relevant historical details, corresponding discussions in a pedagogical manner, and additional reference.

The first way which was used to derive the QHD equations [Manfredi 2001] (with $\mathbf{\Sigma}$ given by Eq.(2.12)) is based on the equation governing the evolution of the one-particle Wigner function in mean field approximation (the

quantum Vlasov equation)*

$$\left(\frac{\partial}{\partial t}+\mathbf{v}\cdot\nabla\right)f_W(\mathbf{r},\mathbf{v},t)-\frac{im_e}{\hbar}\int\int\frac{\mathrm{d}\mathbf{s}}{(2\pi\hbar)^3}\mathrm{d}\mathbf{v}'e^{im_e(\mathbf{v}-\mathbf{v}')\mathbf{s}/\hbar}$$
$$\times\left[V_{\mathrm{eff}}\left(\mathbf{r}+\frac{\mathbf{s}}{2}\right)-V_{\mathrm{eff}}\left(\mathbf{r}-\frac{\mathbf{s}}{2}\right)\right]f_W(\mathbf{r},\mathbf{v},t)=0, \quad (2.13)$$

where $\mathbf{v}$ is the electron velocity, V_{eff} is the total self-consistent potential, and f_W is the one-particle Wigner function [Wigner 1932, Bonitz 2016]

$$f_W(\mathbf{x},\mathbf{v},t)=\frac{m_e}{(2\pi\hbar)^3}\sum_{i=1}^{K}w_i\int_{-\infty}^{\infty}\mathrm{d}\mathbf{s}\,\psi_i^*\left(\mathbf{r}+\frac{\mathbf{s}}{2},t\right)\psi_i\left(\mathbf{r}-\frac{\mathbf{s}}{2},t\right)e^{im_e\mathbf{v}\,\mathbf{s}/\hbar} \quad (2.14)$$

with w_i being the probability that the system is in state i.

The zero and first order moments of the one-particle Wigner distribution function give the density distribution, $n(\mathbf{x},t)=\int f_W(\mathbf{x},\mathbf{v},t)\mathrm{d}\mathbf{v}$, and the velocity distribution, $v(\mathbf{x},t)=\frac{1}{n_0}\int\mathbf{v}f_W(\mathbf{x},\mathbf{v},t)\mathrm{d}\mathbf{v}$, respectively; here n_0 denotes the mean number density of the electrons. In Ref. [Manfredi 2001], the QHD model based on closure (2.12) was derived assuming that $\psi_i(\mathbf{r},t)=A(\mathbf{r})\exp(iS(\mathbf{r},t)/\hbar)$, where *all orbitals have the same amplitudes* $A_i(\mathbf{r})=A(\mathbf{r})$, and taking the first two moments of Eq. (2.13). This model was used for the study of a large variety of processes involving quantum electrons such as linear and non-linear waves, screening etc. [Shukla 2011]. In this formulation, the electronic pressure and Bohm potential are used in the following form:

$$P=P_F^D(T_e,n_0)\left(\frac{n(\mathbf{r})}{n_0}\right)^{(D+2)/D}, \quad (2.15)$$

$$V_B=\gamma\frac{\hbar^2}{8m}\left(\left|\frac{\nabla n}{n}\right|^2-2\frac{\nabla^2 n}{n}\right), \quad (2.16)$$

where P_F^D is the Fermi pressure of a D-dimensional fermion system, n_0 is the mean electronic density, and γ is a correction coefficient.

An alternative approach—well known in the field of solid-state physics—to derive the closure relation (2.12) (at $\theta\ll 1$) is based on the variational principle [Ying 1974, Eguiluz 1975],

$$\delta\int_{t_1}^{t_2}L[n(\mathbf{r},t),w(\mathbf{r},t)]\mathrm{d}t=0, \quad (2.17)$$

*This approach can be improved by taking into account electronic correlations by using, e.g., famous BBGKY hierarchical equations [Bonitz 2016].

applied to the Lagrangian

$$L[n(\mathbf{r},t),w(\mathbf{r},t)] = \int n(\mathbf{r},t)\frac{\partial w(\mathbf{r},t)}{\partial t}\mathrm{d}\mathbf{r} - H[n(\mathbf{r},t),w(\mathbf{r},t)], \tag{2.18}$$

where w is the scalar field defined as $\mathbf{v} = -\nabla w$, and H is a semi-classical electronic Hamiltonian, a further discussion of which is given in chapter 3.

In Refs. [Manfredi 2005, Eliasson 2008], the choice $D = 1$ was made in order to study the high frequency electronic oscillations, but—at the same time—using k_F for the three-dimensional system. This was justified by the agreement with the correct RPA result for the plasmon dispersion relation. Because of the same reason, the Bohm potential (2.16) with the pre-factor $\gamma = 1$ was used. Further, an approximate exchange-correlation potential for the static (equilibrium) case at $\theta \ll 1$ was added to the Bohm potential in order to extend the model to the case of correlated electrons [Crouseilles 2008]. Similarly, in plasmonics, the QHD model is used with fitting parameters [Yan 2015, Yan 2016, Ciracì 2016] corresponding to additional prefactors of the Fermi pressure and the Bohm potential and with an exchange correlation potential which is derived for the the static (equilibrium) case. In general, it was found that these parameters depend on the characteristic length-scale and time-scale of the physical problem and, moreover, these pre-factors are found to be a function of the density and temperature; thereby, resulting in complicated parametric dependencies [Haas 2015, Eliasson 2008, Moldabekov 2015b, Stanton 2015]. This led to some confusion and, therefore, to the usage of the QHD model beyond its range of applicability. For example, applying the QHD model for the description of the screening of a point-like ion charge by fully degenerate electrons with the assumption $\gamma = 1$, the discovery of a new attraction mechanism between ions was reported [Shukla 2012, Akbari-Moghanjoughi 2013]. This was clearly shown to be an artifact due to the usage of the QHD model outside the scope of applicability [Bonitz 2013a, Bonitz 2013c]. Finally, it was revealed that the "novel attractive force" from Ref. [Shukla 2012] is just the result of the invalid description of the well-known Friedel oscillations [Moldabekov 2015b] and that a more accurate description of the static screening at $\theta \ll 1$ is provided by the choice $\gamma = 1/9$. Another example is the implementation of the correction factor of $1/9$ to study the propagation of surface waves in a half-space quantum plasma in Ref. [Khalilpour 2015]. This was consequently criticized because this factor was derived for the static case only [Akbari-Moghanjoughi 2016].

Therefore, the QHD model with the above mentioned correction factors is far from being a reliable model for the large scale simulation of dense quantum plasmas. For instance, if the interaction of the ion beam with an quantum plasma or a streaming dense plasma is considered [Ludwig 2010], the relevant frequency is given by the relation $\omega = \mathbf{k} \cdot \mathbf{v}$ and, thereby, neither of the correction factors describing different liming cases (high or low frequency) can be used (where v is the penetrating ion or streaming velocity, and $\mathbf{k}$ is the wave vector which varies during the simulation). Additionally, the QHD model, in this formulation, has the following drawbacks:

- The quantum non-locality is taken into account approximately by the Bohm potential, which is the first order correction due to quantum diffraction effects in the non-interacting electron limit [Michta 2015, Moldabekov 2015b]. Therefore, in this sense, the QHD model cannot provide a full quantum mechanical treatment even in the case of ideal electrons.

- The exchange-correlation term derived for the equilibrium case and incorporated on the basis of the variational principle [Crouseilles 2008, Yan 2015, Ciracì 2016], is applicable only for the low frequency case and the use of it for the study of the high frequency phenomena like plasmon dynamics is unjustified in the absence of a benchmark by a more accurate method.

Knowing the limitations and drawbacks of the previously used QHD equations, in the next chapter the QHD equations at finite temperature and the needed closure relations are formulated in a more consistent way and with a clear discussion of the introduced approximations.

In a nutshell, in this chapter: The plasma state under consideration in terms of both dimensional and dimensionless parameters was described. Recent experiments in which the considered plasma parameters were realized were specified. The multi-scale approach, which lies at the heart of most theoretical considerations of the two component electron-ion plasma, was discussed. Limitations and open questions of the previously used QHD models, and the motivation for the revision of them from the very foundations were provided.

Chapter 3

Quantum hydrodynamics of electrons at finite temperature

Contents

After setting the framework from both the theoretical and the experimental perspective, in this chapter the consistent formulation of the QHD equations at finite temperature and the derivation of the closure relations determining the potentials for the QHD are presented. The latter allows to take into account quantum non-locality as well as exchange-correlation effects in the QHD description of a dense plasma. Moreover, the determined QHD model agrees with the OF-DFT in the static limit. Further, a generalized fully non-local Bohm potential is proposed. As an application of the obtained closure relations and of the generalized non-local Bohm potential, the existing QHD results are revised and, in part, improved with a clear description of the used approximations. Additionally,

the density gradient correction to a non-interacting free energy density functional and the Bohm potential for the two- and one-dimensional cases are derived and analyzed. The applicability of the QHD equations in the presence of an external magnetic field is discussed. The formulas for functional derivatives needed to follow the derivations in this chapter are listed in Appendix A. The results presented in this chapter were published in Refs. [Moldabekov 2018a, Moldabekov 2017a].

3.1 Derivation of the QHD equations at finite temperature

As discussed in chapter 2, there are two ways to derive the QHD equations. One can employ a kinetic equation to derive relations between the zero and first order moments of the one particle distribution function. Alternatively a derivation can be realized in a field-theoretical manner by variation of the semiclassical Lagrangian of the electrons. In this chapter an approach equivalent to the latter procedure is used. Starting from a semi-classical Hamiltonian of the electrons, we derive the QHD equations by using Hamilton's equations. This is possible due to the simultaneous existence of a one-body density $n(\mathbf{r})$ and a velocity field $v(\mathbf{r})$ realized by a determinantal (antisymmetrized) wave function for $N \geq 4$ particles [Lieb 2013].

We start from the magnetic field free case with the semi-classical Hamiltonian of the electrons in the form:

$$H[n(\mathbf{r},t),w(\mathbf{r},t)] = E[n(\mathbf{r},t)] - \int eV_{\text{ext}}n(\mathbf{r},t)\mathrm{d}\mathbf{r} + \int \frac{m_e n(\mathbf{r},t)}{2}\left|\nabla w\left(\mathbf{r},t\right)\right|^2 \mathrm{d}\mathbf{r} + \frac{e^2}{2}\int \frac{n(\mathbf{r},t)n(\mathbf{r}',t)}{|\mathbf{r}-\mathbf{r}'|}\mathrm{d}\mathbf{r}\mathrm{d}\mathbf{r}', \quad (3.1)$$

where w is the scalar potential determining the velocity field by $\mathbf{v} = -\nabla w$, $E[n] = E_{\text{id}}[n] + E_{\text{xc}}[n]$ is the sum of the kinetic and the exchange-correlation energy functionals, and V_{ext} refers to the external electric potential.

Hamilton's equations, with $n(\mathbf{r},t)$ and $m_e w(\mathbf{r},t)$ being canonically conjugate field variables, read [Lurie 1968]:

$$\frac{\delta H[n(\mathbf{r},t),w(\mathbf{r},t)]}{m_e \delta w(\mathbf{r},t)} = -\frac{\partial n(\mathbf{r},t)}{\partial t}, \quad (3.2)$$

$$\frac{\delta H[n(\mathbf{r},t),w(\mathbf{r},t)]}{\delta n(\mathbf{r},t)} = m_e \frac{\partial w(\mathbf{r},t)}{\partial t}. \quad (3.3)$$

Using Eq. (3.1) in Hamilton's equations (3.2) and (3.3), the following equations of motion, which are the basis of the QHD are obtained [Ying 1974, Banerjee 2000]:

$$\frac{\partial}{\partial t} n\left(\mathbf{r},t\right) = \nabla\cdot\left[n\left(\mathbf{r},t\right)\nabla w\left(\mathbf{r},t\right)\right], \tag{3.4}$$

$$m_e\frac{\partial}{\partial t} w\left(\mathbf{r},t\right) = \frac{\delta E[n]}{\delta n} - eV_{\text{ext}} + e^2\int\frac{n(\mathbf{r}',t)}{|\mathbf{r}-\mathbf{r}'|}\mathrm{d}\mathbf{r}' + \frac{1}{2}m_e\left|\nabla w\left(\mathbf{r},t\right)\right|^2. \tag{3.5}$$

Taking into account the relations $\mathbf{v} = -\nabla w$ and $(\mathbf{v}\cdot\nabla)\mathbf{v} = \frac{1}{2}\nabla(\nabla w)^2$, the QHD equations can be formulated in terms of the average density $n\left(\mathbf{r},t\right)$, velocity $v\left(\mathbf{r},t\right)$, and the generalized force $-\nabla\mu\left[\mathbf{r},t\right]$ [Ying 1974, Banerjee 2000]

$$\frac{\partial}{\partial t} n\left(\mathbf{r},t\right) = -\nabla\cdot\left[n\left(\mathbf{r},t\right)\mathbf{v}\left(\mathbf{r},t\right)\right], \tag{3.6}$$

$$m_e\frac{\partial}{\partial t}\mathbf{v}\left(\mathbf{r},t\right) + m_e\left[\mathbf{v}\left(\mathbf{r},t\right)\cdot\nabla\right]\mathbf{v}\left(\mathbf{r},t\right) = -\nabla\mu\left(\mathbf{r},t\right), \tag{3.7}$$

$$\mu[n(\mathbf{r},t)] = \frac{\delta E[n(\mathbf{r},t)]}{\delta n(\mathbf{r},t)} + e\varphi(\mathbf{r},t), \tag{3.8}$$

where the following effective potential is introduced:

$$\varphi(\mathbf{r},t) = e\int\frac{n(\mathbf{r}',t)}{|\mathbf{r}-\mathbf{r}'|}\mathrm{d}\mathbf{r}' - V_{\text{ext}}. \tag{3.9}$$

The derived QHD equations describe a curl-free flow.

The QHD equations (3.6), (3.7), and (3.8) are formulated in the micro-canonical ensemble, as they are derived from the semi-classical Hamiltonian (3.1). In previous works [Yan 2015, Michta 2015], Eqs. (3.7) and (3.8) were derived for the case of fully degenerate electrons ($\theta \ll 1$), where the utilized potential $\mu[n(\mathbf{r},t)]$ was obtained by substituting the following Tomas-Fermi energy density functional including the first order density gradient correction into Eq. (3.8):

$$E_{\text{id}}([n],T) = \bar{\alpha}\int\mathcal{E}_0[n(\mathbf{r})]\mathrm{d}\mathbf{r} + \gamma\frac{\hbar^2}{8m_e}\int\frac{|\nabla n(\mathbf{r})|^2}{n(\mathbf{r})}\,\mathrm{d}\mathbf{r}. \tag{3.10}$$

In Eq. (3.10), $\mathcal{E}_0$ is the energy density in the local density approximation, $\bar{\alpha}$ and γ are the correction factors that were introduced in chapter 2. The Bohm potential appears in quantum hydrodynamics via $\mu[n(\mathbf{r},t)]$ due to the functional derivative of the leading order term of the density gradient

correction (the second term on the right hand side of Eq. (3.10)), which is found using Eq. (A.2):

$$V_B = \gamma \frac{\hbar^2}{8m_e} \frac{\delta}{\delta n} \left(\int \frac{|\nabla n(\mathbf{r})|^2}{n(\mathbf{r})} \mathrm{d}\mathbf{r} \right) = -2 \frac{\hbar^2}{8m_e} \gamma \frac{\nabla^2 n(\mathbf{r})}{n(\mathbf{r})} + \mathcal{O}\Big((\tilde{n}/n_0)^2 \Big), \quad (3.11)$$

where $\tilde{n} = n(\mathbf{r}) - n_0$ is the density perturbation. A discussion of the coefficients $\bar{\alpha}$ and γ will be provided later in subchapter 3.4, after a more general closure relation that determines $\mu[n(\mathbf{r}, t)]$ is derived.

The applicability of the aforementioned low temperature QHD model to high-energy-density plasmas is severely limited due to the importance of thermal excitations in such systems. To properly extend the QHD equations to finite temperature the grand canonical ensemble is employed. Note that the considered system is infinite and quasi-neutral so that the pair interaction is screened. Therefore, according to Ref. [Campa 2009], the conditions for *the equivalence of the different statistical ensembles* are fulfilled*. At finite temperature, equations (3.4) and (3.5) have the same form, but the quantities n, $\mathbf{v}$ (with corresponding w), and μ (or equivalently $\frac{\delta E}{\delta n}$) are replaced by their expectation values in the grand canonical ensemble [Zubarev 1971]. The following relation holds for the expectation value in the grand canonical ensemble of the functional derivative of the energy with respect to the density variation [Zubarev 1971]:

$$\left\langle \frac{\delta E}{\delta n} \right\rangle = \frac{\delta \Omega}{\delta n}, \quad (3.12)$$

with the grand potential

$$\Omega[n(\mathbf{r})] = F[n(\mathbf{r})] - \mu_0 N, \quad (3.13)$$

where $F[n]$ is the free energy functional, $\mu_0 = \text{const}$ is the chemical potential of the system in thermodynamic equilibrium, and $N = \int n(\mathbf{r}) \mathrm{d}\mathbf{r}$ is the mean number of particles in the grand canonical ensemble. The proof of the equality (3.12) is given in Appendix B.

* Non-neutral plasmas and self-gravitating systems are examples for which the ensemble equivalence does not hold [Campa 2009].

Using Eqs. (3.8), (3.12), and (3.13), we find the following potential of the generalized force at finite temperature:

$$\mu[n(\mathbf{r},t),T]+\mu_0=\frac{\delta F[n(\mathbf{r},t)]}{\delta n(\mathbf{r},t)}+e\varphi(\mathbf{r},t). \tag{3.14}$$

Further, $F[n]=F_{\rm id}[n]+F_{\rm xc}[n]$ is decomposed into the ideal (non-interacting) contribution, $F_{\rm id}[n]$, and the exchange-correlation part, $F_{\rm xc}[n]$ *.

3.2 Non-interacting free energy functional

First, the ideal system is considered, where $F_{\rm xc}[n]=0$. In the previous works (discussed in chapter 2) electronic quantum non-locality effects were taken into account via the Bohm potential (3.11), which in the case of a weak density perturbation is proportional to $\nabla^2 n/n$. This approximation is valid in the long wavelength limit [Perrot 1979], i.e., far from a test charge that induces the electronic density perturbation. At large wavenumbers (short distances) the previously used QHD model is not applicable. In the next chapter, the investigation of the structural properties of strongly coupled ions in quantum plasmas will reveal that the inclusion of the large wavenumbers in the treatment of the electronic subsystem is vital at $\theta\lesssim 0.1$. Another example that shows the importance of quantum non-locality effects is presented in Appendix C, where a quantum wakefield in dense plasmas is considered. Thus, it is important to inquire whether the long wavelength approximation can be avoided.

The basic idea is to compute the density response function, $\Pi_{\rm QHD}(k,\omega)=\delta\tilde{n}(k,\omega)/e\delta\tilde{\varphi}(k,\omega)$, of the electrons to the perturbation by the effective field $\delta\tilde{\varphi}(k,\omega)$ (cf. Eq. (3.9)) using the QHD under the condition that it coincides with the polarization function of linear response theory in the whole frequency-wavenumber range. In the case of uncorrelated electrons the obvious choice is hence to use the RPA polarization function, i.e,

$$\Pi^{\rm id}_{\rm QHD}(k,\omega)\equiv\Pi_{\rm RPA}(k,\omega), \tag{3.15}$$

*It should be noted that in the static long wavelength limit, the determination of the generalized force, $-\nabla\mu[n(\mathbf{r},t),T]$, is equivalent to setting the pressure tensor $\overline{\overline{\mathbf{P}}}$ in the standard fluid theory [Chihara 2001],

$$\nabla\cdot\overline{\overline{\mathbf{P}}}=n(\mathbf{r},t)\nabla\frac{\delta F[n(\mathbf{r},t)]}{\delta n(\mathbf{r},t)}.$$

where $\Pi^{\mathrm{id}}_{\mathrm{QHD}}(k,\omega)$ is the QHD polarization function when assuming that $F_{\mathrm{xc}}[n] = 0$. This ansatz will result in a generalized fully non-local Bohm potential since the RPA polarization function is non-local.

From Eq. (3.14), for an equilibrium density profile $n_0(\mathbf{r})$ (that is current-free, with $w_0(\mathbf{r}) = 0$ and $\mu[n(\mathbf{r},t),T] = 0$) the following Euler-Lagrange equation underlying OF-DFT can be easily obtained

$$\frac{\delta F[n_0(\mathbf{r})]}{\delta n_0(\mathbf{r})} + e\varphi_0(\mathbf{r}) = \mu_0, \tag{3.16}$$

where μ_0 is a constant (the chemical potential at equilibrium). Now, the equilibrium system satisfying Eq. (3.16) is subject to an external perturbation. This leads to $n(\mathbf{r},t) = n_0(\mathbf{r}) + n_1(\mathbf{r},t)$, $w(\mathbf{r},t) = w_1(\mathbf{r},t)$, $\varphi(\mathbf{r},t) = \varphi_0(\mathbf{r}) + \varphi_1(\mathbf{r},t)$, with n_1, w_1 being the change in density, and velocity field potential, respectively, induced by the perturbation, $\varphi_1(\mathbf{r},t)$. In this case the Taylor expansion of the functional derivative of the free energy is given by

$$\frac{\delta F[n]}{\delta n(\mathbf{r})} = \frac{\delta F[n]}{\delta n(\mathbf{r})}\bigg|_{\mathrm{n=n_0}} + \int \mathrm{d}\mathbf{r}' \, \frac{\delta^2 F[n]}{\delta n(\mathbf{r},t)\delta n(\mathbf{r}')}\bigg|_{\mathrm{n=n_0}} n_1(\mathbf{r}') + \dots. \tag{3.17}$$

In first order in the perturbation, using Eqs. (3.16) and (3.17) in combination with the continuity and the momentum equations we find

$$\frac{\partial n_1(\mathbf{r},t)}{\partial t} - \nabla\cdot(n_0\nabla w_1) = 0, \tag{3.18}$$

$$m_e\frac{\partial w_1(\mathbf{r},t)}{\partial t} = e\varphi_1(\mathbf{r},t) + \int \mathrm{d}\mathbf{r}' \, \frac{\delta^2 F[n]}{\delta n(\mathbf{r},t)\delta n(\mathbf{r}',t)}\bigg|_{\mathrm{n=n_0}} n_1(\mathbf{r}',t), \tag{3.19}$$

where w_1, by definition, determines the velocity perturbation, $\mathbf{v}_1 = -\nabla w_1$. The last term on the right hand side of Eq. (3.19) represents the total potential incorporating the Fermi pressure, Bohm potential and, in general, the exchange-correlation terms when $F_{\mathrm{xc}}[n] \neq 0$.

Now, in order to connect the term $\frac{\delta^2 F[n]}{\delta n(\mathbf{r},t)\delta n(\mathbf{r}',t)}\Big|_{\mathrm{n=n_0}}$ with the polarization (density) response function from linear response theory, the equilibrium density is assumed to be uniform. Using the Fourier transform to frequency and wavenumber space (k,ω), which is denoted by $\mathfrak{F}$, Eqs. (3.18) and (3.19) yield

$$-i\omega\tilde{n}_1 + k^2 n_0 \tilde{w}_1 = 0, \tag{3.20}$$

$$-i\omega\tilde{w}_1 = \frac{e\tilde{\varphi}_1}{m_e} + \mathfrak{F}\left[\left.\frac{\delta^2 F[n]}{\delta n(\mathbf{r},t)\delta n(\mathbf{r}',t)}\right|_{\mathrm{n=n_0}}\right]\frac{\tilde{n}_1}{m_e}. \tag{3.21}$$

The QHD result for the inverse polarization function $\Pi^{-1}_{\mathrm{QHD}}(k,\omega) = e\tilde{\varphi}_1/\tilde{n}_1$ is deduced from Eqs. (3.20) and (3.21):

$$\Pi^{-1}_{\mathrm{QHD}}(k,\omega) = \frac{m_e\omega^2}{n_0 k^2} - \mathfrak{F}\left[\left.\frac{\delta^2 F[n]}{\delta n(\mathbf{r},t)\delta n(\mathbf{r}',t)}\right|_{\mathrm{n=n_0}}\right]. \tag{3.22}$$

For the non-interacting case, i.e., $F_{\mathrm{xc}}[n] = 0$, and $\Pi^{\mathrm{id}}_{\mathrm{QHD}} = \Pi_{\mathrm{RPA}}$, we find the following relation:

$$-\mathfrak{F}\left[\left.\frac{\delta^2 F_{\mathrm{id}}}{\delta n(\mathbf{r},t)\delta n(\mathbf{r}',t)}\right|_{\mathrm{n=n_0}}\right] = \frac{1}{\Pi_{\mathrm{RPA}}(k,\omega)} - \frac{1}{\Pi^0(\omega)}, \tag{3.23}$$

where $\Pi^0(\omega)$ denotes the long-wavelength limit of the RPA polarization function,

$$\Pi^0(\omega) \equiv \lim_{k\to 0}\Pi_{\mathrm{RPA}}(k,\omega) = \frac{k^2}{\omega^2}\frac{n_0}{m_e}. \tag{3.24}$$

As was mentioned previously, Eq. (3.23) takes into account both the Fermi and Bohm potential.

Note that, in the static limit where $\left[\Pi^0(\omega=0)\right]^{-1} = 0$, the relation (3.23) reduces to that which is used in the OF-DFT for the construction of a non-interacting free energy functional for the application in dense plasma and warm dense matter simulations [Sjostrom 2013a].

The next question to be addressed is how correlation effects can be consistently included in the QHD description. This question is discussed in the following subchapter.

3.3 Exchange-correlation potential for QHD

At this point we also take into account the exchange-correlation contribution to $F[n]$. Thereby, the polarization function is extended from the ideal to the interacting one, $\Pi^{\mathrm{id}}_{\mathrm{QHD}} \to \Pi_{\mathrm{QHD}}$. Previously, for the case $\theta \ll 1$, exchange-correlation contributions were included in QHD only in a phenomenological manner [Crouseilles 2008].

It is known from DFT and linear response theory that the exchange-correlation effects can be included using a so-called local field correction

[Sjostrom 2014b, Ichimaru 1982]. We use this approach to take into account the exchange-correlation potential in the QHD model.

First of all, substituting $F = F_{\rm id} + F_{\rm xc}$ into Eq. (3.22) we find:

$$\frac{1}{\Pi_{\rm QHD}(k,\omega)} = \frac{1}{\Pi^0(\omega)} - \mathfrak{F}\left[\left.\frac{\delta^2 F_{\rm id}[n]}{\delta n(\mathbf{r},t)\delta n(\mathbf{r}',t)}\right|_{\rm n=n_0}\right] - \mathfrak{F}\left[\left.\frac{\delta^2 F_{\rm xc}[n]}{\delta n(\mathbf{r},t)\delta n(\mathbf{r}',t)}\right|_{\rm n=n_0}\right]. \quad (3.25)$$

Taking into account Eq. (3.23) we have

$$\frac{1}{\Pi_{\rm QHD}(k,\omega)} = \frac{1}{\Pi_{\rm RPA}(k,\omega)} - \mathfrak{F}\left[\left.\frac{\delta^2 F_{\rm xc}[n]}{\delta n(\mathbf{r},t)\delta n(\mathbf{r}',t)}\right|_{\rm n=n_0}\right]. \quad (3.26)$$

The polarization function given by Eq. (3.26) can be rewritten in a more familiar form as

$$\Pi_{\rm QHD}(k,\omega) = \frac{\Pi_{\rm RPA}(k,\omega)}{1 - \mathfrak{F}\left[\left.\frac{\delta^2 F_{\rm xc}}{\delta n(\mathbf{r})\delta n(\mathbf{r}')}\right|_{\rm n=n_0}\right]\Pi_{\rm RPA}(k,\omega)}. \quad (3.27)$$

On the other hand, the polarization function of a correlated electron gas can be expressed in terms of a local field correction as [Ichimaru 1982]:

$$\Pi_{\rm LFC}(k,\omega) = \frac{\Pi_{\rm RPA}(k,\omega)}{1 + \tilde{u}(k)G(k,\omega)\Pi_{\rm RPA}(k,\omega)}, \quad (3.28)$$

with $\tilde{u}(k) = 4\pi e^2/k^2$ being the Fourier transform of the Coulomb potential. From the requirement that the correlated QHD polarization is in agreement with the latter result, i.e., $\Pi_{\rm QHD}(k,\omega) \equiv \Pi_{\rm LFC}(k,\omega)$, we arrive at the closure relation for the exchange-correlation free energy:

$$\mathfrak{F}\left[\left.\frac{\delta^2 F_{\rm xc}}{\delta n(\mathbf{r})\delta n(\mathbf{r}')}\right|_{\rm n=n_0}\right] = -\tilde{u}(k)G(k,\omega). \quad (3.29)$$

Note that a similar result was obtained in the context of TDDFT [Runge 1984, Giuliani 2008].

Now, in the case of the *homogeneous equilibrium (static) density distribution*, we can write down the derived QHD momentum equation taking into account exchange-correlation effects:

$$m_e \frac{\partial w_1(\mathbf{r},t)}{\partial t} = e\varphi_1(\mathbf{r},t) + \left(\frac{\delta F[n(\mathbf{r})]}{\delta n(\mathbf{r})}\right)^{(1)}, \quad (3.30)$$

with the non-local potential

$$\left(\frac{\delta F[n(\mathbf{r})]}{\delta n(\mathbf{r})}\right)^{(1)} = \int \mathrm{d}\mathbf{r}'\, n_1(\mathbf{r}',t)\Bigg[\int \frac{\mathrm{d}\mathbf{k}}{(2\pi)^3}\,\mathrm{d}\omega\, e^{i[\mathbf{k}\cdot(\mathbf{r}-\mathbf{r}')-\omega t]} \left(-\frac{1}{\Pi_{\mathrm{RPA}}(k,\omega)}+\frac{1}{\Pi^0(\omega)}-\frac{4\pi e^2}{k^2}G(k,\omega)\right)\Bigg]\Bigg|_{\mathrm{n}_0}. \quad (3.31)$$

This case, for instance, is relevant to ICF plasmas, where a macroscopic density gradient scale length, $L = n_0/|\nabla n_0| \sim 100\ \mu$m, is larger than all characteristic microscopic length scales [Bates 2018] (for comparison, the wavelength of an ion-acoustic wave is $\lesssim 0.1\ \mu$m).

In the case of the *inhomogeneous equilibrium density distribution*, similarly to the standard approach of the OF-DFT, Eqs. (3.29) and (3.23) determining $\frac{\delta^2 F[n]}{\delta n(\mathbf{r},t)\delta n(\mathbf{r}',t)}\Big|_{\mathrm{n}=\mathrm{n}_0}$ allow to find a proper non-local free energy density (e.g., Refs. [Wang 1992, Garcia-Aldea 2012, Sjostrom 2013a, Huang 2010, Sjostrom 2014b, Witt 2018]). In the next subchapter, this will be demonstrated by re-deriving the fluid equations within the well established Thomas-Fermi (TF) approach with the Kirzhnitz-von Weizsäcker density gradient correction.

To have a closed set of QHD equations the information about the local field correction, $G(k,\omega)$, is needed. In quantum plasma physics, the local field correction has been studied for a long time. For example, the analytic properties of the dynamic local field correction—such as the asymptotic expansion—were studied in detail by Kugler [Kugler 1975], and the interpolation formula for the dynamic local field correction was considered in Refs. [Tanaka 1987, Dabrowski 1986]. Hence, this "input" function can be obtained by a number other methods/approximations.

Let us briefly discuss different methods which can be used to compute the local field correction. The static local field correction, $G(k)$, can be computed using the finite temperature Singwi-Tosi-Land-Sjölander approximation (STLS), which was widely used for the investigation of dense plasma properties [Tanaka 1986, Tanaka 2017, Sjostrom 2013b]. This approximation is discussed and analyzed in more detail in chapter 4 in the context of a quantum plasma with strongly coupled ions. It should be noted that the most reliable result for $G(k)$ can be obtained from *ab initio* quantum Monte Carlo simulations [Dornheim 2016]. In Ref. [Corradini 1998], an analytical formula of $G(k)$ for fully degenerate electrons in the ground state, i.e., $\theta \to 0$,

was obtained by a fit to accurate quantum Monte Carlo data [Moroni 1995]. The *ab initio* calculation of the local field correction at finite temperature for different values of wavenumber was presented in Refs. [Dornheim 2017a, Dornheim 2017b, Groth 2017a]. In the long wavelength limit, the static local field correction is expressed using the exchange-correlation free energy density, f_{xc}, of the uniform electron gas by the relation $G(k \ll 2k_F, 0) \simeq -\frac{k_F^2}{4\pi e}\frac{\partial^2 n f_{\mathrm{xc}}}{\partial n^2}k^2$, where the result for an accurate parametrization of f_{xc} for the case of partial degeneracy from Ref. [Groth 2017b] can be used. Further, the fit formula based on the data from quantum Monte Carlo for both small and large wavenumbers can written in the form $G(k) = A[1 - \exp(-Bk^2)]$ [Vashista 1972, Dandrea 1986], where the values of the coefficients A and B can be extracted from the pair-distribution function of the uniform electron gas, $g(r)$, at $r \to 0$ and $G(k \ll 2k_F, 0)$ [Sjostrom 2014b].

Once a proper static local field correction, $G(k, 0)$, is obtained, the dynamic result, $G(k, \omega)$, can be approximately computed using the method of moments [Arkhipov 2010]. Alternatively, the dynamic STLS approximation can be employed to compute the dynamic local field correction [Kumar 2009]. Another approximation often used in warm dense matter and dense plasma studies is the so-called dynamic collision frequency approach [Reinholz 2000, Veysman 2016]. The application of this approximation in QHD will be discussed later in this chapter.

3.4 Local density approximation with gradient corrections

As was discussed earlier, all previous works on the QHD description of quantum plasmas are based on the LDA taking into account the leading order density gradient correction and relying on various fit parameters. Despite the wide usage, the previously used QHD models suffer from a number of inconsistencies as discussed in subchapter 2.4. As an application of the derived closure relation (3.23), the results of previous works on QHD are revised and improved in this and the next subchapters.

First, in order to derive a potential related to the Fermi pressure and the Bohm potential, we set $F_{\mathrm{xc}}[n] = 0$ and consider the following free energy functional for the case of a non-uniform (inhomogeneous) electron distribu-

tion:

$$F_{\mathrm{id}}[n] = F_0[n(\mathbf{r},t)] + \int \mathrm{d}\mathbf{r}\, a_2\,[n(\mathbf{r},t)] \mid \nabla\tilde{n}(\mathbf{r},t) \mid^2, \tag{3.32}$$

where $\tilde{n}(\mathbf{r},t) = n(\mathbf{r},t) - n_0$ is the density perturbation relative to the constant mean density n_0. The term F_0 is defined via the free energy density

$$F_0[n] = \int f_0[n(\mathbf{r},t)]\mathrm{d}\mathbf{r}. \tag{3.33}$$

Here, $f_0[n]$ and $a_2[n]$ are unknown functions which must be found. Functionals in the form of Eq. (3.32) are often referred to as the generalized Thomas-Fermi (TF) model with the von Weizsäcker-type density gradient correction [Garcia-Aldea 2012].

In first order in the perturbation, the second order functional derivative of Eq. (3.32) at $n = n_0$ reads

$$\left.\frac{\delta^2 F_{\mathrm{id}}}{\delta n(\mathbf{r},t)\delta n(\mathbf{r}',t)}\right|_{\mathrm{n=n_0}} = \left.\frac{\partial^2 f_0[n]}{\partial n^2}\right|_{\mathrm{n=n_0}} \delta(\mathbf{r}-\mathbf{r}') + 2a_2[n_0]\nabla\cdot\nabla'\delta(\mathbf{r}-\mathbf{r}'), \tag{3.34}$$

where Eqs. (A.1) and (A.2) were used. The Fourier transform of Eq. (3.34) is given by

$$\mathfrak{F}\left[\left.\frac{\delta^2 F_{\mathrm{id}}}{\delta n(\mathbf{r},t)\delta n(\mathbf{r}',t)}\right|_{\mathrm{n=n_0}}\right] = \left.\frac{\partial^2 f_0[n]}{\partial n^2}\right|_{\mathrm{n=n_0}} + 2a_2[n_0]k^2. \tag{3.35}$$

Equation (3.23) allows us to express $f_0[n]$ and $a_2[n]$ systematically using the RPA. In what follows we will need the real part of the RPA polarization function, which in equilibrium at arbitrary temperature reads [Arista 1984]

$$\mathrm{Re}\,\Pi_{\mathrm{RPA}}(k,\omega) = -\frac{k^2\chi_0^2}{16\pi e^2 z^3}\left[g(u+z) - g(u-z)\right], \tag{3.36}$$

where $u = \omega/(kv_F)$ and $z = k/(2k_F)$ are the dimensionless frequency and wavenumber, respectively, $\chi_0^2 = (\pi k_F a_B)^{-1} \simeq r_s/6.03$, and $k_F = (3\pi^2 n)^{1/3}$. In Eq. (3.36), the function $g(x)$ is given by

$$g(x) = -g(-x) = \int \frac{y\,\mathrm{d}y}{\exp(y^2/\theta - \eta) + 1} \ln\left|\frac{x+y}{x-y}\right|. \tag{3.37}$$

This explicit expression of the RPA polarization was used to study various limiting cases with respect to frequency and wavenumber. In particular,

in the limiting case of large or small values of z, we need the following expansion of the inverse of the real part of the RPA polarization function [Arista 1984, Wang 2000]:

$$\frac{1}{2\,\mathrm{Re}\,\Pi_{\mathrm{RPA}}(z,u)} \simeq \tilde{a}_0 + \tilde{a}_2(2k_F)^2\ z^2 + \tilde{a}_4(2k_F)^4\ z^4 + ... + cu^2$$
$$\simeq \tilde{a}_0 + \tilde{a}_2 k^2 + \tilde{a}_4 k^4 + ... + \frac{1}{2}\frac{\omega^2}{k^2}\frac{m_e}{n_0}. \quad (3.38)$$

Substituting Eq. (3.35) into Eq. (3.23) and using expansion (3.38) we derive the following equations determining $f_0[n]$ and $a_2[n]$:

$$\tilde{a}_0[n_0] = -\frac{1}{2}\frac{\partial^2 f_0[n]}{\partial n^2}\bigg|_{\mathrm{n=n_0}}, \quad (3.39)$$

$$\tilde{a}_2[n_0] = -a_2[n_0]. \quad (3.40)$$

Equations (3.39) and (3.40) are related to the *stiffness* theorem. The latter connects the free-energy perturbation (energy, in the case of ground state) due to an applied external field with an inverse linear response function. For the proof of this theorem in the ground state see Ref. [Giuliani 2008]. Further, in Appendix D the discussion of the *stiffness* theorem at finite temperature for the case of a perturbation by an external electric field is given. Additionally, the consistency of the results of this work with this theorem is discussed.

In accordance with the standard concept of the LDA, after the coefficients $\tilde{a}_0[n_0]$ and $a_2[n_0]$ are obtained, the equilibrium density is allowed to vary in space and time, $n_0 \to n(\mathbf{r},t)$. In the LDA, the Bohm potential for any degeneracy parameter is computed from the second term on the right hand side of Eq. (3.32) using Eq. (A.2):

$$V_B = \frac{\delta}{\delta n}\int \mathrm{d}\mathbf{r}\, a_2\,[n]\ |\ \nabla n(\mathbf{r})\ |^2$$
$$= |\nabla n|^2\,\frac{\partial a_2[n]}{\partial n} - 2\left(a_2[n]\nabla^2 n + \nabla n\cdot\nabla a_2[n]\right), \quad (3.41)$$

where the abbreviation $n(\mathbf{r}) = n(\mathbf{r},t)$ is introduced.

It should be stressed that the coefficients $\tilde{a}_0$ and a_2 depend on the considered limits for k and ω. Obviously, this affects the value of the Bohm potential. To make this point conspicuous, in the ground state (i.e., at

$\theta = k_B T/E_F \sim T \times n^{-2/3} \to 0$), we rewrite the Bohm potential (3.11) using Eq. (A.2) in the form:

$$V_B(\omega, k) = \gamma(\omega, k)\frac{\hbar^2}{8m}\left(\left|\frac{\nabla n}{n}\right|^2 - 2\frac{\nabla^2 n}{n}\right), \tag{3.42}$$

where the coefficient γ is now determined by $a_2([n]; \theta \ll 1) = \gamma\hbar^2/(8mn)$, as it can be seen by comparing Eq. (3.10) with Eq. (3.32) (note that in the ground state $F \to E$). The coefficient γ depends on the considered values of the wavenumber and frequency.

The Fermi pressure is related to the functional derivative of the first term on the right hand side of Eq. (3.32), which at $\theta \to 0$ can be written as:

$$\frac{\delta F_0[n]}{\delta n} = \frac{\partial f_0[n]}{\partial n} = -\int 2\tilde{a}_0\left([n], \theta \to 0\right)\mathrm{d}n = \bar{\alpha}(\omega, k)E_F, \tag{3.43}$$

where the coefficient $\bar{\alpha}$ depends on the considered limit on the k–ω plane. Eq. (3.43) represents the consistent derivation of the previously artificially added coefficient $\bar{\alpha}$ (see Eq. (3.10)), but now this coefficient is not an arbitrary fitting parameter, i.e., $\tilde{a}_0\left([n], \theta \to 0\right)$ determines the coefficient $\bar{\alpha}$.

Eqs. (3.39) and (3.40), derived on the basis of the closure relation (3.23), provide a unified general picture for the understanding of the complex parametric dependencies of the pre-factors of both Fermi pressure and Bohm potential on frequency, wavenumber, density and temperature. Now, using Eqs. (3.39) and (3.40), we analyze different limits for the coefficients $\tilde{a}_0[n]$ and $a_2[n] = -\tilde{a}_2$, for different frequency-wavenumber ranges.

In what follows, the coefficients $\tilde{a}_0[n]$ and $a_2[n]$ are expressed in terms of the density $n(\mathbf{r})$ and the dimensionless chemical potential, $\eta = \beta\mu$, where $\beta = 1/(k_B T)$ is the inverse temperature. We use the relation $n(\mathbf{r}) = \frac{\sqrt{2}m^{3/2}}{\pi^2\beta^{3/2}\hbar^3} I_{1/2}[\eta(\mathbf{r})]$, which is valid in the local density approximation, to write the following partial derivatives needed to find the Bohm potential (3.41),

$$\frac{\partial\eta}{\partial n} = C\frac{1}{I_{-1/2}(\eta)}, \tag{3.44}$$

$$\nabla\eta = C\frac{\nabla n(\mathbf{r})}{I_{-1/2}(\eta)}, \tag{3.45}$$

where $C = \frac{2\pi^2\beta^{3/2}\hbar^3}{\sqrt{2}m^{3/2}} = \frac{4}{3n}\theta^{-3/2}$, and I_ν is the Fermi-Dirac integral of order ν.

3.4.1. Low frequency and long wavelength limit

First we consider the static long wavelength case, $k \ll 2k_F$. The results obtained in this case are valid also for low frequencies, i.e., $u \ll 1$ or $\omega \ll kv_F$. This case is important for the investigation of the screening of a test charge and the dispersion of low-frequency waves (e.g., ion-acoustic waves) in plasmas. In a number of publications the static screening of an ion charge in a quantum plasma was treated incorrectly using the wrong factor $\gamma = 1$ for the Bohm potential [Shukla 2012, Shukla 2008], which—while being valid for the high-frequency case—is almost by a factor of ten larger than the proper value for the static case ($\gamma = 1/9$). This resulted in the unphysical prediction of an attraction between ions in an equilibrium dense plasma, for detailed discussions see Refs. [Bonitz 2013a, Bonitz 2013b, Bonitz 2013c].

In the present limiting case, the coefficients $\tilde{a}_0[n]$ and $a_2[n]$ of the expansion (3.38) read [Perrot 1979, Moldabekov 2015b]:

$$\tilde{a}_0\,[n] = -\frac{\pi e^2}{2k_F^2\chi_0^2 H_1(\eta)}, \tag{3.46}$$

$$a_2\,[n] = -\frac{\hbar^2 H_2(\eta)}{72 m_e n H_1^2(\eta)}, \tag{3.47}$$

with

$H_1(\eta) = \frac{\sqrt{\theta[n]}}{2}\, I_{-1/2}(\eta), \quad H_2(\eta) = \frac{1}{2\sqrt{\theta[n]}}\, I_{-3/2}(\eta).$

Substituting Eq. (3.47) into Eq. (3.32) we recover the density gradient correction derived in Ref. [Perrot 1979] for finite temperatures. This density gradient correction was used recently to study the ion screening by quantum electrons [Stanton 2015]. In the case $k_BT \ll E_F$, we have $H_1 \simeq 1$ and $H_2 \simeq -1$. In this limit Eq. (3.47) gives the asymptotic result $a_2 \to \hbar^2/(72mn)$. Therefore, for the coefficient in front of the Bohm potential in Eq. (3.42) we have $\gamma = 1/9$ [Perrot 1979, Kirzhnitz 1957]. The convergence of the expansion (3.38) in the static case at $k < 2k_F$ is discussed in Appendix E.

On the other hand, for the static case ($\omega = 0$), it is known that $f_0 \equiv f_{\mathrm{TF}}$, where f_{TF} is the free energy density in the Thomas-Fermi approximation:

$$f_{\mathrm{TF}}\,([n], \theta) = \frac{\sqrt{2} m^{3/2}}{\hbar^3 \pi^2 \beta^{5/2}} \left(\eta I_{1/2}(\eta) - \frac{2}{3} I_{3/2}(\eta) \right). \tag{3.48}$$

The second order partial derivative of Eq. (3.48), $-\frac{1}{2}\frac{\partial^2 f_{TF}[n]}{\partial n^2}$, in the static long wavelength limit ($k \ll 2k_F$) exactly matches $\tilde{a}_0[n]$ given by Eq. (3.46)

[Perrot 1979]. Finally, the functional derivative of the Thomas-Fermi term yields:

$$\frac{\delta F_{\mathrm{TF}}}{\delta n} = \frac{\eta}{\beta}. \tag{3.49}$$

In the limit $\theta \ll 1$, we have $\eta = \beta E_F$. This leads to the well-known result $\delta E_0/\delta n = E_F$ (e.g., see Ref. [Michta 2015]). On the other hand, using the first term on the right hand side of Eq. (3.10), we have $\delta E_0/\delta n = \bar{\alpha} E_F$. Thus, in the static long wavelength limit it is $\bar{\alpha} = 1$.

From the relations (3.44) and (3.45), taking into account the dependence $\theta[n] \sim n^{-2/3}$, the finite-temperature generalization of the Bohm potential can be obtained by substituting Eq. (3.47) into Eq. (3.41). By regrouping terms, we write the Bohm potential (3.41) as

$$V_B = V_1 + V_2, \tag{3.50}$$

where

$$V_1 = -2a_2[n]\nabla^2 n, \tag{3.51}$$

and

$$\begin{aligned} V_2 &= |\nabla n|^2 \frac{\partial a_2[n]}{\partial n} - 2\nabla n \cdot \nabla a_2[n] \\ &= |\nabla n|^2 \frac{\partial \eta}{\partial n}\frac{\partial a_2[n]}{\partial \eta} - 2(\nabla n \cdot \nabla \eta)\frac{\partial a_2[n]}{\partial \eta} \\ &= -|\nabla n|^2 \frac{C}{I_{-1/2}(\eta)}\frac{\partial a_2[n]}{\partial \eta}. \end{aligned} \tag{3.52}$$

The last line of Eq. (3.52) was found by making use of Eqs. (3.44) and (3.45). To make the finite temperature Bohm potential look similar to its zero temperature form, the coefficient γ is generalized to finite temperature:

$$\gamma[n] = a_2[n]\left(\frac{\hbar^2}{8m_e n}\right)^{-1} = -\frac{2}{9}\frac{I_{-3/2}(\eta)}{I^2_{-1/2}(\eta)}\theta^{-3/2}, \tag{3.53}$$

which equals $1/9$ at $\theta \ll 1$. We use this coefficient in V_1 to find

$$V_1 = \gamma[n]\frac{\hbar^2}{8m_e}\left(-2\frac{\nabla^2 n}{n}\right). \tag{3.54}$$

For V_2, taking into account that $C = \frac{4}{3n}\theta^{-3/2}$, we obtain:

$$V_2 = -\gamma[n]\frac{\hbar^2}{8m_e}\frac{2I_{-1/2}(\eta)I_{1/2}(\eta)}{I_{-3/2}(\eta)}\frac{\partial a_2[n]}{\partial \eta} \times \frac{|\nabla n|^2}{n^2}. \tag{3.55}$$

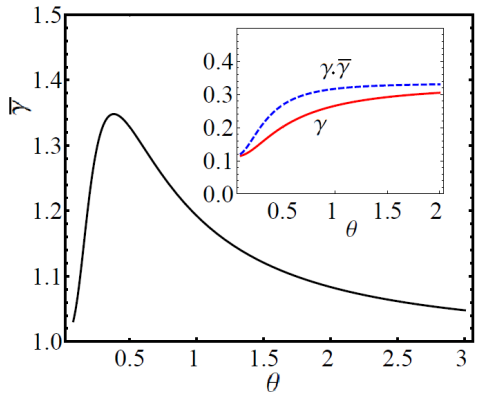

Figure 3.1: The factors $\bar{\gamma}$, γ, and $\gamma\bar{\gamma}$ for the long-wavelength case. From reference [Moldabekov 2018a].

Further, we introduce one more coefficient:

$$\bar{\gamma}[n] = -\frac{2I_{1/2}(\eta)I_{-1/2}(\eta)}{I_{-3/2}(\eta)}\frac{\partial}{\partial\eta}\left(\frac{I_{-3/2}(\eta)}{I^2_{-1/2}(\eta)}\right). \tag{3.56}$$

Substituting Eqs. (3.54) and (3.55) into Eq. (3.50), and taking into account the definition of the coefficient $\bar{\gamma}$, Eq.(3.56), the following expression for the finite-temperature Bohm potential in the static long wavelength limit is derived:

$$V_B(\theta) = \gamma(\theta)\frac{\hbar^2}{8m}\left(\bar{\gamma}(\theta)\left|\frac{\nabla n}{n}\right|^2 - 2\frac{\nabla^2 n}{n}\right). \tag{3.57}$$

The dependence of γ, $\gamma\bar{\gamma}$, and the correction coefficient $\bar{\gamma}$ on θ are shown in Fig. 3.1. In the case of fully degenerate electrons, $\theta \to 0$, and in the classical limit, $\theta \gg 1$, the correction coefficient tends to unity, $\bar{\gamma} \to 1$. As can be seen from Fig. 3.1, the correction coefficient $\bar{\gamma}$ is expected to be important for a partially degenerate plasma with $\theta \sim 0.5$.

For completeness, it should be mentioned that the finite-temperature Bohm potential was also recently considered in Ref. [Haas 2015]. In this work, the coefficient γ given by Eq. (3.53) was found by comparing the linearized QHD result to the RPA result, but the correction coefficient $\bar{\gamma}$ was omitted. The reason for the latter is that the first term of the Bohm potential in Eq. (3.57) is proportional to $(n_0/n_1)^2$, where $n_1/n_0 \ll 1$. Thereby, in Ref. [Haas 2015], after the linearization of the QHD equations the information about the term $\sim (n_0/n_1)^2$ and the related coefficient $\bar{\gamma}$ was lost.

3.4.2. Short wavelength limit at low frequencies

It is known that in the limit of short wavelengths, the plasma behaves like a collection of individual particles [Pines 1952], in contrast to pronounced collective behavior in the long-wavelength limit. The behavior of the coefficients $\tilde{a}_0$ and a_2, determining $F_0[n]$ and the gradient correction in Eq. (3.32), at the transition from the long wavelength to the short wavelength limit is important for the analysis of QHD results for currently interesting topics such as plasmonics [Ciracì 2016, Pitarke 2007], quantum plasmas [Haas 2000] and the application of OF-DFT to dense plasmas (warm dense matter) [Sjostrom 2014a, Starrett 2017, Karasiev 2012].

In the short wavelength limit, as was shown in Ref. [Jones 1971] for the degenerate electron gas, the first order density gradient correction has the form of the von Weizsäcker gradient correction with $a_2[n] = \frac{\hbar^2}{8m_e n}$ [Weizsäcker 1935]. In this case we have $\gamma = 1$ for the Bohm potential. Note that the von Weizsäcker gradient correction correctly reproduces the Kato-Steiner cusp condition [Kato 1957, Steiner 1963] for the electron distribution close to a test charge (core) [Plumper 1983, Ladányi 1992].

First, we need the expansion of the function $\Delta g = g(u+z) - g(u-z)$ (cf. Eq. (3.37)) in the limit $z \gg 1$, which reads [Arista 1984]:

$$\Delta g \simeq 2g(z) + u^2 g''(z), \tag{3.58}$$

where

$$g(z) = \frac{2}{3z} + \frac{I_{3/2}\theta^{5/2}}{3z^3}. \tag{3.59}$$

Using Eqs. (3.58) and (3.59) we find

$$\frac{z}{\Delta g} \simeq -\frac{3}{8} I_{3/2}(\eta)\theta^{5/2} + \frac{3z^2}{4} - \frac{3u^2}{4} + ... \tag{3.60}$$

Substituting Eq. (3.60) into the formula (3.36) for the inverse polarization function,

$$\frac{1}{\mathrm{Re}\,\Pi_{\mathrm{RPA}}(k,\omega)} = -\frac{4\pi e^2}{\chi_0^2 k_F^2}\frac{z}{\Delta g}, \tag{3.61}$$

and subsequently using the obtained result in the expansion (3.38), we derive the coefficients $\tilde{a}_0[n]$ and $a_2[n]$ in the short wavelength case:

$$\tilde{a}_0[n] = -\frac{4\pi e^2}{k_F^2 \chi_0^2} \times \frac{3}{16} I_{3/2}(\eta)\theta^{5/2}[n], \tag{3.62}$$

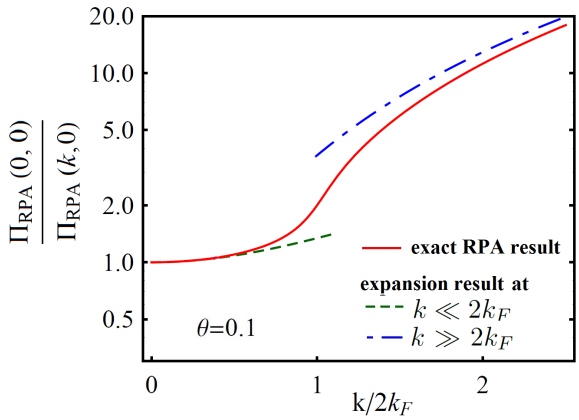

Figure 3.2: $\Pi_{\mathrm{RPA}}(0,0)/\Pi_{\mathrm{RPA}}(k,0)$ at $\theta = 0.1$ and various approximations to it (see the text). From reference [Moldabekov 2018a].

$$a_2\,[n] = \frac{\hbar^2}{8m_e n}. \tag{3.63}$$

Now, we use Eqs. (3.62) and (3.63) to find the coefficients $\bar{\alpha}$ and γ. At $\theta \ll 1$, by substituting Eq. (3.62) into Eq. (3.39) and subsequently integrating the result for $\frac{\partial^2 f_0[n]}{\partial n^2}$ over n, we find that:

$$\frac{\delta F_0[n]}{\delta n} \simeq \frac{3}{5}E_F. \tag{3.64}$$

A finite temperature correction is obtained by expanding $\tilde{a}_0$ around $\theta = 0$,

$$\frac{\delta F_0[n]}{\delta n} \simeq \frac{3}{5}E_F + \frac{3\pi^2}{8}E_F\theta^2. \tag{3.65}$$

The value of $\bar{\alpha}$ is determined by the pre-factor in front of E_F on the right hand side of Eq. (3.64). Therefore, the transition from the long wavelength to the short wavelength limit results in a change of $\bar{\alpha}$ in Eq. (3.10) from 1 to 3/5. Additionally, from Eq. (3.63) we find that the coefficient in front of the Bohm potential in Eq. (3.42) becomes $\gamma = a_2 \cdot \frac{8m_e n}{\hbar^2} = 1$ [Jones 1971], and independent of temperature.

Interestingly, in the considered limit $k/k_F \gg 1$, which can also be understood as a vanishing number density of the electrons ($k_F \to 0$), the von Weizsäcker gradient correction is the leading term in F_{id} given by Eq. (3.32)

[Plumper 1983]. Thus, one can neglect F_0 and use Eqs. (3.14) and (3.7) to find the momentum equation which coincides with the Madelung equation* [Madelung 1926, Madelung 1927],

$$m_e \frac{\partial}{\partial t} w(\mathbf{r},t) - \frac{1}{2} m_e (\nabla w(\mathbf{r},t))^2 = -\frac{\hbar^2}{2m_e} \frac{\nabla^2 \sqrt{n}}{\sqrt{n}} - eV_{\text{ext}}, \tag{3.66}$$

where the following identity was used:

$$V_B(k/2k_F \gg 1) = \frac{\hbar^2}{8m_e} \left(\left| \frac{\nabla n}{n} \right|^2 - 2\frac{\nabla^2 n}{n} \right) = -\frac{\hbar^2}{2m_e} \frac{\nabla^2 \sqrt{n}}{\sqrt{n}}. \tag{3.67}$$

Therefore, we arrive at the conclusion that in the short wavelength limit defined as $k/k_F \gg 1$, indeed, electrons behave like a collection of non-interacting individual particles with negligible quantum statistical effects.

The applicability of the results obtained in the short wavelengths case can be gauged by comparing the inverse RPA polarization function with the expansion result at $k/2k_F \gg 1$. Such a comparison is presented in Fig. 3.2. Obviously, the convergence of the expansion in the limit $k/2k_F \gg 1$ to the RPA result is rather slow. In contrast, the convergence of the expansion in the long-wavelength limit, which is also shown in Fig. 3.2, is very good and it is applicable up to $k \simeq k_F$.

3.4.3. High frequency limit, $\omega \gg \hbar k^2/2m_e$

This case is important for plasma electrodynamics and related to such processes like the optical (Langmuir) oscillations of the electrons as well as the high-frequency electromagnetic field propagation in plasmas (or interaction with plasmas).

To find the correct values of the factors γ and $\bar{\alpha}$ in the limit $u \gg z$ ($\omega \gg \hbar k^2/2m_e$), we need the following expressions [Arista 1984]

$$g(u+z) - g(u-z) = 2zg'(u) + \frac{z^3}{3} g'''(u), \tag{3.68}$$

$$g(u) = \frac{2}{3u} + \frac{I_{3/2}\theta^{5/2}}{3u^3}. \tag{3.69}$$

*In the original work by Madelung, the field w was defined using $\mathbf{v} = \nabla w$, whereas here it is $\mathbf{v} = -\nabla w$.

Eqs. (3.68) and (3.69) yield

$$\frac{z}{\Delta g} \simeq -\frac{9}{8} I_{3/2}(\eta)\theta^{5/2} + \frac{3z^2}{4} - \frac{3u^2}{4} + ... \tag{3.70}$$

Substituting Eq. (3.70) into Eq. (3.61) and using the obtained result in Eq. (3.38), we deduce the coefficients $\tilde{a}_0[n]$ and $a_2[n]$ in the high frequency limit,

$$\tilde{a}_0\,[n] = -\frac{4\pi e^2}{k_F^2 \chi_0^2} \times \frac{9}{16} I_{3/2}(\eta)\theta^{5/2}[n], \tag{3.71}$$

$$a_2\,[n] = \frac{\hbar^2}{8 m_e n}. \tag{3.72}$$

Further, in the case $\theta \ll 1$, Eqs. (3.71) and (3.39) allow us to obtain the following formula for the functional derivative of $F_0[n]$ at $\omega \gg \hbar k^2/2m_e$:

$$\frac{\delta F_0[n]}{\delta n} \simeq \frac{9}{5} E_F + \frac{9\pi^2}{8} E_F \theta^2, \tag{3.73}$$

where the expansion of $I_{3/2}(\eta)$ at $\theta \ll 1$ and the equality $I_{3/2}(\theta \to 0) = \frac{2}{5}\theta^{-5/2}$ were used.

From the first term on the right hand side of Eq. (3.73) it follows that, in the high-frequency limit, for the QHD equations we have the factor $\bar{\alpha} = 9/5$ at $\theta \to 0$. This result agrees with previous works [Yan 2015, Halevi 1995], where this factor was empirically included to find the correct plasmon dispersion relation from the linearized QHD equations. Thereby, in the long wavelength limit, the transition from the low frequency to high frequency regime leads to the change of the factor $\bar{\alpha}$ from 1 to 9/5.

In the past, the foregoing feature of the factor $\bar{\alpha}$ led to some confusion due to the lack of a unifying picture of the various versions of QHD. For example, in Ref. [Caizergues 2014], $\bar{\alpha} = 1$ was used to compute a photoabsorption cross section at high frequencies.

From Eq. (3.72) we see that the pre-factor in front of the Bohm potential equals $\gamma = 1$ as in the short wavelength limit. In the case of high frequencies, the coefficient $a_2[n]$ is independent of the temperature. Therefore, at finite temperature the Bohm potential is given by Eq. (3.42). This is reasonable since the movement of the electrons is not affected by thermal excitations at sufficiently high frequency of the perturbing electric field.

The correctness of the derived coefficients $\tilde{a}_0$ and a_2 for the high-frequency case can be checked by using them to derive the well-known plasmon dispersion on the basis of the QHD equations:

$$\omega^2(k) = \omega_p^2 - 2\left[\tilde{a}_0([n_0],\theta) - a_2([n_0],\theta)k^2\right]\frac{n_0}{m_e} \times k^2, \tag{3.74}$$

which, at $\theta \ll 1$, leads to

$$\omega^2(k) = \omega_p^2 + \frac{3}{5}v_F^2k^2 + \frac{\hbar^2k^4}{4m_e^2}, \tag{3.75}$$

where it is taken into account that $2\tilde{a}_0[n_0]n_0/m_e \to -\frac{3}{5}v_F^2$, at $\theta \ll 1$, and that, in the considered case, $a_2[n] = \hbar^2/8m_en$.

In the opposite limit of high temperatures, i.e., $\theta \gg 1$, we have $\tilde{a}_0[n_0] \to -\frac{3}{2}\frac{k_BT}{n_0}$, which yields

$$\omega^2(k) = \omega_p^2 + 3v_{\text{th}}^2k^2 + \frac{\hbar^2k^4}{4m_e^2}, \tag{3.76}$$

with $v_{\text{th}} = \sqrt{\frac{k_BT}{m_e}}$ being the thermal velocity.

In the case of fully degenerate electrons, it has thus been shown that the value of the factors γ and $\bar{\alpha}$ depends on the characteristic wavelengths and frequencies of the phenomena involved. To illustrated this finding, the different results for the coefficients γ and $\bar{\alpha}$ in the k–ω plane are summarized in Fig. 3.3. Additionally, the obtained coefficients $a_2[n], \gamma$ and $\tilde{a}_0[n]$, $\bar{\alpha}$ are collected in tables 3.1 and 3.2.

Finally, note that the Bohm potential is commonly expressed via $\sqrt{n}$ using Eq. (3.67) [Shukla 2011]. However, from the considered case of low frequencies and long wavelengths at finite temperature, we see that the equality (3.67) for the Bohm potential is not always valid. It is evident that the identity (3.67) holds at finite temperature only if high frequencies ($\omega \gg \hbar k^2/2m_e$) or short wavelengths ($k \gg 2k_F$) are considered.

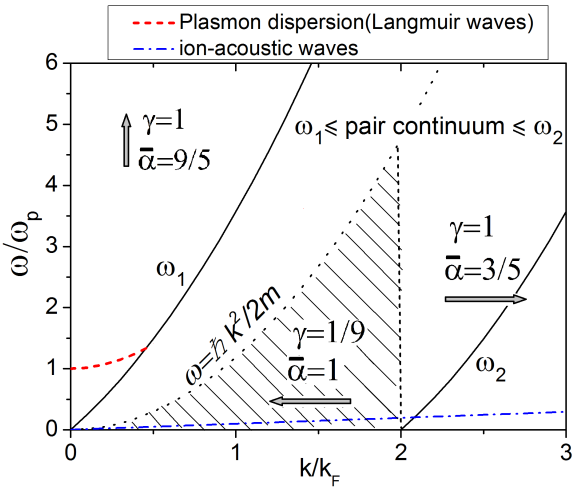

Figure 3.3: The factors γ in Eq. (3.42) and $\bar{\alpha}$ in Eq.(3.43) for different limiting cases (indicated by arrows) at $\theta \ll 1$ (given in Tables 3.2 and 3.1). The dashed line indicates the well-known plasmon dispersion $\omega = \omega_p^2 + (3/5)k^2 v_F^2 + (1/4)\hbar^2 k^4/m_e^2$ in the RPA. The dash-dot line represents the ion-acoustic waves multiplied by the factor m_p/m_e. The static long wavelength limit corresponds to the dashed area. The so-called pair continuum takes place in the area between curves ω_1 and ω_2. From reference [Moldabekov 2018a].

Table 3.1: The value of γ at $\theta \ll 1$ [cf. Eq. (3.42)] and the result for the coefficient $a_2[n]$ in different limits.

	$a_2[n]$	γ
$\omega \ll \hbar k^2/2m_e$ $k \ll 2k_F$	$-\dfrac{\hbar^2 H_2(\eta)}{72 m_e n H_1^2(\eta)}$	1/9
$\omega \ll \hbar k^2/2m_e$ $k \gg 2k_F$	$\dfrac{\hbar^2}{8m_e n}$	1
$\omega \gg \hbar k^2/2m_e$	$\dfrac{\hbar^2}{8m_e n}$	1

Table 3.2: The value of $\bar{\alpha}$ [cf. Eq. (3.43)] and the result for the coefficient $\tilde{a}_0[n]$ in different limits.

	$\tilde{a}_0[n]$	$\bar{\alpha}$
$\omega \ll \hbar k^2/2m_e$ $k \ll 2k_F$	$-\frac{\pi e^2}{2k_F^2\chi_0^2 H_1(\eta)}$	1
$\omega \ll \hbar k^2/2m_e$ $k \gg 2k_F$	$-\frac{4\pi e^2}{k_F^2\chi_0^2} \times \frac{3}{16} I_{3/2}(\eta)\theta^{5/2}$	3/5
$\omega \gg \hbar k^2/2m_e$	$-\frac{4\pi e^2}{k_F^2\chi_0^2} \times \frac{9}{16} I_{3/2}(\eta)\theta^{5/2}$	9/5

3.4.4. Summary for the LDA case

On the basis of the closure relation for the non-interacting free energy, the LDA approximation—most commonly used in dense plasma physics—with the leading order gradient correction was extensively analyzed in this subchapter. However, it is known from TDDFT, that in case of an inhomogeneous electronic system the exchange-correlation kernel (the second-order functional derivative of F_{xc}) is not rapidly decaying with $|\mathbf{r} - \mathbf{r}'|$; in contrast to the homogenous case where the exchange-correlation kernel is short-ranged. This leads to the so-called ultra-non-locality problem of time-depended DFT, which states that a frequency-dependent adiabatic local density approximation of an inhomogeneous electronic system does not exist [Giuliani 2008, Runge 1984]. Nevertheless, the local density approximation for the exchange-correlation potential can be used if the characteristic length scale on which the time-dependent potential changes is much smaller than that of the equilibrium density distribution [Giuliani 2008, Harbola 1998]. In this case, the applicability condition of the QHD equations can be deduced from the continuity equation (3.18)

$$\frac{\partial n_1(\mathbf{r},t)}{\partial t} = \nabla\cdot(n_0\nabla w_1) = n_0\nabla^2 w_1\left(1+\frac{\nabla n_0\cdot\nabla w_1}{n_0\nabla^2 w_1}\right).$$

Here the information contained in the last term in the brackets vanishes in a uniform electron gas. The ensuing consequence of this is that the LDA is valid only if $\left|\frac{\nabla n_0\cdot\nabla w_1}{n_0\nabla^2 w_1}\right| \ll 1$. In terms of the velocity, $|\nabla n_0\cdot\mathbf{v}| \ll n_0|\nabla\cdot\mathbf{v}|$,

the latter condition yields:

$$\frac{|\nabla n_0|}{n_0} \ll \frac{|\nabla \cdot \mathbf{v}|}{|\mathbf{v}|}. \tag{3.77}$$

Therefore, the characteristic length scale over which the density distribution changes must be substantially larger than that of corresponding change of the velocity.

3.5 Fully non-local Bohm potential

Next it is demonstrated how a fully non-local Bohm potential, that goes beyond previous works, can be introduced using relation (3.23). We start from the following ansatz:

$$F_{\mathrm{id}}[n] = F_0[n(\mathbf{r})] + \int \mathrm{d}\mathbf{r}\,\mathrm{d}\mathbf{r}'\, K([n_0]; |\mathbf{r}-\mathbf{r}'|) n_1(\mathbf{r},t)\, n_1(\mathbf{r}',t), \tag{3.78}$$

where the kernel K is symmetric with respect to permutation of $\mathbf{r}$ and $\mathbf{r}'$. Taking the first order functional derivative of the second term on the right hand side of Eq. (3.78) yields the generalized non-local Bohm potential:

$$V_B = \frac{\delta}{\delta n}\left(\int \mathrm{d}\mathbf{r}\,\mathrm{d}\mathbf{r}'\, K([n_0]; |\mathbf{r}-\mathbf{r}'|) n_1(\mathbf{r},t)\, n_1(\mathbf{r}'.t) \right). \tag{3.79}$$

Further, using Eqs. (3.33), (A.1) and (A.3), from Eq. (3.78) we find:

$$\mathfrak{F}\left[\frac{\delta^2 F_{\mathrm{id}}}{\delta n(\mathbf{r},t)\delta n(\mathbf{r}',t)}\bigg|_{\mathrm{n=n_0}} \right] = \frac{\partial^2 f_0[n]}{\partial n^2}\bigg|_{\mathrm{n=n_0}} + 2\widetilde{K}([n_0]\mathbf{k}), \tag{3.80}$$

where $\widetilde{K}([n_0];\mathbf{k})$ is the Fourier transform of the kernel K.

Substituting Eq. (3.80) into Eq. (3.23), we can express the kernel $\widetilde{K}$ in terms of the known RPA response function and the ideal free energy,

$$\widetilde{K}([n_0];\mathbf{k}) = \frac{1}{2}\left[-\frac{1}{\Pi_{\mathrm{RPA}}(k,\omega)} + \frac{1}{\Pi^0(\omega)} - \frac{\partial^2 f_0[n]}{\partial n^2}\bigg|_{\mathrm{n=n_0}} \right]. \tag{3.81}$$

Thus, the generalized non-local Bohm potential in the first order of the density perturbation reads

$$V_B \simeq \int 2K([n_0]; |\mathbf{r}-\mathbf{r}'|) n_1(\mathbf{r}')\mathrm{d}\mathbf{r}' + \mathcal{O}\Big((n_1/n_0)^2 \Big), \tag{3.82}$$

where the functional $K([n_0];|\mathbf{r}-\mathbf{r}'|)$ is given by the inverse Fourier transformation of Eq. (3.81).

Eqs. (3.79) and (3.81) can be used to rederive the results of the LDA from the previous subchapter. To show this, we neglect the imaginary part of the response function and use Eq. (3.36). Now, we expand the kernel K in Fourier space*,

$$\widetilde{K}([n_0];\mathbf{k}) = \tilde{a}_2[n_0]k^2 + \tilde{a}_4[n_0]k^4 + ..., \tag{3.83}$$

and perform the inverse Fourier transformation,

$$K([n_0];|\mathbf{r}-\mathbf{r}'|) = a_2[n_0]\nabla\cdot\nabla'\delta(\mathbf{r}-\mathbf{r}')+a_4[n_0](\nabla)^2(\nabla')^2\delta(\mathbf{r}-\mathbf{r}')+.... \tag{3.84}$$

Then we find, taking into account Eq. (3.39), that Eq. (3.79) yields the Bohm potential in the form of Eq. (3.41) if the first term of the expansion (3.83) is retained.

As another example of the utility of relation (3.23), the force field $\mu[n(\mathbf{r},t)]$, Eq. (3.14), can be computed via the ansatz [Wang 1992]:

$$F_{\mathrm{id}} = F_{\mathrm{TF}} + F_{\mathrm{vW}} + \int \mathrm{d}\mathbf{r}\mathrm{d}\mathbf{r}'\ [n(\mathbf{r},t)]^a\, W\left(\mathbf{r}-\mathbf{r}', T, n_0\right)\left[n(\mathbf{r}',t)\right]^b, \tag{3.85}$$

where F_{TF} is defined by the Thomas-Fermi free energy density (3.48) and F_{vW} has the same form as the gradient correction in Eq. (3.32) with $a_2 = \hbar^2/8m_e n$ (i.e., $\gamma = 1$), and $a = b = 5/6$.

Using the relation (3.23), the kernel $W\left(\mathbf{r}-\mathbf{r}', T, n_0\right)$ is determined using its Fourier transform as

$$\widetilde{W}\left(k,\omega\right) = -\frac{1}{2abn_0^{(a+b-2)}}\left[\frac{1}{\Pi_{\mathrm{RPA}}(k,\omega)} - \frac{1}{\Pi^0(\omega)}\right] + \frac{(\tilde{a}_0 - a_2)}{abn_0^{(a+b-2)}}, \tag{3.86}$$

where $\tilde{a}_0$ is given by Eq. (3.46), and a_2 is defined by Eq. (3.72). Recently, the static version of Eqs. (3.86) and Eq. (3.85) were successfully used for the description of the thermodynamical properties of hydrogen at warm dense matter conditions on the basis of the OF-DFT with the accuracy comparable to that of Kohn-Sham DFT simulations [Sjostrom 2013a].

The ansatz defined by Eqs. (3.85) and (3.86) (or by Eqs. (3.78) and (3.81)) can be used in the momentum equation (3.14) to simulate the dynamics of the non-uniform electron gas within the QHD formalism.

*Since K is real due to the usage of only the real part of Π_{RPA}, meaning $\widetilde{K}(-\mathbf{k}) = \widetilde{K}(\mathbf{k})$. Thus, the expansion (3.83) contains only even powers of $\mathbf{k}$.

3.6 Collision effects in the relaxation-time approximation

As an example of the application of relation (3.29) for the exchange-correlation potential, we consider the relaxation time approximation. In this approximation, the polarization function is given by

$$\Pi_{\mathrm{LFC}}(k,\omega) = \frac{\Pi_{\mathrm{RPA}}(k,\omega)}{1 + i\hbar\nu\tilde{\Pi}(k,\omega)}, \tag{3.87}$$

where

$$\tilde{\Pi}(k,\omega) = \frac{1}{\hbar\omega}\left[\frac{\Pi_{\mathrm{RPA}}(k,\omega)}{\Pi_{\mathrm{RPA}}(k,0)} - 1\right]. \tag{3.88}$$

The electron collision frequency ν [Mermin 1970, Ludwig 2010] takes into account all scattering processes [Bonitz 2016] and must, thus, incorporate a contribution from both electron-electron collisions [Barriga-Carrasco 2006, Daligault 2017] and electron-ion (neutral) collisions.

From Eqs. (3.28) and (3.87), we see that

$$\frac{4\pi e^2}{k^2}G(k,\omega) = \frac{i\nu}{\omega}\left[\frac{1}{\Pi_{\mathrm{RPA}}(k,0)} - \frac{1}{\Pi_{\mathrm{RPA}}(k,\omega)}\right]. \tag{3.89}$$

Making use of the expansion (3.38) in the limit $k/2k_F \ll 1$, we find,

$$\frac{4\pi e^2}{k^2}G(k,\omega) \simeq \frac{i\nu}{\omega}\left[2\Big(\tilde{a}_0^0[n_0] - \tilde{a}_0[n_0]\Big) + 2\Big(\tilde{a}_2^0[n_0] - \tilde{a}_2[n_0]\Big)k^2 - \frac{1}{\Pi^0(\omega)}\right] \tag{3.90}$$

$$\simeq -\frac{im_e}{n_0}\frac{\omega\nu}{k^2}, \tag{3.91}$$

where the coefficients $\tilde{a}_0[n_0]$ and $\tilde{a}_2[n_0]$ are given by Eqs. (3.71) and (3.72), respectively, and the coefficients $\tilde{a}_0^0[n_0]$ and $\tilde{a}_2^0[n_0]$ are defined by Eqs. (3.46) and (3.47), respectively.

Eq. (3.91) results in a friction force in the momentum equation (3.21),

$$\int \mathrm{d}\mathbf{r}' \left.\frac{\delta^2 F_{\mathrm{xc}}[n]}{\delta n(\mathbf{r},t)\delta n(\mathbf{r}',t)}\right|_{\mathrm{n=n_0}} n_1(\mathbf{r}',t) = \mathfrak{F}^{-1}\left[-\frac{4\pi e^2}{k^2}G(k,\omega)\tilde{n}_1\right] = \mathfrak{F}^{-1}\left[\frac{im_e}{n_0}\frac{\omega\nu}{k^2}\tilde{n}_1\right] = \mathfrak{F}^{-1}\left[\nu\tilde{w}_1 m_e\right] = \nu w_1(\mathbf{r},t)\, m_e, \quad (3.92)$$

where the expression $\tilde{w}_1 = \frac{i\omega}{k^2 n_0}\tilde{n}_1$, and the relation (3.29) were used. The so-called hydrodynamic Drude model that is often used in plasmonics [Halevi 1995, Yan 2015, Fernández-Domínguez 2012, Teng 2017] is recovered if one uses Eq. (3.90) retaining the terms scaling as $\sim \tilde{a}_0$ and $\sim \tilde{a}_2$.

The Mermin polarization function with a constant collision frequency is the simplest analytical model which takes into account correlations. This model was substantially improved by introducing a dynamical collision frequency, $\nu = \nu(\omega)$ [Reinholz 2000]. This approximation is widely used for the description of dense plasmas and warm dense matter [Thiele 2008, Sperling 2013, Neumayer 2010]. The required information about the dynamical collision frequency can be obtained using the Green functions method or semiclassical molecular dynamics simulations [Reinholz 2000, Morozov 2005]. In appendix C, the dynamical collision frequency approach is employed to evaluate the impact of the correlations on quantum wakefield.

3.7 Bohm potential and gradient correction for systems of reduced dimensionality

The QHD and OF-DFT equations for dense quantum plasmas formally have the same form as those used in plasmonics. Therefore, as another example of the utility of the derived relation (3.23), gradient corrections for the systems of 2D and 1D electrons are investigated in this subchapter.

Previous works mainly focused on 3D systems and, thereby, much less is known about density gradient corrections at finite temperature for systems of reduced dimensionality. The accuracy of the OF-DFT computations depends on the non-interacting free energy functional as well as the exchange-correlation energy functional. The LDA was proven to be a very accurate approximation for two-dimensional systems [Koivisto 2008, Eschrig 1996, Trappe 2016a]; even with bound states or strong inhomogeneity.

In Refs. [Holas 1991] and [Salasnich 2007] the gradient correction for the ground state was obtained using the expansion of the inverse ideal polarization function of electrons and the so-called Kirzhnitz expansion method, respectively. In particular, it was found that the leading term of the gradient correction to the kinetic energy is zero in 2D and negative in 1D. Recently, in Ref. [Putaja 2012] it was revealed that in the ground state all higher order terms of the density gradient correction to the kinetic energy vanish in 2D. However, at finite temperature it has been shown that the density gradient correction to the kinetic energy in 2D is non-zero [van Zyl 2011].

In the aforementioned works a kinetic energy functional rather than a free energy functional was studied. However, the Fermi temperature in 2D and 1D systems can be comparable to temperatures that occur in experiments [Pouget 2016]. Therefore, for the adequate description of physical phenomena, such as screening and transport [Das Sarma 2015], the finite temperature DFT and QHD which are based on the free energy functional must be used. In what follows the density gradient correction to the non-interacting free energy and related Bohm potential at finite temperature are derived.

To facilitate a comparison of the finite temperature result with the previous zero temperature results, it is convenient to rewrite Eq. (3.32) in the form:

$$F_{\mathrm{id}}([n],T) = \int f_0[n(\mathbf{r})]\mathrm{d}\mathbf{r} + \frac{\hbar^2}{8m_e}\int \gamma_D\,(n,T)\,\frac{|\,\nabla n(\mathbf{r})\,|^2}{n(\mathbf{r})}\,\mathrm{d}\mathbf{r}, \tag{3.93}$$

where D indicates the dimensionality.

Using Eq. (3.93), for the Bohm potential we find:

$$V_B = \frac{\hbar^2}{8m_e}\,\frac{\delta}{\delta n}\left(\int \gamma_D\,(n,T)\,\frac{|\,\nabla n(\mathbf{r})\,|^2}{n(\mathbf{r})}\,\mathrm{d}\mathbf{r}\right) \tag{3.94}$$

$$= -2\frac{\hbar^2}{8m_e}\gamma_D\,(n,T)\,\frac{\nabla^2 n}{n} + \mathcal{O}\Big(\,(n_1/n_0)^2\,\Big), \tag{3.95}$$

and according to Eqs. (3.39) and (3.40), for f_0 and γ_D we have

$$\tilde{a}_0[n_0] = -\,\frac{1}{2}\frac{\partial^2 f_0[n]}{\partial n^2}\bigg|_{\mathrm{n=n_0}}, \qquad \text{(3.39 revisited)}$$

$$\tilde{a}_2[n_0] = -\gamma_D(n_0,T)\frac{\hbar^2}{8mn_0}. \tag{3.96}$$

For example, if $D = 3$, for long wavelengths and low frequencies from Eqs. (3.96) and (3.47) we have:

$$\gamma_3[n] = \frac{1}{9} 4\theta^{-3/2} \frac{I'_{-1/2}(\eta)}{I^2_{-1/2}(\eta)}, \tag{3.97}$$

where the derivatives of $I_{-1/2}$ are taken with respect to η. In the zero temperature limit, γ_3 coincides with the previously introduced coefficient γ, i.e, $\gamma_3(\theta \to 0) = 1/9$. For high frequencies Eq. (3.72) yields $\gamma_3\left(\omega \gg \frac{\hbar k^2}{2m_e}\right) = 1$.

To proceed further, we need the polarization function of ideal electrons in 2D and 1D. For the 2D case, we use the polarization function expressed in terms of the dimensionless variables $u = \omega/(kv_F)$ and $z = k/(2k_F)$* [Bret 1993]:

$$\Pi^{\mathrm{D=2}}_{\mathrm{RPA}}(k,\omega) = -\frac{k_F^2 \chi_0^2}{2\pi e^2 k} \left[g_2(u+z) - g_2(u-z)\right]. \tag{3.98}$$

where $\chi_0^2 = 1/(\pi k_F a_B)$, and $k_F = (2\pi n)^{1/2}$ (the Fermi wavenumber for the two dimensional electron gas). The function g_2 in Eq. (3.98) is defined as:

$$g_2(x) = 2\pi \frac{x}{|x|} \int_0^x \frac{y\,\mathrm{d}y}{[\exp(y^2\theta^{-1} - \eta) + 1]\sqrt{x^2 - y^2}} - 2i\pi \int_x^\infty \frac{y\,\mathrm{d}y}{[\exp(y^2\theta^{-1} - \eta) + 1]\sqrt{y^2 - x^2}}, \tag{3.99}$$

where the dimensionless chemical potential, $\eta = \mu/k_B T$, can be computed using the identity $\eta = \ln\left(\exp\left(\theta^{-1}\right) - 1\right)$.

In the 1D case, the electronic polarization function [Jérome 1982] is

$$\Pi^{\mathrm{D=1}}_{\mathrm{RPA}}(k,\omega) = \frac{2}{L} \sum_k \frac{f(\epsilon_k) - f(\epsilon_{k-q})}{\epsilon_k - \epsilon_{k-q} - \hbar\omega + i\hbar\eta^+}, \tag{3.100}$$

where $f(\epsilon_k)$ is the Fermi-Dirac function, L is the system length, and $\eta^+ \to +0$ is a positive infinitesimal assuring a causal response of the system. A discussion of the polarization function for the 1D case is given, e.g., in

*Following Ref. [Arista 1984], in Ref. [Bret 1993] the variables u and z were used to analyze the polarization function in 2D.

Ref. [Bonitz 2016]. Following Refs. [Arista 1984] and [Bret 1993], the real part of the polarization function of the 1D electron gas is written as

$$\mathrm{Re}\,\Pi^{\mathrm{D=1}}_{\mathrm{RPA}}(k,\omega) = -\frac{k_F\chi_0^2}{e^2 k}\left[g_1(u+z) - g_1(u-z)\right], \tag{3.101}$$

where u, z, and χ_0 are defined as in the 2D and 3D cases (see Eqs. (3.36) and (3.98), respectively), but with $k_F = \pi n/2$. The function g_1 is given by the principal value of the following integral:

$$g_1(x) = \mathrm{P}\int_{-\infty}^{\infty} \frac{\mathrm{d}y}{[\exp(y^2\theta^{-1} - \eta) + 1](x+y)}. \tag{3.102}$$

In Eq. (3.102), the dimensionless chemical potential, $\eta = \mu/k_BT$, is connected to the degeneracy parameter of the 1D electron gas by the relation $2\theta^{-1/2} = I_{-1/2}(\eta)$. Note that the expansion of the inverse RPA polarization function in the 2D and 1D cases has the same form as in the 3D case, Eq. (3.38).

The expansion of the polarization functions for 2D and 1D allow to find the coefficient γ_D and, thereby, compute both the density gradient correction and the Bohm potential at finite temperature. First, we start with the static long-wavelength limit for the 2D and 1D cases, and continue with the high frequency limit.

3.7.1. Low frequency and long wavelength limit: 2D electron gas

As was discussed in subchapter 3.4, the static long wavelength limit is important for the description of screening at large distances. The results obtained in the static case are applicable for low frequencies ($u \ll z$) as well. For this case, we find from Eq. (3.98):

$$\Pi^{\mathrm{D=2}}_{\mathrm{RPA}}(k,\omega=0) = -\frac{2k_F^2\chi_0^2}{e^2 k}\int_0^z \frac{y\mathrm{d}y}{[\exp(y^2\theta^{-1} - \eta) + 1](z^2-y^2)^{1/2}}, \tag{3.103}$$

which in the long wavelength limit leads

$$\Pi^{\mathrm{D=2}}_{\mathrm{RPA}}(k \ll 2k_F, \omega=0) \simeq -\frac{k_F\chi_0^2}{e^2}\frac{1}{[1+\exp\left(\frac{2z^2}{3\theta} - \eta\right)]}. \tag{3.104}$$

Using Eq. (3.104) the following coefficients of the expansion (3.38) are obtained:

$$\tilde{a}_0(n,T) = -\frac{\pi e^2 a_B}{2}\left[1+\exp(-\eta)\right], \tag{3.105}$$

$$\tilde{a}_{2l}(n,T) = -\frac{\pi e^2 a_B}{2}\left(\frac{2}{3}\right)^l \frac{\exp(-\eta)}{l!\,\theta^l (2k_F)^{2l}}, \tag{3.106}$$

where $l = 1, 2, 3, ...$ are integer values.

For the discussion of the convergence of the expansion of the inverse RPA polarization function, Eq. (3.38), the following dimensionless inverse static polarization function is introduced:

$$\overline{\Pi}^{-1}_{\mathrm{RPA}}(k) = \frac{\Pi^{\mathrm{D}}_{\mathrm{RPA}}(k=0)}{\Pi^{\mathrm{D}}_{\mathrm{RPA}}(k)} = 1 + \frac{\tilde{a}_2}{\tilde{a}_0}k^2 + ... + \frac{\tilde{a}_{2l}}{\tilde{a}_0}k^{2l} + ... \tag{3.107}$$

In Fig. 3.4, the convergence of the expansion (3.107)—or equivalently of the expansion (3.38)— is illustrated for different θ using Eqs. (3.105) and (3.106) for the 2D case. In the limit of low temperatures, $\theta \simeq 0.1$, the zero order term, $\Pi^{-1}_{\mathrm{RPA}}(0) = 2\tilde{a}_0$, provides an accurate description at small wavenumbers (up to $k/2k_F \simeq 0.4$). However, at large wavenumbers ($k \gtrsim k_F$), the convergence of the expansion (3.107) is unsatisfactory. At higher temperatures ($\theta = 0.75$ and $\theta = 1.5$), retaining the term $(\tilde{a}_2/\tilde{a}_0)k^2$ in the expansion (3.107) provides an excellent approximation of $\overline{\Pi}^{-1}_{\mathrm{RPA}}(k)$ at $k < k_F$. Therefore, it is expected that the long wavelength approximation is very accurate at any degeneracy as long as $k < k_F$.

Now, $\gamma_2[n]$ determining the first order gradient correction in Eq. (3.93) and the Bohm potential (3.94) for the 2D electron gas is obtained using Eqs. (3.106) and (3.96):

$$\gamma_2\,[n] = \frac{1}{3}\frac{\theta^{-1}}{\exp(\theta^{-1})-1}. \tag{3.108}$$

From Eq. (3.108), we see that in the zero temperature limit ($\theta \ll 1$), the leading term of the gradient correction for the 2D case tends to zero as $\sim \exp\left(-\theta^{-1}\right)$. In the opposite limit of high temperatures ($\theta \gg 1$), we have $\gamma_2 = 1/3$.

Note that the result obtained in Ref. [van Zyl 2011] for the gradient correction to the kinetic energy can be found using the relation $f_0(n.T) =$

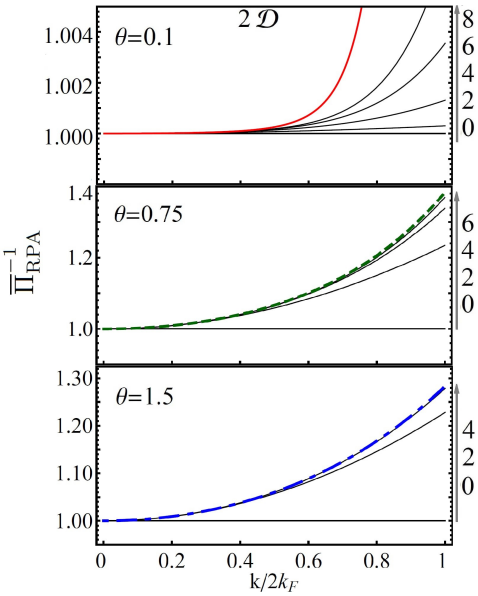

Figure 3.4: Convergence of the expansion (3.107) for different values of θ in the 2D case. The coefficients of the expansion are given by Eqs. (3.105) and (3.106). Solid thin (black) curves represent approximations with different maximum orders in the expansion that are retained, as indicated on the right hand side of the figure. At $\theta = 0.75$ and $\theta = 1.5$, the curves corresponding to the higher order corrections are visually indistinguishable from the exact curves at this scale. From reference [Moldabekov 2017a].

$\tau_0(n,T) - T\sigma(n,T)$ between the free energy density, the kinetic energy density, and the entropic contribution ($\sigma = -\left.\frac{\partial f_0}{\partial n}\right|_T$). In the limit $\theta \ll 1$ (ground state), substituting Eq. (3.39) into Eq. (3.105), one can recover the well-known result for the kinetic energy density in the LDA, $f_0[n] \to \tau[n] = \frac{\hbar^2\pi}{2m}n^2$.

3.7.2. Low frequency and long wavelength limit: 1D electron gas

Now we consider the static long wavelength limit for the 1D electron gas. In this case, Eq. (3.101) reduces to

$$\Pi^{\mathrm{D=1}}_{\mathrm{RPA}}(k,\omega=0) = \frac{k_F}{\pi E_F}\int_0^\infty \frac{\mathrm{d}y}{[\exp(y^2\theta^{-1}-\eta)+1](y^2-z^2)}. \tag{3.109}$$

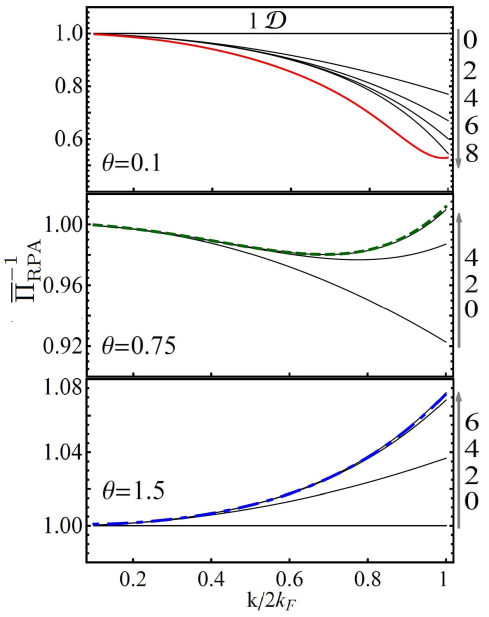

Figure 3.5: The same as in Fig 3.4, but with the coefficients defined by Eqs. (3.112) and (3.113). From reference [Moldabekov 2017a].

In the limit $z = k/2k_F \ll 1$, the expansion $\frac{1}{y^2-z^2} \simeq \frac{1}{y^2} + \frac{z^2}{y^4} + ... + \frac{z^{2j}}{y^{2j+2}} + ..$, with $j = 1, 2, ...$, allows to write the following expansion in terms of Fermi integrals:

$$\Pi^{\mathrm{D=1}}_{\mathrm{RPA}}(k \ll 2k_F, \omega = 0) \simeq \frac{k_F}{\pi E_F}\left(\frac{1}{2\theta^{1/2}} I_{-3/2}(\eta) + \frac{1}{8k_F^2\theta^{3/2}} I_{-5/2}(\eta)k^2 + ...\right). \tag{3.110}$$

We find, using Eq. (3.110), that

$$\frac{1}{2\Pi^{\mathrm{D=1}}_{\mathrm{RPA}}(k)} = \frac{\pi E_F \theta^{1/2}}{k_F I_{-3/2}(\eta)(1 + \sum b_i z^{2i})}, \qquad b_i\left([n], \theta\right) = \frac{\theta^{-i} I_{-i-3/2}(\eta)}{I_{-3/2}(\eta)}. \tag{3.111}$$

From Eq. (3.111), for the first five non-vanishing coefficients of the ex-

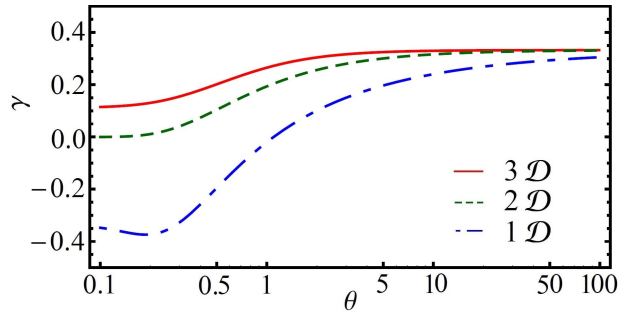

Figure 3.6: Dependence of the coefficient γ_D in Eqs. (3.93) and (3.94) on θ in the static case. In the high temperature limit γ_D tends to 1/3. In the zero temperature limit ($\theta \ll 1$): $\gamma_1 = -1/3$, $\gamma_2 = 0$, and $\gamma_3 = 1/9$. From reference [Moldabekov 2017a].

pansion (3.38), we find:

$$\tilde{a}_0(n,T) = \frac{\pi E_F \theta^{1/2}}{k_F I_{-3/2}(\eta)}, \quad \frac{\tilde{a}_2(n,T)}{\tilde{a}_0(n,T)} = -\frac{b_1}{4k_F^2}, \quad \frac{\tilde{a}_4(n,T)}{\tilde{a}_0(n,T)} = \frac{b_1^2 - b_2}{16k_F^4}, \tag{3.112}$$

$$\frac{\tilde{a}_6(n,T)}{\tilde{a}_0(n,T)} = \frac{-b_1^3 + 2b_1b_2 - b_3}{64k_F^6}, \quad \frac{\tilde{a}_8(n,T)}{\tilde{a}_0(n,T)} = \frac{b_1^4 - 3b_1^2b_2 + b_2^2 + 2b_1b_3 - b_4}{256k_F^8}. \tag{3.113}$$

The convergence of the expansion (3.107) for the 1D case, with the coefficients given by Eqs. (3.112) and (3.113), is illustrated in Fig. 3.5. In the low temperature limit ($\theta = 0.1$), the convergence is slower in comparison to the 2D case as well as the 3D case, which is discussed in Appendix E. In contrast, at high temperatures ($\theta = 0.75$ and $\theta = 1.5$) the quality of the convergence of the expansion (3.107) is much better, e.g., taking into account the first two terms of the expansion (3.107) provides a very accurate description of the exact static RPA result at $k < k_F$. The power expansion of the inverse polarization function is the Fourier transformation of the density gradient expansion of the second order functional derivative of free energy (see Eqs. (3.34) and (3.35)). Therefore, the foregoing discussion of the expansion convergence indicates that in the 1D case the LDA with gradient corrections can be used at partial degeneracy.

From Eqs. (3.112) and (3.96) we deduce $\gamma_1[n]$ needed for the computation of the gradient correction to the non-interacting free energy and the Bohm

potential:

$$\gamma_1[n] = \frac{1}{3} 2\theta^{-1/2} \frac{I''_{-1/2}(\eta)}{I'^2_{-1/2}(\eta)}. \tag{3.114}$$

In the limit $\theta \ll 1$, we find from Eq. (3.114) that $\gamma_1 = -1/3$, in agreement with the results of Refs. [Salasnich 2007, Holas 1991]. At high temperatures ($\theta \gg 1$), Eq. (3.114) yields $\gamma_1 = 1/3$.

The results for γ_D, obtained for the electron gas in 1, 2, and 3 dimensions, are presented in the Fig. 3.6. At finite temperature, γ_D depends only on the degeneracy parameter. From this figure we see that the coefficient γ_D in the high temperature limit approaches 1/3 for all considered cases, D=1, 2, 3. Note that γ_1 changes its sign at $\theta \simeq 1.1$. Another interesting feature of the pre-factor γ_1 is that it has an absolute minimum $\gamma_1(\theta_{\min}) \simeq -0.374$ at $\theta_{\min} \simeq 0.19$, while both γ_2 and γ_3 have their minima at $\theta = 0$.

The negative sign of γ_1 means that the uniform state is not stable bellow a certain temperature, i.e., any small perturbation of the density causes the system to decrease its free energy. This behavior is the well-known Peierls instability [Pouget 2016, Jérome 1982], which leads to such phenomena as charge density waves and periodic lattice distortions. From Fig. 3.6 one can see that thermal electronic excitations (at degeneracy parameters $\theta \gtrsim 1.1$) can stabilize the uniform state due to a positive per-factor γ_1, in accordance with more elaborate studies [Pouget 2016].

The results given by Eqs. (3.108) and (3.114) are applicable at low frequencies ($\omega < kv_F$), but not in the high frequency limit ($\omega \gg \hbar^2 k^2/2m$). Therefore, we now turn to the high frequency regime.

3.7.3. High frequency limit in the 2D and 1D cases

In the case of high frequencies ($\omega \gg \hbar^2 k^2/2m$), by analyzing the aforementioned polarization functions at $k \ll 2k_F$ it is found that in the 2D case $\gamma_2 = 0$, and in the 1D case $\gamma_1 = 1$. Additionally, it is revealed that $\tilde{a}_0 = -\frac{3\pi\hbar^2}{2m}\theta^2 I_1(\eta)$ for the 2D case, and in the 1D case $\tilde{a}_0 = -\frac{\pi^2\hbar^2}{8m}n$.

In Refs. [Akbari-Moghanjoughi 2014, Zhang 2017], plasmons in 2D systems in the limit of full electronic degeneracy ($\theta \ll 1$) were investigated employing the QHD approach with the ad hoc non-zero Bohm potential with the pre-factor $\gamma = 1$. This is one more example of the inconsistencies in previously used QHD models. On the other hand, it is clear that the result $\gamma_2 = 0$ (for the high frequency regime and in the static ground state)

does not imply that there is no quantum non-locality in 2D systems. For example, going well beyond the LDA for the 2D system, in Ref. [van Zyl 2014] the non-vanishing density gradient correction introduced in the static case by applying the so-called average-density approximation. Furthermore, in Ref. [Trappe 2016b]—also for the static case—a non-zero gradient correction was obtained in terms of an effective potential for the DFT (formulated as a joint functional of both the single-particle density and the effective potential energy [Englert 1992]). The relation (3.23) presented in this work can be used for the construction of the fully non-local free energy functional and the Bohm potential for the consideration of the electronic dynamics in 2D and 1D systems (similarly to the 3D case discussed in subchapter 3.5).

The results presented in this subchapter improve, to some degree, the understanding of the non-interacting electronic free energy functional of inhomogeneous quantum systems of reduced dimensionality. The density gradient correction to the non-interacting free energy and the quantum Bohm potential *at any degeneracy* for QHD in the 2D and 1D cases are the new results.

3.8 QHD equations with an external magnetic field

Up to this point the magnetic field free case has been considered. Recent progress towards inertial confinement fusion (ICF) [Higginson 2017, Perkins 2013] shows that an external magnetic field (with $B > 10^5$G (10T)) can significantly facilitate the solution of the ICF related problems (like the improvement of the alpha particles energy deposition into a DT fuel). Therefore, in this subchapter we add a magnetic field to the QHD equations and discuss the range of applicability of these equations with respect to the strength of the applied external magnetic field.

The QHD equations can be found from the following Hamiltonian

$$\begin{aligned} H[n(\mathbf{r},\mathbf{B}),w(\mathbf{r},\mathbf{B})] &= E[n(\mathbf{r},\mathbf{B})] + \frac{e^2}{2}\int \frac{n(\mathbf{r},\mathbf{B})n(\mathbf{r}',\mathbf{B})}{|\mathbf{r}-\mathbf{r}'|}\mathrm{d}\mathbf{r}\mathrm{d}\mathbf{r}' \\ &- \int eV_{\mathrm{ext}}n(\mathbf{r},\mathbf{B})\mathrm{d}\mathbf{r} + \int \frac{m_e n(\mathbf{r},\mathbf{B})}{2}\left|\nabla w\left(\mathbf{r},\mathbf{B}\right) - \frac{e}{cm}\mathbf{A}\right|^2 \mathrm{d}\mathbf{r}, \end{aligned} \tag{3.115}$$

where $\mathbf{B} = \nabla \times \mathbf{A}$, the velocity field is defined using the scalar potential w and a vector potential of an external magnetic field $\mathbf{A}$ by the relation $\mathbf{v} = -\nabla w + \frac{e}{cm}\mathbf{A}$. In Eq. (3.115), m is the electron mass, c is the speed

of light, $E[n(\mathbf{r},\mathbf{B})]$ is the sum of the kinetic and the exchange-correlation energy functionals, $\mathbf{B}$ denotes an external constant magnetic field, and V_{ext} refers to the external electric potential. For simplicity, in Eq. (3.115), the time variables are not explicitly written. Additionally, in Eq. (3.115), terms corresponding to spin-magnetic field and spin-spin interactions are not included.

Starting from the Hamiltonian (3.115), in the same way as the QHD equations were derived in subchapter 3.1, we arrive at the QHD equations that take into account an external magnetic field:

$$\frac{\partial}{\partial t} n\left(\mathbf{r},t\right) + \nabla \cdot \left[n\left(\mathbf{r},t\right)\mathbf{v}\left(\mathbf{r},t\right)\right] = 0, \tag{3.116}$$

$$m_e \frac{\partial}{\partial t}\mathbf{v}\left(\mathbf{r},t\right) + m_e(\mathbf{v}\left(\mathbf{r},t\right)\cdot\nabla)\mathbf{v}\left(\mathbf{r},t\right) = -\nabla\mu\left(\mathbf{r},t\right) - \frac{e}{c}\mathbf{v}\times\mathbf{B}, \tag{3.117}$$

and

$$\mu[n(\mathbf{r},t)] = \frac{\delta F_{\text{id}}[n(\mathbf{r},t)]}{\delta n(\mathbf{r},t)} + \frac{\delta F_{\text{xc}}[n(\mathbf{r},t)]}{\delta n(\mathbf{r},t)} + e^2\int\frac{n(\mathbf{r}',t)}{|\mathbf{r}-\mathbf{r}'|}\mathrm{d}\mathbf{r}' - eV_{\text{ext}}, \tag{3.118}$$

where the relation $(\mathbf{v}\cdot\nabla)\mathbf{v} + \frac{e}{cm}[\mathbf{v}\times(\nabla\times\mathbf{A})] = \frac{1}{2}\nabla[\left(\nabla w - \frac{e}{cm}\mathbf{A}\right)^2]$ was used [Eguiluz 1976].

With a choice of an ansatz for F (e.g., see Eq. (3.78) or Eq. (3.85)), the following closure relations are needed:

$$\mathfrak{F}\left[\left.\frac{\delta^2 F_{\text{id}}}{\delta n(\mathbf{r},t)\delta n(\mathbf{r}',t)}\right|_{\text{n=n}_0}\right] = -\left[\frac{1}{\Pi_{\text{RPA}}(k,\omega;\ \mathbf{B})} - \frac{1}{\Pi^0(\omega;\ \mathbf{B})}\right], \tag{3.119}$$

where $\Pi_{\text{RPA}}(k\to 0,\omega;\ \mathbf{B}) = \Pi^0(\omega;\ \mathbf{B})$, and

$$\mathfrak{F}\left[\left.\frac{\delta^2 F_{\text{xc}}}{\delta n(\mathbf{r})\delta n(\mathbf{r}')}\right|_{\text{n=n}_0}\right] = -\frac{4\pi e^2}{k^2}G(k,\omega;\mathbf{B}). \tag{3.120}$$

The quantum polarization function in the RPA with an external magnetic field—with $\mathbf{B}$ in the z direction—is given by [Nersisyan 2007]

$$\Pi_{\text{RPA}}(\mathbf{k},\omega;\mathbf{B}) = -\frac{1}{4\pi^2 e^2 k_z^2 \lambda_B^2 a_B}\sum_{\sigma=\pm 1/2}\sum_{n;n'=0}^{\infty} F_{nn'}^2(\xi)$$
$$\times\left\{G_{n\sigma}(Q_-) + G_{n\sigma}(Q_+) + \frac{ik_z}{\pi|k_z|}\left[f(E_{n\sigma}(Q_-)) - f(E_{n\sigma}(Q_+)\right]\right\}, \tag{3.121}$$

where $\lambda_B^2 = \hbar/(m_e\omega_c)$, $\xi = (k_x^2+k_y^2)\lambda_B^2/2$, $Q_\pm = k_z/2+\frac{m}{\hbar k_z}\left[\omega_c(n'-n)\mp\omega\right]$, f is the Fermi-Dirac distribution function, $E_{n\sigma} = \hbar^2k_z^2/2m_e + \hbar\omega_c(n+\sigma+1/2)$, the function $F_{nn'}(\xi)$ is given in terms of the generalized Laguerre polynomials $L_n^{n'}(\xi)$ by

$$F_{nn'}(\xi) = \left(\frac{n!}{n'!}\right)^{1/2} \xi^{(n'-n)/2} e^{-\xi/2} L_n^{n'-n}(\xi), \tag{3.122}$$

and the function $G_{n\sigma}(Q)$ is defined by the principal value of the following integral:

$$G_{n\sigma}(Q) = \int_{-\infty}^{+\infty} dq \frac{f(E_{n\sigma}(q))}{Q-q}. \tag{3.123}$$

$\Pi_{\rm RPA}(\mathbf{k}\to 0,\omega;\mathbf{B}) = \Pi^0(\omega;\ \mathbf{B})$ obtained from Eq. (3.121) reads

$$\Pi^0(\omega;\ \mathbf{B}) = \frac{k^2}{4\pi e^2}\left[\frac{\omega_p^2}{\omega^2}\cos^2(b) + \frac{\omega_p^2}{\omega^2-\omega_c^2}\sin^2(b)\right], \tag{3.124}$$

where b is the angle between the wave vector $\mathbf{k}$ and the magnetic field.

The RPA polarization function (3.121) was analyzed considering different limiting cases in Refs. [Zyryanov 1961, Zyryanov 1962, Mermin 1964, Horing 1965, Greene 1969, Das 1976, Nersisyan 2007]. Eq. (3.121) was used to study the induced charge density by a test charge in Ref. [Perrot 1995], where it was shown that at $B/B_0 \sim 1$ the magnetic field induced anisotropy in the polarized electron cloud around a test charge becomes important (with $B_0 = 2.3505\times 10^9$G being the magnetic field that corresponds to an electron cyclotron energy equal to one Hartree (or equivalently two times the binding energy of an electron in a hydrogen atom)). An extended study of the electron-ion collision and stopping power on the basis of Eq. (3.121) is given in Ref. [Nersisyan 2007].

The Hamiltonian (3.115) is valid if the magnetic field is non-quantizing; here a *quantizing magnetic field* is referred to the situation when most of the electrons are on the few lowest Landau levels [Potekhin 2013]. In order to estimate corresponding magnetic field strength, we need the dimensionless parameter $\zeta = \hbar\omega_c/\langle K\rangle$ defined as the ratio of the electron cyclotron energy to the characteristic quantum-kinetic energy of electrons, $\langle K\rangle \simeq \sqrt{(k_BT)^2+(E_F)^2}$; here $\omega_c = eB/m_ec$ is the electron cyclotron frequency. In terms of the degeneracy and density parameters (θ and r_s,

respectively), ζ is expressed as

$$\zeta = \frac{\hbar\omega_c}{\langle K\rangle} \simeq \frac{r_s^2}{18.4\sqrt{\theta^2+1}} \times \frac{B}{B_0}. \tag{3.125}$$

The inverse value of ζ gives the approximate number of the involved Landau levels.

In the limits of quantum and classical plasmas, from Eq. (3.125) we find the following conditions for the regime with a non-quantizing magnetic field:

$$\left.\begin{array}{l}\zeta \ll 1\\ \theta < 1\end{array}\right] \rightarrow \frac{B}{B_0} \ll \frac{18.4}{r_s^2}, \qquad \left.\begin{array}{l}\zeta \ll 1\\ \theta \gg 1\end{array}\right] \rightarrow \frac{B}{B_0} \ll 18.4 \times \frac{\theta}{r_s^2}. \tag{3.126}$$

At the considered plasma densities, $r_s \lesssim 2$, the non-quantizing regime is realized when $B/B_0 \ll 4$. Note that the electron cyclotron energy, $\hbar\omega_c$, is much less than the electron rest energy, $m_e c^2$, if $B \ll 4.4\times 10^{13}$ G $\sim 10^5\ B_0$. Thus, at $B/B_0 \ll 4$, relativistic effects related to electronic cyclotron oscillations can be neglect.

Another important parameter is the ratio of the cyclotron frequency to the electronic plasma frequency, $\beta = \omega_c/\omega_p$. This parameter determines whether the plasma electrons are magnetized ($\beta > 1$) or not ($\beta < 1$). For classical plasmas [Ott 2018], the ratio ω_c/ω_p describes the importance of the magnetic field impact. The parameters ζ and β can be expressed via each other as $\zeta/\beta \simeq \sqrt{r_s/(1+\theta^2)}$. At $\beta > 1$, the electrons become magnetized. In this case the conditions for a non-quantizing magnetic field in quantum and classical plasmas read

$$\left.\begin{array}{l}\zeta \ll 1\\ \theta < 1\\ \omega_c/\omega_p > 1\end{array}\right] \rightarrow r_s \ll 1, \qquad \left.\begin{array}{l}\zeta \ll 1\\ \theta \gg 1\\ \omega_c/\omega_p > 1\end{array}\right] \rightarrow r_s \ll \theta^2. \tag{3.127}$$

In other words, *in order to have magnetized quantum electrons in non-quantizing magnetic field, the density must be such that* $r_s \ll 1$. Note that at $r_s < 0.1$, relativistic effects must be taken into account. If $\omega_c/\omega_p < 1$, the inequalities given by Eq. (3.126) remain valid.

In a two-component plasma, one more parameter, the ratio of the ion cyclotron frequency to the ionic plasma frequency, $\omega_{ci}/\omega_{pi} = (\omega_c/\omega_p) \times \sqrt{m_e/m_i}$, is of interest. If the ions are magnetized (meaning that the elec-

trons are, also, strongly magnetized), we have the following conditions:

$$\left.\begin{array}{l}\zeta \ll 1\\ \theta < 1\\ \omega_{ci}/\omega_{pi} > 1\end{array}\right] \rightarrow r_s \ll \frac{1}{(m_i/m_e)}, \quad \left(\begin{array}{c}\text{ultrarelativistic}\\ \text{quantum plasmas}\end{array}\right) \tag{3.128}$$

and

$$\left.\begin{array}{l}\zeta \ll 1\\ \theta \gg 1\\ \omega_{ci}/\omega_{pi} > 1\end{array}\right] \rightarrow r_s \ll \frac{1}{(m_i/m_e)} \times \theta^2. \tag{3.129}$$

Therefore, *the plasma with quantum electrons and magnetized ions is a relativistic quantum plasma*. This case is out of the scope of our considerations.

To sum up, the momentum equation (3.117) can be used for the description of quantum electrons if the inequalities given by Eqs. (3.126) and (3.127) for $\theta < 1$ are hold. Corresponding parameters cover the range of densities, temperatures, and applied external magnetic field strengths in experimental ICF studies [Higginson 2017, Perkins 2013].

3.9 Summary

In the presented chapter the QHD equations at finite temperature and the closure relations that determine the force field were derived. The fully non-local potential for the QHD description of the quantum non-ideal electrons was deduced making link with linear response theory. This represents the first unifying picture of various QHD models used earlier for the study of different phenomena in quantum plasmas. Clearly understanding the limitations of the previous formulations of QHD, the present work goes beyond all earlier models by invoking the quantum RPA and local field corrections approach. The latter is essential for the adequate description of quantum plasmas with the density parameter $r_s > 1$. In this case electronic correlations cannot be discarded. The quantum non-locality is expected to be important at $\theta < 1$. The importance of the inclusion of the electronic correlations and degeneracy for the description of the quantum plasma with strongly coupled ions is demonstrated in the next chapter.

Chapter 4

Structural properties of strongly coupled ions

Contents

The multi-scale approach facilitates the description of a two-component plasma with quantum electrons and classical ions. The quantum electrons can be described using continuous variables governed by the QHD equations and the ions can be considered as immersed into an electronic medium. In this case the choice of the approximation in the treatment of the electronic component must be done taking into account the resulting consequences for the ionic subsystem. Therefore, in this chapter the structural properties of strongly coupled ions in dense plasmas with non-ideal quantum electrons are investigated. The radial pair distribution function (RPDF) and static structure factor (SSF) are investigated in detail. Different theoretical models describing the screened ion-ion interaction—within linear response theory—are considered including the Singwi-Tosi-Land-Sjölander (STLS) approximation, local field corrections obtained from ground-state quantum Monte Carlo data, the RPA, and analytical models obtained from the long wavelength approximation to the RPA. Taking into account the considerable number of models (approximations) needed to be analyzed and the relatively wide range of plasma parameters under consideration, the hypernetted chain approximation (HNC) is employed as a fast alternative to the

much more computationally involved molecular dynamics simulation (MD). Before carrying out the bulk of the calculations, the applicability of the HNC approach in the considered range of plasma parameters was verified using a so-called effective coupling parameter [Ott 2014]. The latter was introduced in previous works on the basis of MD data for one component systems of the charged particles interacting via the Yuakwa potential to provide a description by a single dimensionless parameter under different coupling strengths and characteristic screening lengths. It is revealed that the HNC correctly captures the relative differences in RPDFs and SSFs obtained for different ion-ion pair interaction potentials. Therefore, the HNC was used to investigate the effect of electronic correlations and degeneracy on the structural properties of strongly coupled ions, and subsequently the main conclusions were verified by MD simulations. The results presented in this chapter were published in Refs. [Moldabekov 2018b, Moldabekov 2017b].

4.1 Decoupling of ionic dynamics from the electrons

First, we briefly discuss the assumptions that allow to decouple the dynamics of the ions from that of the electrons. To proceed further, we need to define the electron-ion coupling parameter $\Gamma_{\text{ei}} = Ze^2/ak_BT_e$ (additionally to the dimensionless parameters introduced in chapter 2). This parameter is used to gauge the validity of the linear response based approach, which is used in this chapter. For $\Gamma_{\text{ei}} < 1$, the ions can be represented as a system of charged particles with a screened ion-ion pair interaction potential, i.e., the effect of electrons is given by the modification of the ion potential. In this weak electron-ion coupling regime, a modified ion potential can be described on the basis of linear response theory. This approach is inadequate if the coupling between the electronic and ionic subsystems is strong, $\Gamma_{\text{ei}} > 1$. In this case, the linear response based treatment fails in the vicinity of an ion. Fortunately, in dense plasmas it usually holds $\Gamma_{\text{ei}} \lesssim 1$ [Clérouin 2015a, More 1986], as explained in chapter 2, which was confirmed by simulations using orbital-free density functional theory [Clérouin 2015a]. Additionally, it is clear that a more realistic parameter describing the electron-ion coupling should be of the form $\tilde{\Gamma}_{\text{ei}} = \Gamma_{\text{ei}} \times \exp(-\kappa)$, which takes into account the screening. At the considered temperatures and densities, the characteristic screening length in units of a is in the range $\kappa \sim 1 - 2$. Thereby, the real

electron-ion coupling is reduced due to strong screening. For simplicity, we always take $Z = 1$ without loss of generality.

The electronic and ionic subsystems are coupled via the interaction energy,

$$U_{\rm ei} = \frac{1}{2\Omega} \sum_{\mathbf{k}\neq 0} \tilde{\varphi}_{\rm ei}(\mathbf{k}) \tilde{n}_i(\mathbf{k}) \tilde{n}_e(-\mathbf{k}), \tag{4.1}$$

where $\tilde{n}$ is the deviation from the mean density, and the Fourier transform of the bare electron-ion interaction potential is denoted as $\tilde{\varphi}_{\rm ei}(\mathbf{k})$. The electron-ion interaction can be considered as a perturbation when the electronic quantum kinetic energy exceeds the potential energy $U_{\rm ei}$. For example, if $\Gamma_{\rm ei} \ll 1$—the lowest order approximation—one can set $U_{\rm ei} = U_{\rm ei}^{(1)} = 0$ (e.g., for an extremely dense plasma, $r_s \ll 1$, or very hot electrons). In this limit, the ions can be described as a system of particles interacting through the bare Coulomb potential. This corresponds to the picture where the electrons do not respond to the field of the ions and their role is a neutralizing uniform background.

In the second order approximation, using the the static electron-density response function $\chi_e(\mathbf{k})$, we can write the electronic density induced by the weak perturbing field of an ion as $\tilde{n}_e(-\mathbf{k}) = \chi_e(\mathbf{k}) \tilde{\varphi}^*_{\rm ei}(\mathbf{k}) \tilde{n}_i(-\mathbf{k})$. By substituting this result into Eq. (4.1), we get

$$U_{\rm ei}^{(2)} = \frac{1}{2\Omega} \sum_{\mathbf{k}\neq 0} |\tilde{\varphi}_{\rm ei}(\mathbf{k})|^2 \, \chi_e(\mathbf{k}) \tilde{n}_i(\mathbf{k}) \tilde{n}_i(-\mathbf{k}). \tag{4.2}$$

Note that in Eq. (4.2), $U_{\rm ei}^{(2)}$ is expressed using solely the variables of the ions. Further, by introducing an effective ion-ion interaction potential of the form [Hansen 2013]

$$\Phi(\mathbf{r}_{j'}, \mathbf{r}_j) = \frac{Z^2 e^2}{|\mathbf{r}_{j'} - \mathbf{r}_j|} + \int \frac{{\rm d}^3 k}{(2\pi)^3} \, |\tilde{\varphi}_{\rm ei}(\mathbf{k})|^2 \, \chi_e(\mathbf{k}) \; e^{i\mathbf{k}\cdot(\mathbf{r}_{j'} - \mathbf{r}_j)} \quad , \tag{4.3}$$

we are able to write total Hamiltonian of the system as the sum of an ionic Hamiltonian with the potential (4.3) and that of a uniform electron gas without any perturbation by the field of the ions,

$$H = H_i \left(\mathbf{R}, \mathbf{P}\right) + H_e[n_e], \tag{4.4}$$

where the complete set of ionic coordinates and momenta is denoted as $\mathbf{R} = \mathbf{r}_1, ..., \mathbf{r}_{N_i}$ and $\mathbf{P} = \mathbf{p}_1, ..., \mathbf{p}_{N_i}$, respectively.

The ionic Hamiltonian is given by

$$H_i\left(\mathbf{R},\mathbf{P}\right)=K_i\left(\mathbf{P}\right)+\sum_{j=1}^{N_i}\sum_{j'>j}^{N_i}\Phi(\mathbf{r}_{j'},\mathbf{r}_j), \tag{4.5}$$

whit K_i being the kinetic energy.

Next, substituting the Coulomb potential as the bare electron-ion interaction potential, $\tilde{\varphi}_{\mathrm{ei}}(\mathbf{k})=4\pi Ze^2/k^2$, into Eq. (4.3) we arrive at the widely used expression for the screened potential,

$$\Phi(\mathbf{r})=\int\frac{\mathrm{d}^3k}{2\pi^2}\frac{Q^2}{k^2\epsilon(\mathbf{k},\omega=0)}\,e^{i\mathbf{k}\cdot\mathbf{r}}\quad, \tag{4.6}$$

expressed in terms of the inverse dielectric response function of the electrons

$$\epsilon^{-1}(\mathbf{k},\omega)=1+\frac{4\pi e^2}{k^2}\chi_e(\mathbf{k},\omega). \tag{4.7}$$

It is important to note that in the general case of an arbitrary electron-ion pseudopotential (such as the so-called empty core potential), Eq. (4.6) is not appropriate and the more general form Eq. (4.3) must be used.

Further, all electronic correlation effects are conviently incorporated in the so-called local field correction G that enters the density response function via

$$\chi_e^{-1}(\mathbf{k},\omega)=\chi_0^{-1}(\mathbf{k},\omega)+\frac{4\pi e^2}{k^2}\left[G(\mathbf{k},\omega)-1\right], \tag{4.8}$$

where χ_0 denotes the finite temperature ideal density response function of the electron gas.

4.2 Electronic density response function

Let us recall the relation between the polarization function, Π, used in the previous chapter 3, and the density response function, χ_e. The polarization function is defined as the electronic density response to a screened test charge field (cf., Eq. (3.9)), while the density response function is introduced as the response to a bare test charge potential. Therefore, these two functions are connected via the following equation:

$$\frac{1}{\Pi(\mathbf{k},\omega)}=\frac{1}{\chi_e(\mathbf{k},\omega)}+\frac{4\pi e^2}{k^2}. \tag{4.9}$$

For example, using relation (4.9), Eq. (4.7) can be equivalently written as [Bonitz 2016]

$$\epsilon(\mathbf{k},\omega) = 1 - \frac{4\pi e^2}{k^2}\Pi(\mathbf{k},\omega). \tag{4.10}$$

In the case of non-interacting quantum electrons, the ideal response function, χ_0, in Eq. (4.8), is equal to Π_{RPA} [Giuliani 2008] (with the real part given by Eq. (3.36)). Therefore, Eq. (4.8)—describing non-ideal electrons—is equivalent to Eq. (3.28).

In the following, we introduce five different approximations for the description of the electronic density response function, which are subsequently employed to study the impact of the electronic quantum degeneracy and correlation effects on the structural properties of strongly coupled ions in subchapter 4.4.

4.2.1. STLS approximation

Among the theoretical models describing quantum electrons, the STLS approximation gained wide usage. Indeed, STLS-based methods were used to investigate variety of dense plasma properties; e.g. transport and relaxation [Bennadji 2009, Reinholz 1995, Benedict 2017], stopping power [Wang 1997, Zwicknagel 1999, Montanari 2017, Gauthier 2013, Barriga-Carrasco 2009], thermodynamics [Bennadji 2011, Tanaka 2017, Schweng 1991], and the dynamical as well as the static structure factor [Fortmann 2010, Gregori 2007, Plagemann 2012, Saumon 2012].

The STLS scheme is based on the following self-consistent closed set of nonlinear equations [Singwi 1968, Tanaka 1986]:

$$G^{\text{STLS}}\Big(\left[S^{\text{STLS}}\right], \mathbf{k}, \omega = 0\Big) = -\frac{1}{n}\int \frac{\mathrm{d}\mathbf{k}'}{(2\pi)^3}\frac{\mathbf{k}\cdot\mathbf{k}'}{k'^2}\left[S^{\text{STLS}}(\mathbf{k}-\mathbf{k}')-1\right], \tag{4.11}$$

and

$$S^{\text{STLS}}\Big(\left[G^{\text{STLS}}\right], \mathbf{k}\Big) = -\frac{1}{\beta n}\sum_{l=-\infty}^{\infty}\frac{\chi_0(\mathbf{k},z_l)}{1+\frac{4\pi e^2}{k^2}\left[G^{\text{STLS}}(\mathbf{k},z_l)-1\right]\chi_0(\mathbf{k},z_l)}, \tag{4.12}$$

where the latter is the well-known fluctuation-dissipation theorem involving the static structure factor S^{STLS}. In Eq. (4.12) the summation is over the Matsubara frequencies, $z_l = 2\pi i l/\beta\hbar$.

The STLS scheme has its roots in classical many-particle physics, where a classical two particle distribution function is approximated as

$$f(\mathbf{r},\mathbf{p};\mathbf{r}',\mathbf{p}';t) = f(\mathbf{r},\mathbf{p};t)f(\mathbf{r}',\mathbf{p}';t)g(|\mathbf{r}-\mathbf{r}'|), \tag{4.13}$$

with $g(|\mathbf{r}-\mathbf{r}'|)$ being the equilibrium value of the electron-electron RPDF. Substituting ansatz (4.13) into the equation of motion of the classical distribution function $f(\mathbf{r}',\mathbf{p}';t)$, results in the following force (in addition to the Hartree mean field and the external field forces):

$$\nabla V_{\mathrm{xc}}^{\mathrm{STLS}}(\mathbf{r},t) = \int \left[g(|\mathbf{r}-\mathbf{r}'|)-1\right]\nabla\frac{e^2}{|\mathbf{r}-\mathbf{r}'|}n_1(\mathbf{r}',t)\mathrm{d}\mathbf{r}', \tag{4.14}$$

where $n_1(\mathbf{r}',t)$ is the time-dependent density perturbation. The Fourier transform of Eq. (4.14), in combination with the relation $V_{\mathrm{xc}}^{\mathrm{STLS}}(k,\omega) = -\frac{4\pi e^2}{k^2}G(k)n_1(k,\omega)$, gives Eq. (4.11) [Giuliani 2008].

The screened ion potential (4.3), which is computed using $\chi_e(k,\omega=0)$ on the basis of G^{STLS} is what will be called the *STLS potential* throughout the remaining of this work*.

4.2.2. Quantum Monte-Carlo data based result

An exact benchmark for $G(k.0)$ with all exchange-correlation effects included is highly desirable. Despite recent progress in *ab initio* quantum Monte-Carlo simulations (QMC) at finite temperature [Dornheim 2017a, Groth 2017a], the QMC data on the static density response function of electrons at finite temperature [Dornheim 2017a, Groth 2017a] have yet insufficient k-resolution for the computation of the screened ion potential. Therefore, in order to be able to gauge other approximations, we use the following parametrization of the ground state quantum Monte Carlo data [Moroni 1995] from Ref. [Corradini 1998]:

$$G(k) = Ck^2 + \frac{Bk^2}{\tilde{g}+k^2} + \tilde{\alpha}k^4\exp\left(-\tilde{\beta}k^2\right), \tag{4.15}$$

where C, B, $\tilde{g}$, $\tilde{\alpha}$, $\tilde{\beta}$ are fit parameters depending on the electronic density; for more details, the interested reader is referred to Refs. [Moroni 1995, Corradini 1998].

* An improved version of the STLS for classical plasmas was recently derived in Refs. [Kählert 2014, Kählert 2015].

The quantum Monte Carlo data presented in Ref. [Moroni 1995], correspond to the ground state with $r_s = 2,\ 5,\ 10$ and 100. In the context of the parameters that are of interest to the present work, the ground state $G(k)$ data of Ref. [Corradini 1998] at $r_s = 2$ is used in Eqs. (4.8)–(4.6) for the quasiground state with $\theta = 0.01$. In the following, the potential computed in this way will be referred to as the *QMC potential*.

At this point, it is important to note that often parametrizations of the local field correction similar to the one from Ref. [Ichimaru 1982] (based on STLS) were used (e.g., Ref. [Reinholz 1995, Sjostrom 2014b]). This class of parametrizations includes the restriction $G(k \to \infty) < 1$. This restriction originated from the works of Refs. [Shaw 1970] and [Niklasson 1974], and became widely used after the seminal work by Ichimaru [Ichimaru 1982]. However, it turned out that the condition $G(k \to \infty) < 1$ is wrong. The correct asymptotic form of the local field correction is $G(k \to \infty) \sim k^2$, as it was proven in Ref. [Holas 1991] and subsequently confirmed by the ground state QMC simulations [Moroni 1995]. A recent overview of various theoretical approaches for the uniform electron gas and a comparison to QMC data at finite temperature can be found in Ref. [Dornheim 2018].

4.2.3. Exact RPA result

It is important to compare the results obtained invoking a local field correction to those computed using the ideal density response (RPA polarization) function. For this purpose, the static polarization function given by Eq. (3.36), with $\omega = 0$, is used in Eqs. (4.10) and (4.6), where $G = 0$. In the following, the potential calculated in the RPA will be referred to as the *RPA potential*. The properties of the RPA potential are well-known; an exponential decay at intermediate distances (characterized by a screening length) and an oscillatory tail at large distances are among its main features. The latter is known as the Friedel oscillations with the asymptotics $\sim \cos(2k_F r)/r^3$ [Friedel 1952] in the fully degenerate electron limit. Further, thermal excitations lead to a faster decay as $\sim \cos(2k_F r)/r^2 \exp(-wr)$, where $w = \sqrt{2m}\pi k_B T_e/\sqrt{\mu}\hbar$ [Grassme 1993].

Essentially, the RPA potential does not include electronic non-ideality (correlations), but does fully take into account the quantum non-locality embedded into the ideal response function of the non-interacting electrons.

4.2.4. First order long wavelength approximation to RPA

Yukawa-type potentials are the most often used screened pair potentials in plasma physics. These include: the Debye-Hückel potential for a classical plasma, and the Thomas-Fermi potential which is due to the screening by fully degenerate electrons. A general form of the Yukawa potential interpolating between the classical and quantum limits can be found simply by considering the first order result of the long wavelength expansion of the static inverse RPA polarization function of the electrons

$$\Pi^{-1}_{\mathrm{RPA}}(k \to 0, \omega = 0) \approx 2\tilde{a}_0(n, T_e), \tag{4.16}$$

with $\tilde{a}_0(n, T_e) = 2\pi e^2/k_Y^2$ (cf. Eq. (3.38)). Substituting this expansion into Eq. (4.10) and subsequently using the resulting static dielectric function in Eq. (4.6), we arrive at the well-known formula,

$$\Phi_Y(r; n, T) = \frac{Q_i^2}{r}\, e^{-k_s r}, \tag{4.17}$$

where the finite-temperature inverse screening length, k_s, is equal to $k_Y = \left[\frac{1}{2}k_{TF}^2\theta^{1/2}I_{-1/2}(\mu/k_BT_e)\right]^{1/2}$. Note that even at $\theta \sim 1$, the potential (4.17) is often referred to as the Thomas-Fermi potential (TF).

4.2.5. Second order long wavelength approximation to RPA

Another analytical model, which is often considered as a significant improvement for the description of the screened ion potential [Stanton 2015] in comparison to Eq. (4.17), is based on the second order result of the long wavelength expansion of the static inverse RPA response function,

$$\Pi^{-1}_{\mathrm{RPA}}(k \ll 2k_F, \omega = 0) \approx 2\tilde{a}_0(n, T_e) + 2\tilde{a}_2(n, T_e) \cdot k^2, \tag{4.18}$$

with $\tilde{a}_2(n, T_e) = -a_2(n, T_e)$ (see Eq. (3.47)). Using expansion (4.18), one recovers the analytical model by Stanton and Murillo (SM) [Stanton 2015]

$$\phi(r; n, T) = \frac{Q_i^2}{2r}\left[(1+b)\, e^{-k_+ r} + (1-b)\, e^{-k_- r}\right], \tag{4.19}$$

where $b = 1/\sqrt{1-\alpha^{SM}}$ and $k_\pm = k_{TF}(1 \mp \sqrt{1-\alpha^{SM}})^{1/2}/\sqrt{\alpha^{SM}/2}$, $\alpha^{SM} = 3\sqrt{8\beta}\lambda I'_{-1/2}(\beta\mu)/\pi$, $\lambda = 1/9$, and $I'_p(\beta\mu)$ is the derivative of the Fermi integral with respect to $\beta\mu$; the inverse Thomas-Fermi screening length at

finite temperature is given by $k_{TF} = (4I_{-1/2}(\eta_0)/\pi\sqrt{2\beta})^{1/2}$. In a certain range of densities and temperatures (at $\alpha^{SM} > 1$), the SM potential has an oscillatory pattern. Thereby, in this case, Eq. (4.19) was expressed in a different form to make conspicuous the appearance of the oscillatory pattern [Stanton 2015]. This can be achived using Euler's formula relating trigonometric functions and the complex exponential function. Nevertheless, both forms of the potential give essentially the same value of the potential, meaning that potential (4.19) can be used regardless of the value of α^{SM}.

In Ref. [Stanton 2015], the potential (4.19) was derived starting from the Thomas-Fermi model with the first order gradient correction (Eq. (3.32) with a_2 given by Eq. (3.47)). In Ref. [Akbari-Moghanjoughi 2015], the potential (4.19) was independently derived by considering the ideal density response function of the fully degenerate electron gas.

It should be stressed that the Yukawa potential totally disregards the quantum non-locality related to finite values of the wavenumber, while the SM potential takes into account the quantum non-locality as a correction in the limit of small wavenumbers. Overall, the Yukawa and SM potentials are, in fact, lower order approximations with respect to the full (nonlocal) RPA description.

To sum up the discussion of the described different approximation, we have—to some extent—the following hierarchy of models:

(i) The QMC potential is the most accurate which, in linear response, exactly takes into account quantum-non locality and electronic correlations.

(ii) The STLS potential includes both quantum-non locality and electronic correlation effects, but the latter approximated on the basis of ansatz (4.13).

(iii) The RPA potential exactly takes into account the quantum non-locality on the level of non-interacting quantum electrons, but totally neglects electronic correlations.

(iv) The SM potential takes into account quantum non-locality as a correction and provides a description of the RPA potential at large distances; similarly, electronic correlations are not taken into account.

(v) The Yukawa potential totally discards both the quantum-non locality and electronic correlations; it represents a truly local density approximation without any gradient corrections.

With these five models we are now prepared for the in-depth investigation of the impact of the electronic quantum and non-ideality effects on the structural properties of strongly coupled ions in dense plasmas.

4.3 The hypernetted chain approximation

To investigate the structural properties of ions in a relatively wide range of plasma parameters on the basis of five different screened ion potentials, we solve the Ornstein-Zernike equation in the hypernetted chain approximation, instead of computationally significantly more costly MD simulations. But first, the applicability of the HNC at the considered plasma parameters is verified.

The Ornstein-Zernike relation [Hansen 2013] for a homogenous system is given by

$$h(r) = c(r) + n \int c(r')h(|\mathbf{r} - \mathbf{r}'|)\mathrm{d}\mathbf{r}' \,, \tag{4.20}$$

with the formally exact closure

$$g(r) = \exp\{[-\beta u(r) + h(r) - c(r) + B(r)]\}, \tag{4.21}$$

where $\beta = (k_B T)^{-1}$, $u(r)$ is the pair interaction potential, $g(r)$ denotes the radial pair distribution function (RPDF), $c(r)$ the direct correlation function, $h(r) = g(r) - 1$ the total correlation function, and $B(r)$ is the bridge function. The HNC corresponds to setting $B(r) = 0$.

The static structure factor is related to the Fourier transform of the direct correlation function, $\tilde{c}(k)$, by

$$S(k) \equiv 1 + n \int [g(r) - 1] \exp(i\mathbf{k} \cdot \mathbf{r})\mathrm{d}\mathbf{r} = \frac{1}{1 - n\tilde{c}(k)}. \tag{4.22}$$

Note that the SSF, $S(k)$, is directly measured using the X-ray Thomson scattering technique [Glenzer 2009] and, thereby, the computation of $S(k)$ is needed for the interpretation of experimental observations. Additionally, the accurate calculation of $S(k)$ is needed, e.g., for the investigation of the optical properties of dense plasmas on the basis of the dynamical collision

frequency approach [Veysman 2016] and for the calculation of the plasma resistivity on the basis of the Rousseau-Ziman formula [Bennadji 2009].

First, we shall give a brief discussion of the key assumption underlying the HNC from the point of view of the classical density functional theory. For this, the starting point can be the *intrinsic* free energy of classical ions,

$$\mathcal{F}_i[n_i] = F_i[n_i] - \int Q_i \tilde{n}_i(\mathbf{r}) V_{\text{ext}}(\mathbf{r}) \mathrm{d}\mathbf{r} = \mathcal{F}_{\text{id}}[n_i] + \mathcal{F}_{\text{ex}}[n_i], \tag{4.23}$$

which has been decomposed into the sum of the ideal and excess part (with $\tilde{n}_i$ being the deviation of the ion density from the mean ionic density, n_0); here, the ideal part is given in the LDA with the free energy density of the non-interacting classical gas. Additionally, we need the relation $h(r) = \tilde{n}_i(r)/n_0 = g(r) - 1$; this can be understood as a density distribution around an ion at the origin. Further, the excess part of the intrinsic free energy can be expanded around the mean density as

$$\begin{aligned}\mathcal{F}_{\text{ex}}[n_i] = \mathcal{F}_{\text{ex}}[n_0] + \int \mathcal{K}_{\text{ex}}\left(\mathbf{r} - \mathbf{r}'; n_0\right) \tilde{n}(\mathbf{r}) \tilde{n}(\mathbf{r}') \mathrm{d}\mathbf{r}\mathrm{d}\mathbf{r}' \\ + \int \mathcal{L}_{\text{ex}}\left(\mathbf{r}, \mathbf{r}', \mathbf{r}''; n_0\right) \tilde{n}(\mathbf{r}) \tilde{n}(\mathbf{r}') \tilde{n}(\mathbf{r}'') \mathrm{d}\mathbf{r}\mathrm{d}\mathbf{r}'\mathrm{d}\mathbf{r}'' + \ldots\end{aligned} \tag{4.24}$$

By definition, the direct correlation function reads

$$c(\mathbf{r} - \mathbf{r}') \equiv -(k_B T_i) \frac{\partial \mathcal{F}_{\text{ex}}[n_i]}{\partial n_i(\mathbf{r}) \partial n_i(\mathbf{r}')}. \tag{4.25}$$

Now, keeping the terms up to the one with the kernel $\mathcal{K}_{\text{ex}}$ and dropping the higher order terms on the r.h.s. of Eq. (4.24), we find from Eq. (4.25):

$$c(\mathbf{r} - \mathbf{r}') \simeq c^{(2)}(\mathbf{r} - \mathbf{r}') = -\frac{\mathcal{K}_{\text{ex}}\left(\mathbf{r} - \mathbf{r}'; n_0\right)}{2 k_B T_i}. \tag{4.26}$$

From Eq. (4.23), taking into account the free energy minimization condition, and Eqs. (4.24)–(4.26), one can find the HNC closure [March 2002],

$$g(r) \simeq \exp\Big\{\Big[-\beta u(r) + h(r) - c^{(2)}(r)\Big]\Big\}.$$

Therefore, the basic idea of the closure (4.21) is to put all higher order correlation terms into the bridge function, $B(r)$, which can then be approximated. As it was mentioned, the HNC follows by setting $B(r) = 0$.

4.3.1. Numerical solution

To solve self consistently the system of nonlinear equations given by (4.20) and (4.3), one can use the method from Ref. [Springer 1973]. The main idea is to rewrite Eqs. (4.20) and (4.3) as

$$\begin{aligned} \tilde{N}_s &= \tilde{c}/(1 - n_0\tilde{c}) - \tilde{c}_s, \\ g(r) &= \exp[N_s(r) - u_s(r)], \\ c_s(r) &= g(r) - 1 - N_s(r), \end{aligned}$$

where $N(r) = h(r) - c(r)$, and

$$\begin{aligned} u_s(r) &= u(r) - u_l(r), \\ c_s(r) &= C(r) + u_l(r), \\ N_s(r) &= N(r) - u_l(r). \end{aligned}$$

Here u_l is an ad hoc, in principle arbitrary function that accelerates convergence.

For the one-component system of charged particles interacting through a bare Coulomb potential (the *Coulomb system*), i.e., $\kappa = 0$, Ng showed that a quick convergence can be achieved by the choice [Ng 1974]

$$u_l(r) = \frac{\Gamma}{r}\,\mathrm{erf}(\alpha r),$$

where $\alpha = 1.08$ and the distance is given in units of a.

In the case of a one-component system interacting via the Yukawa potential (the *Yukawa system*) with $1 < \kappa < 2$ and $\Gamma < 100$, the convergence of the iterations is fast enough without any u_l (i.e., $u_l = 0$). In contrast, at $\kappa < 1$, u_l is needed for the convergence, and a sufficient form was revealed by trial and error to be

$$u_l(r) = \frac{\Gamma}{r}\left[\exp(-\kappa r) - \exp(-\alpha r)\right], \tag{4.27}$$

where $\alpha = 2.16$ and $\kappa = k_s a$ is the screening parameter. In the context of the present work, u_l in the form given by Eq. (4.27) is used to accelerate the convergence of the HNC calculations when the numerically precomputed STLS, RPA and QMC potentials are used.

4.3.2. Test on the basis of the effective coupling parameter

The Ornstein-Zernike equation (4.20) was solved by implementing the foregoing numerical scheme. The correctness of the numerical solution was confirmed for the Yukawa system by comparison with the MD data from Refs. [Ott 2014, Bruhn 2011], as it is illustrated in Fig. 4.1. In this figure, along the HNC and MD results, the RPDF calculated using two different bridge functions from Refs. [Daughton 2000] and [Ng 1974] are shown. In Ref. [Daughton 2000], the bridge function for the Yukawa system was proposed on the basis of the MD data. In Ref. [Ng 1974], the bridge function for the Coulomb system was obtained by compering to the classical Monte Carlo simulation data. Following the notation of Ref. [Bruhn 2011], the result obtained using the bridge function from Ref. [Daughton 2000] and Ref. [Ng 1974] are denoted as the IHNC ("improved HNC") and AHNC ("adjusted HNC"), respectively. Evidently, the IHNC data are in excellent agreement with the exact MD data [Daughton 2000].

For completeness, further, test of applicability of the HNC for the present research was done using an effective coupling parameter, Γ_{eff}, defined for the Yukawa system. The main idea of the effective coupling approach is that a single dimensionless parameter can describe a system characterized by two independent parameters; Γ and κ. The point is that different pairs of values of Γ and κ can generate the same RPDF. Thus, Γ_{eff} is a function of Γ and κ and different combinations of Γ and κ can yield the same Γ_{eff}. Such a unifying picture was achieved by mapping the Yukawa system onto the Coulomb system [Ott 2014]. In Ref. [Ott 2014], the following simple parametrization of Γ_{eff} was found by analyzing data from MD simulations:

$$\Gamma_{\text{eff}}(\Gamma,\kappa) = \left(1 - 0.309\kappa^2 + 0.08\kappa^3\right)\cdot\Gamma, \tag{4.28}$$

which is valid in the range $0 \leq \kappa \leq 2$, and $1 \leq \Gamma_{\text{eff}} \leq 150$.

Let us briefly summarize the result of the HNC test on the basis of Γ_{eff}:

- It was found that—similar to the MD results—the HNC results nicely follow a one-to-one mapping between the RPDF of Coulomb and Yukawa systems [Ott 2014]. This is illustrated in Fig. 4.2, where RPDFs with fixed Γ_{eff} but different screening parameters approximately coincide. Some differences are visible, at the given scale, near

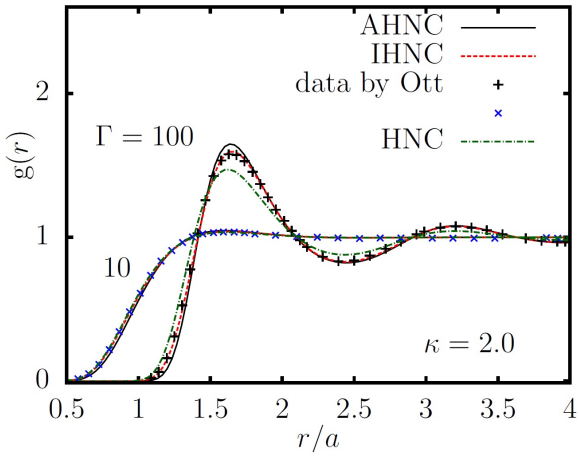

Figure 4.1: The result of the solution of Eqs. (4.20) and (4.3) for the RPDF of the Yukawa system with the screening parameter $\kappa = 2.0$ and different values of the coupling parameter, Γ. Additionally, the comparison with the MD results from Refs. [Ott 2014, Bruhn 2011] at $\Gamma = 10$ and 100 is given. From reference [Moldabekov 2018b].

the first peak of the RPDF. This feature is inherited from the MD results on the basis of which Γ_{eff}, Eq. (4.28), was constructed; a detailed discussion of this feature was given in Ref. [Ott 2014].

- It was found that up to $\Gamma_{\text{eff}} \simeq 10$, HNC provides an accurate description of the RPDF. For instance, the condition $\Gamma_{\text{eff}}(\Gamma, \kappa = 2) = 10$ gives $\Gamma = 25$ as the maximal value of Γ up to which the HNC and MD data on the RPDF are in agreement with each other. This can be seen from Figs. 4.1, 4.2, and 4.3.

The latter point indicates that, if the screening is stronger, $\kappa > 2$, the agreement of the HNC data with MD result extends well beyond $\Gamma = 25$. Indeed, as it will be shown later in this chapter, the HNC data are in agreement with the MD data even at $\Gamma = 50$ when the STLS potential is used at $r_s = 1.8$ and $\theta = 0.1$. Note that due to electronic non-ideality and quantum non-locality effects, the screening is much stronger in the latter case in comparison to the Yukawa potential (4.17) with $\kappa = 2$.

Therefore, the HNC approach allows to analyze the structural properties of the strongly coupled ions by looking at the relative differences (changes)

due to the use of different approximations in the treatment of the electronic density response function. Furthermore, in this work, the main results obtained on the basis of the HNC are verified by MD simulations of ions interacting through a screened ion potential. It should be noted that the screened pair interaction potentials used in this work depend on the temperature and density of the system and, therefore, belong to the class of state-dependent potentials. Many of the widely used integral equations, like the Ornstein-Zernike relation, were originally derived considering a pair interaction which does not have a dependence on the temperature and density (e.g. Coulomb potential). Therefore, the use of the solution of these integral equations on the basis of the screened pair interaction potentials must be done with caution (see discussions in Refs. [Tejero 2009, D'Adamo 2013]).

Finally, it is interesting that even in the regime of strong screening, at $\kappa = 2$, the AHNC leads to relatively good agreement with the IHNC results, as it is can be seen from Figs. 4.1 and 4.3. This is an illustration of a known certain level of universality of the bridge functions [Rosenfeld 1979].

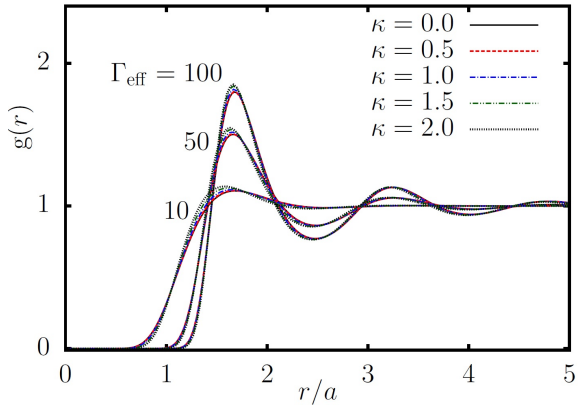

Figure 4.2: The radial pair distribution function computed using the HNC for the various values of the screening parameters, κ, and the effective coupling parameters, $\Gamma_{\rm eff}$. From reference [Moldabekov 2018b].

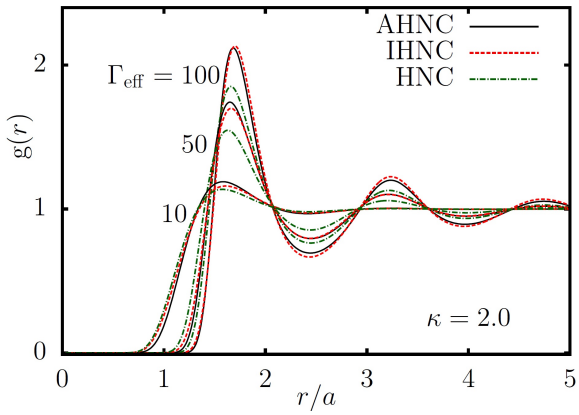

Figure 4.3: The RPDF computed for different $\Gamma_{\rm eff}$, Eq. (4.28), using the HNC, the AHNC (with the bridge function from Ref. [Ng 1974]), and the IHNC (with the bridge function from Ref. [Daughton 2000]). From reference [Moldabekov 2018b].

4.4 Results

The calculations and subsequent analyses were divided into three parts with different electronic density parameters: $r_s \leq 1$, $r_s = 2$, and $1 < r_s < 2$. Accordingly, regarding electronic correlations, these three cases are characterized as weakly ($r_s \leq 1$), strongly ($r_s = 2$), and moderately ($1 < r_s < 2$) non-ideal regimes. Additionally, for each foregoing case the degeneracy parameter is increased starting from $\theta = 0.01$ until the effect of quantum nonlocality significantly diminishes. The latter is gauged by the comparison of more involved descriptions with the results obtained making use of the Yukawa potential, which totally disregards the electronic quantum nonlocality, and on the basis of the SM potential, which takes into account the quantum nonlocality as a first order correction to LDA.

The transition from the higher density, $r_s < 1$, to the lower densities, $r_s \sim 2$, is accompanied by a build up of the inter-electronic correlations. This process is tracked by comparing the data computed using the RPA potential with those calculated using the STLS and QMC potentials. Moreover, the analysis of the results obtained using the STLS potential will allow to identify the applicability range of the STLS approximation. In particular, for the latter purpose, the comparison with the data calculated using the

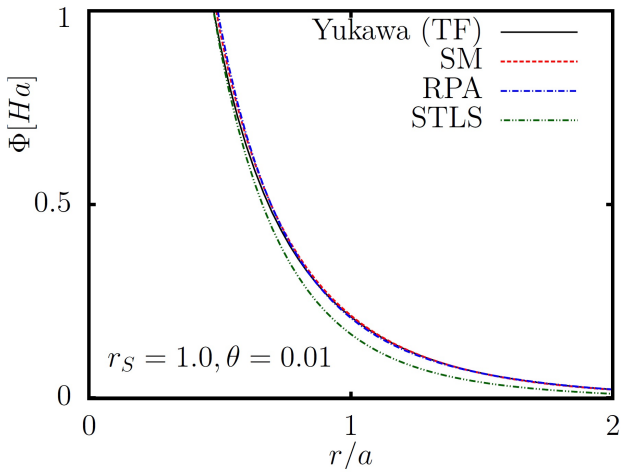

Figure 4.4: Ion potential calculated using different approximations. From reference [Moldabekov 2018b].

QMC potential is important.

4.4.1. Densities $r_s \leq 1$: weakly non-ideal electrons

Let us start from the density parameter $r_s = 1$ and investigate the transition from the ideal to the non-idela domain. In the limit of strongly degenerate electrons, this case is at the edge of the applicability of the RPA description.

In Fig. 4.4, the different considered potentials are shown for the case of strong degeneracy, $\theta = 0.01$. From this figure, first of all, it is apparent that the inter-electronic correlations result in stronger screening in the range $0.5 < r/a \leq 2$ and the Yukawa, SM, and RPA potentials are grouped closely to each other. The RPDFs computed on the basis of various potentials are presented in Fig. 4.5 for $\Gamma = 0.5,\ 1,\ 5,\ 10,\ 25$ and 50. From Fig. 4.5 we see that:

(i) the RPA, Yukawa, and SM potentials result in approximately the same RPDFs up to $\Gamma = 10$, while the STLS potential yields a slightly smaller correlation-hole in the RPDF due to the stronger screening;

(ii) the SM potential, despite being a better approximation to the RPA than the Yukawa potential, gives the RPDF close to that calculated using the Yukawa potential;

(iii) at larger coupling parameters, $\Gamma = 25$ and 50, the RPDFs computed

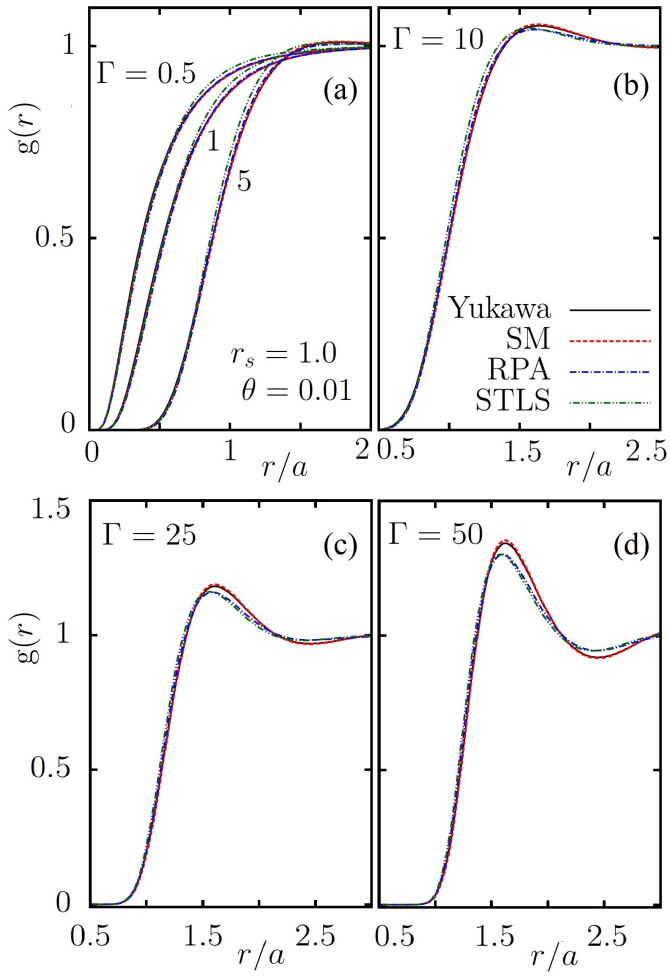

Figure 4.5: Radial pair distribution function computed using different screened ion potentials with: (a) $\Gamma = 0.5,\ 1,\ 5$; (b) $\Gamma = 10$; (c) $\Gamma = 25$; (d) $\Gamma = 50$. From reference [Moldabekov 2018b].

using the RPA potential are much closer to those obtained using the STLS potential rather than to the data found on the basis of the Yukawa and SM potentials.

Observation (iii) indicates that the structural properties of the strongly coupled ions are sensitive to the exact shape of the potential. Therefore, the potentials shown in Fig. 4.4 must be placed under careful scrutiny. This

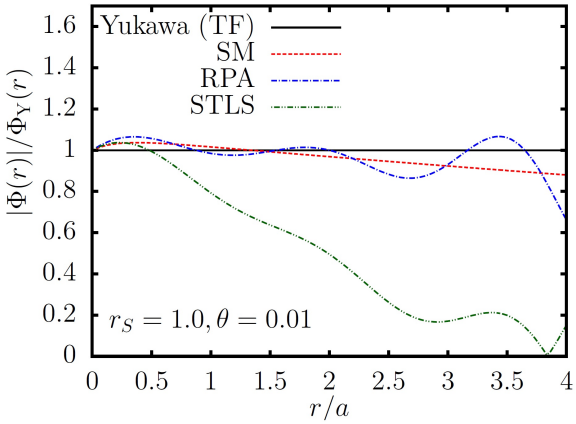

Figure 4.6: Different screened potentials divided by the Yukawa potential (4.17). From reference [Moldabekov 2018b].

is done by looking at the ratio of the considered potentials to the Yukawa potential in Fig. 4.6 and at the difference between the RPA screened potential and other potentials presented in Fig. 4.7. From Figs. 4.6 and 4.7 we see that the RPA potential exhibits oscillations around the decaying SM potential and the STLS potential, too, has such oscillating pattern but with stronger overall screening than that of the RPA potential.

Essentially, the oscillations in the RPA and STLS potentials have a very similar shape (position of local extrema etc.) up to $r/a = 3.75$. This is in contrast to the behavior at $r/a > 5$, where the oscillations in the STLS and RPA potentials turn into the Friedel oscillations. Therefore, we can argue that the aforementioned similarity in the pattern of the RPA and STLS potentials at $r/a \leq 3.75$ is the reason why, at larger coupling parameters, these two potentials give almost the same RPDF. To verify this hypothesis, let us consider the following potential, which is a hybrid of the RPA and Yukawa potentials:

$$\Phi(r; r_c) = \begin{cases} \Phi_{\mathrm{RPA}}(r), & r < r_c \\ \beta(r_c) \times \Phi_Y(r), & r \geq r_c \end{cases} \tag{4.29}$$

where $\beta(r_c) = \Phi_{\mathrm{RPA}}(r_c)/\Phi_Y(r_c)$. We consider $r_c/a = 5.5$, $r_c/a = 2$, and $r_c/a = 1.25$. The distances r_c are chosen such that: at $r > 5.5a$ the RPA potential damps away and only Friedel oscillations remain; at $r > 2a$ and

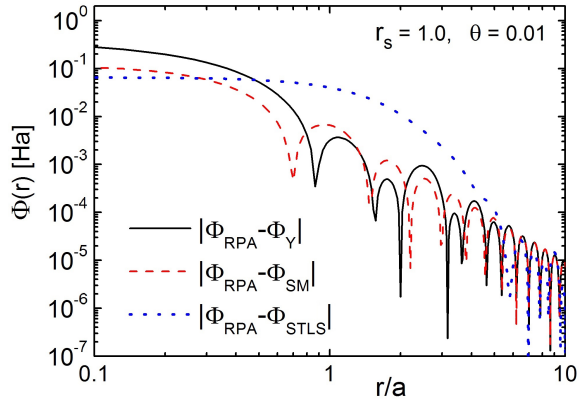

Figure 4.7: The difference between the RPA potential and other potentials. From reference [Moldabekov 2018b].

$r > 1.25a$ the second maximum and the first peak, respectively, of the RPDF are located. In other words, $\Phi(r; r_c)$ is the RPA potential up to r_c followed by the Yukawa-type pattern at $r \geq r_c$. Potential (4.29) is designed to dispose of the impact of the oscillations from different regions and, thus, to examine the sensitivity of the RPDF of the strongly coupled ions to these oscillations.

The RPDFs computed on the basis of $\Phi(r; r_c)$ (with different values of r_c) and the Yukawa potential (Yukawa RPDF) are presented in Fig. 4.8. From this figure we see that: $\Phi(r; r_c = 5.5a)$ yields the same outcome as the RPA potential; $\Phi(r; r_c = 2a)$ leads to a RPDF closer to the Yukawa RPDF at $r/a > 2$ and is in agreement with the RPDF obtained using the RPA potential at $r/a < 2$; $\Phi(r; r_c = 1.25a)$ closely reproduces the Yukawa RPDF (some differences appear as the consequence of matching the RPA potential at $r = r_c$).

Thereby, it is confirmed that the deviation of the RPDF calculated on the basis of the RPA potential from the Yukawa RPDF at $\Gamma = 25$ and 50 is the result of the manifestation of the oscillations in the RPA potential in the intermediate region between very small distances, where bare Coulomb repulsion is dominant, and large distances, where the Friedel oscillations are present. The curves of the static structure factor, $S(k)$, for Γ in the range from 0.5 to 50 are presented in Fig. 4.9. From this figure the following conclusions are drawn out:

- The RPDF computed using the STLS potential has a larger value

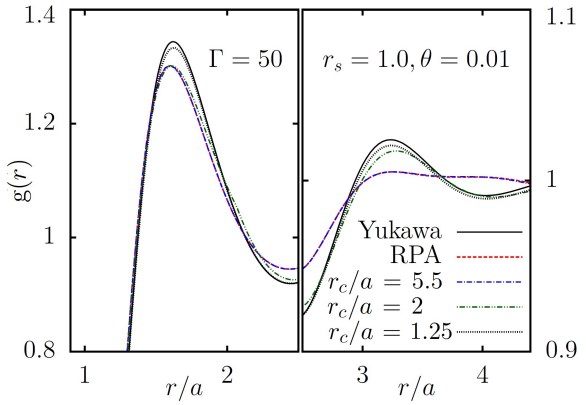

Figure 4.8: RPDF computed using the Yukawa potential (4.17), the RPA potential, and the test potential (4.29). From reference [Moldabekov 2018b].

of $S(0)$ than those calculated neglecting the electronic correlations. Note that the ionic isothermal compressibility can be expressed as $S(0)/(nk_BT_i)$ [March 2002]. Therefore, *the inter-electronic correlations increase the isothermal compressibility of the ions.*

- At $ka < 3$, at considered coupling parameters, the SSF obtained using the RPA potential is in very good agreement with the Yukawa and SM potentials based results. Therefore, *the Friedel oscillations do not affect the structural properties of the ions in dense quantum plasmas.*
- At $ka > 2.5$, the STLS result for the SSF agrees with that obtained from the RPA, Yukawa, and SM potentials up to $\Gamma = 10$. In contrast, at $\Gamma > 10$ and $ka > 3$, the RPA and STLS results deviate from the data computed using the Yukawa and SM potentials. This, again, is due to the aforementioned manifestation of the electronic quantum non-locality in the form of potential oscillations at intermediate distances.

These conclusions remain valid for all $1 \leq r_s \leq 2$, as the following investigations at different density parameters will show.

As one can expect, the impact of the electronic quantum non-locality and correlation effects diminishes at higher densities. This is illustrated in Fig. 4.10, where the RPDF and SSF at $r_s = 0.5$ are presented. From this figure the agreement of the results obtained making use of different approximations for the ion-ion interaction potential is clearly seen up to $\Gamma = 25$. However, at $\Gamma = 50$, a slight difference around the first peaks is observable. Therefore, at even higher coupling parameters, $\Gamma \gg 50$, (which

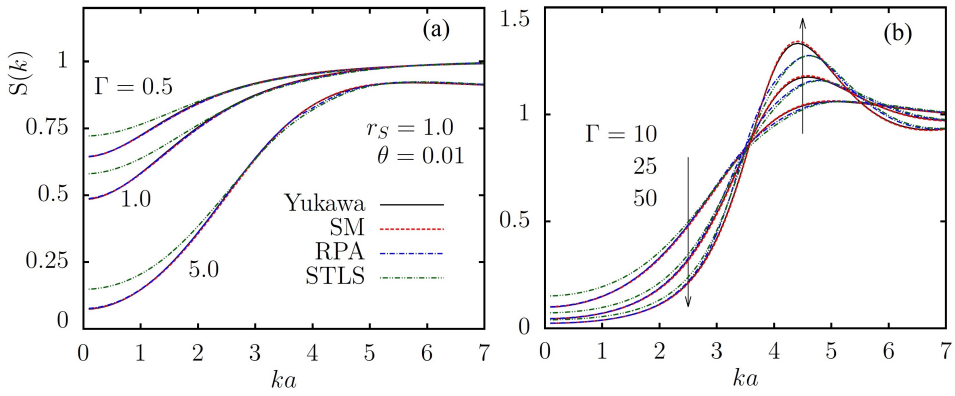

Figure 4.9: SSF calculated using different screened potentials for the different values of Γ. In the left figure (a) the curves for Γ = 5.0 are shifted for the better visibility. From reference [Moldabekov 2018b].

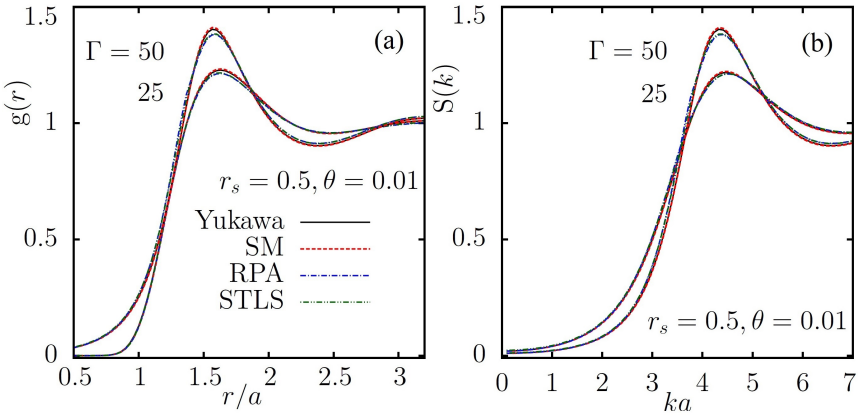

Figure 4.10: (a) Radial pair distribution function and (b) static structure factor obtained using different screened potentials for various values of Γ at $r_s = 0.5$ and $\theta = 0.01$. From reference [Moldabekov 2018b].

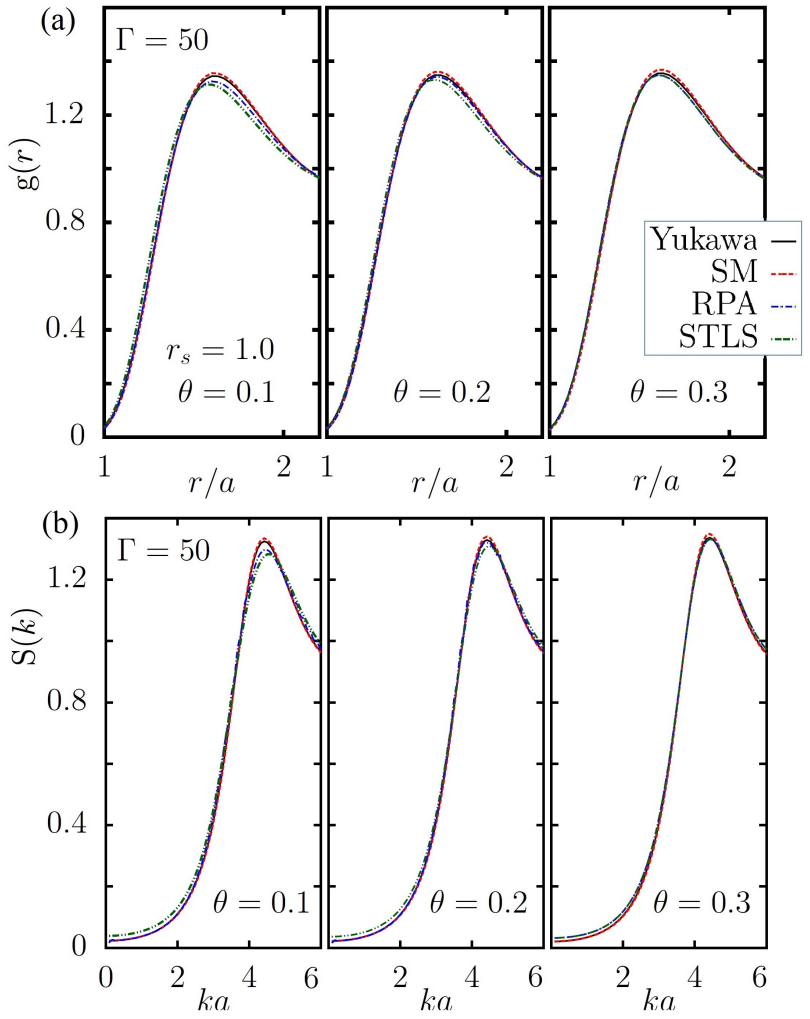

Figure 4.11: RPDF and SSF calculated for different values of the degeneracy parameter θ of the electrons at $r_s = 1.0$ and $\Gamma = 50$. From reference [Moldabekov 2018b].

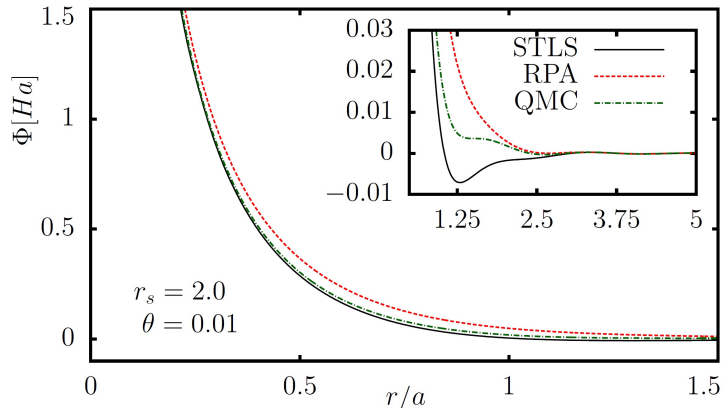

Figure 4.12: The STLS , RPA, and QMC potentials at $r_s = 2.0$ and $\theta = 0.01$. From reference [Moldabekov 2017b].

beyond the scope of this work) the aforementioned effects due to quantum non-locality and non-idelity can manifest at higher densities, $r_s < 1$.

Next, the influence of electronic thermal excitations is examined for $\theta =$ 0.1, 0.2, and 0.3. The RPDF and SSF calculated at these parameters are presented in Fig. 4.11. All curves collapse to a single one as the electronic degeneracy parameter (temperature) increases. Obviously, at $\theta > 0.3$, the electronic thermal excitations results in a significant suppression of electronic quantum non-locality and non- ideality effects.

4.4.2. Density $r_s = 2$: non-ideal electrons

Now we consider the other limiting case which is characterized by strong inter-electronic correlations. As was mentioned, the finite temperature QMC results for the local field correction cannot be used yet for the calculation of the screened ion potential due to insufficient k-resolution. However, in the case $r_s = 2$ and $\theta = 0.01$, the STLS treatment of the electronic subsystem can be gauged by comparing the STLS potential based result to the result obtained using the ground state QMC potential. As mentioned before, the accurate parametrization from Ref. [Corradini 1998] is employed for this purpose.

The STLS, RPA, and QMC potentials, at $r_s = 2$ and $\theta = 0.01$, are presented in Fig. 4.12. We see that at $r/a < 1$ the STLS and QMC potentials are close to each other and show stronger screening in comparison to the

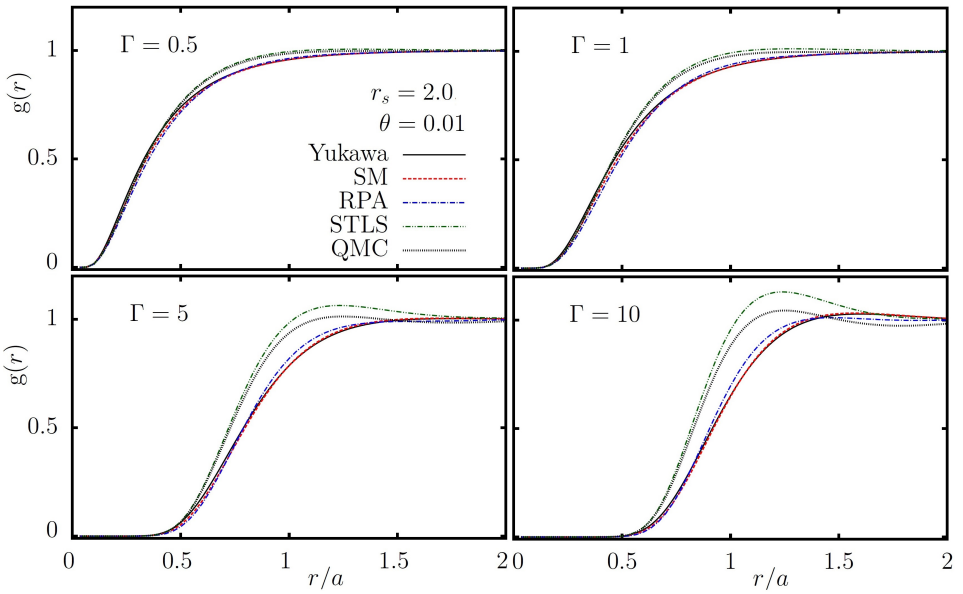

Figure 4.13: Radial pair distribution function of the ions at Γ in the range from 0.5 to 10 calculated on the basis of various screened ion potentials. From reference [Moldabekov 2018b]

RPA potential. At $1 < r/a < 2.5$, both the RPA and QMC potentials remain positive, while the STLS potential has a negative minimum around $r/a = 1.25$. At larger distances, $r/a > 2.5$, all three potentials exhibit Friedel oscillations (not shown in the figure).

The RPDFs calculated using different potentials in the range from $\Gamma = 0.5$ to $\Gamma = 50$ are presented in Figs. 4.13, 4.14, and 4.15. The SSFs computed on the basis of various potentials for $\Gamma = 0.5,\ 1,\ 10$ and $\Gamma = 25$ are given in Figs. 4.16 and 4.17. From these figures, we made the following observations:

• At $\Gamma \leq 1$, the RPDF computed using the STLS potential is close to that of based on the QMC potential, as it is demonstrated in Fig. 4.13.

• At $\Gamma > 1$, the STLS potential yields significantly larger value for the first peak of the RPDF in comparison to the RPDF obtained using the QMC potential, but the position of the first peaks are in agreement (see Figs. 4.14, and 4.15). The former observation is due to the ion-ion attraction (the negative minimum) in the STLS potential, and the latter is due to a similar behavior of the potentials at intermediate distances, $r/a \leq 1$.

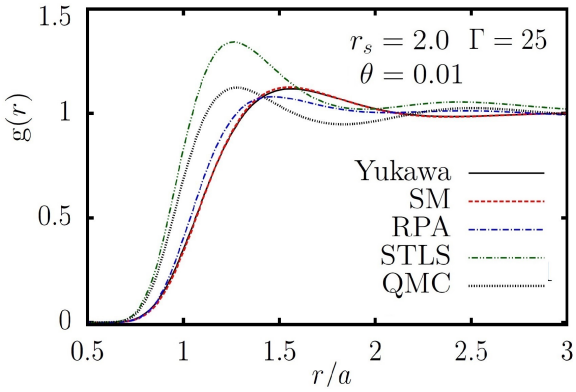

Figure 4.14: RPDF computed using different potentials for $\Gamma = 25$. From reference [Moldabekov 2018b].

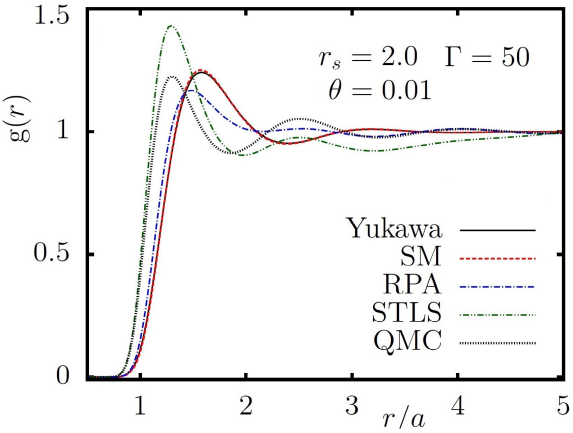

Figure 4.15: The same as in Fig. 4.14 but for $\Gamma = 50$. From reference [Moldabekov 2018b].

• For all considered parameters, the RPA potential based RPDFs and SSFs exhibit a noticeable deviation from the QMC potential based result. Pronounced disagreement between RPDFs (SSFs) obtained using the RPA potential and the Yukawa (SM) potential appears at $\Gamma \gg 1$.

• The SSF computed using the STLS potential has its minimum at $k > 0$ due to the attractive part in the corresponding potential, in contrast to those obtained using other approximations. Particularly, a minimum at $ka \simeq 2$, which becomes more pronounced with increase in Γ, is demonstrated in Figs.

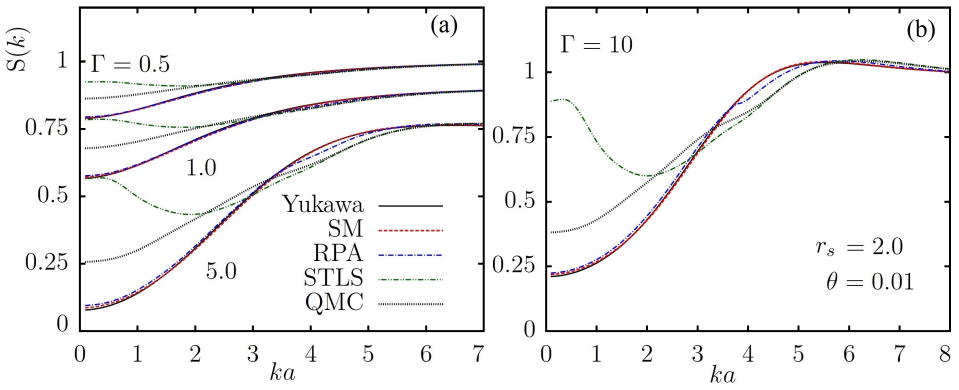

Figure 4.16: Static structure factor calculated on the basis of different ion potentials at different values of Γ. From reference [Moldabekov 2018b].

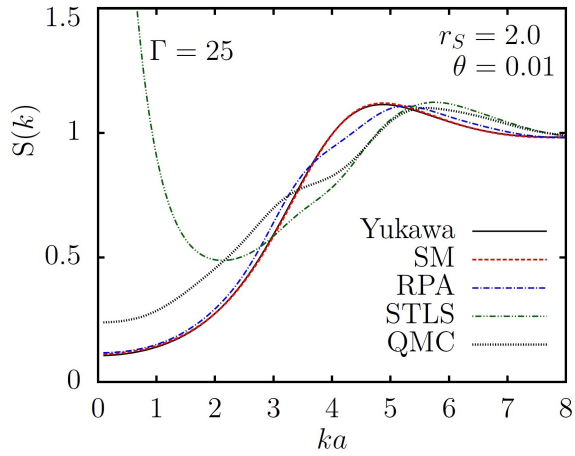

Figure 4.17: SSF calculated using various screened ion potentials at different coupling parameters. From reference [Moldabekov 2018b].

4.16 and 4.17. An important aspect is that the foregoing feature of the SSF does not exist in the SSF calculated using the QMC potential.

From the aforementioned observations, it is evident that *considering electronic screening in the STLS approximation essentially fails to adequately describe the SSF (RPDF)—at small wavenumbers, $ka < 4$ (large distances, $r/a > 1$)—of the strongly coupled ions at certain densities and temperatures in the considered parameters, $r_s \leq 2$ and $\theta \geq 0.01$, due to unphysical at-*

traction between ions. On the other hand, Fig. 4.16 also illustrates that the STLS results and the QMC data based results for the SSF (RPDF) at $ka > 4$ ($r/a < 1$) are in agreement with each other. The reason for this is that the STLS potential correctly reproduces the QMC potential at $r/a < 1$ (see Fig. 4.12).

4.4.3. Density $1 < r_s < 2$: moderately non-ideal electrons

Considering $1 < r_s < 2$, we can understand in more detail how the STLS potential fails to provide correct structure properties of the ions when the density decreases. The curves of the STLS and RPA potentials for $r_s = 1.5$ and 1.8 are shown in Fig. 4.18. As before, inter-electronic correlations yield stronger screening as it is seen by comparing the STLS and RPA potentials. The second point, which is clearly observable from Fig. 4.18 and the previously discussed case $r_s = 1$, is that the first negative minimum of the Friedel oscillations transforms into a single pronounced minimum by decreasing the electronic density. Therefore, the attractive part of the STLS potential is the result of the interplay between screening and the Kohn anomaly [Kohn 1959]. This transition from the strongly oscillatory tail to the specific negative minimum results in dramatic changes in the SSF and RPDF computed using the STLS potential. This is clearly demonstrated in Figs. 4.19 and 4.20, where the RPDFs and SSFs are presented. From these figures we see that:

• At $r_s = 1.5$, the RPDF calculated using the STLS potential has a smaller correlation-hole and the height of the first peak is in between those computed on the basis of the Yukawa (SM) potential and the RPA potential (see Fig. 4.19). In contrast, at $r_s = 1.8$, the height of the first peak of the RPDF found using the STLS potential is higher than those calculated using other approximations (see Fig. 4.19), which is due to the manifestation of the attraction part of the STLS potential.

• The manifestation of the unphysical behavior at $r_s = 1.8$ (see Fig. 4.20) due to the attraction between ions interacting through the STLS potential is more noticeable on the curve of the SSF at $ka < 4$. In contrast, at $r_s = 1.5$, such a feature is absent (see Fig. 4.20).

• In addition, from Figs. 4.19 and 4.20 we see that at $\Gamma = 50$, $\theta = 0.01$, $r_s = 1.5$, and $r_s = 1.8$ the Yukawa and SM potentials are not able to correctly reproduce the results computed using the RPA potential.

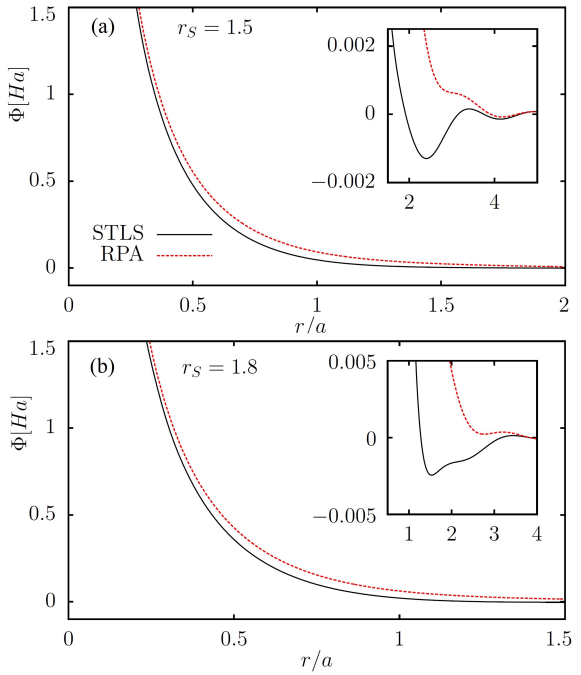

Figure 4.18: The STLS and RPA potentials at the density parameters $r_s = 1.5$ and $r_s = 1.8$ ($\theta = 0.01$). From reference [Moldabekov 2018b].

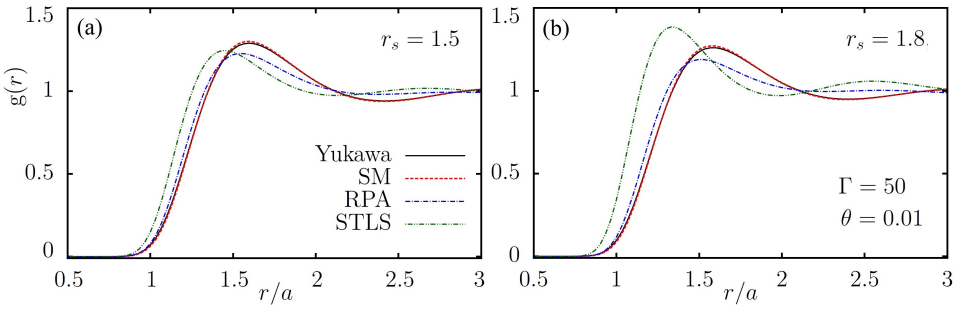

Figure 4.19: RPDF of ions calculated for the density parameters $r_s = 1.5$ and 1.8 at $\theta = 0.01$ and $\Gamma = 50$. From reference [Moldabekov 2018b].

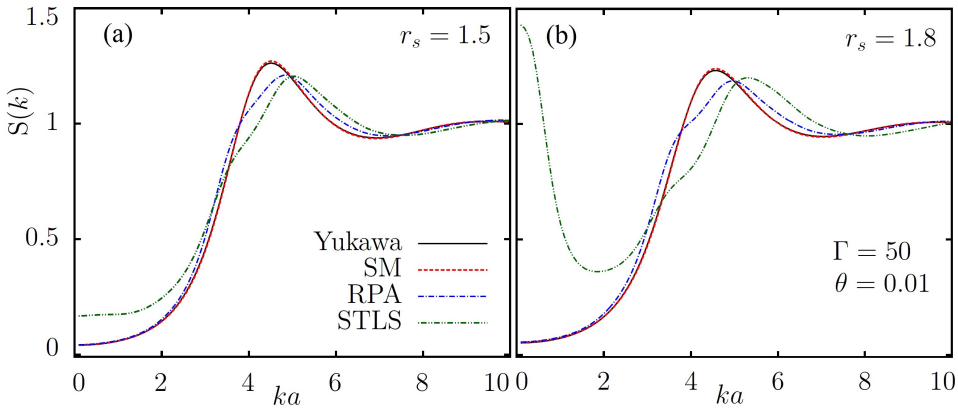

Figure 4.20: Static structure factor of ions computed for the density parameters $r_s = 1.5$ and 1.8 at $\theta = 0.01$ and $\Gamma = 50$. From reference [Moldabekov 2018b].

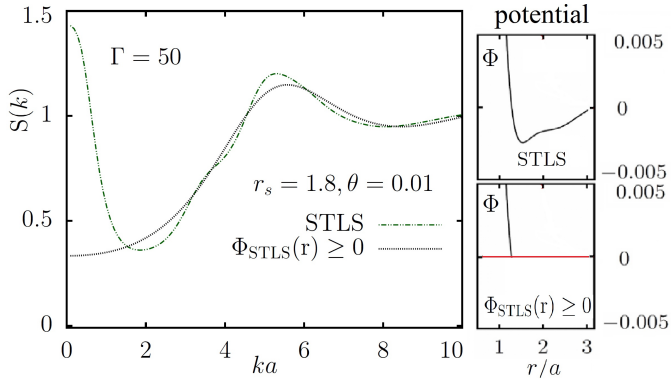

Figure 4.21: Static structure factor of ions for 1.8 at $\theta = 0.01$ and $\Gamma = 50$. The STLS result and the result obtained neglecting the attractive part of the pair interaction potential are compared.

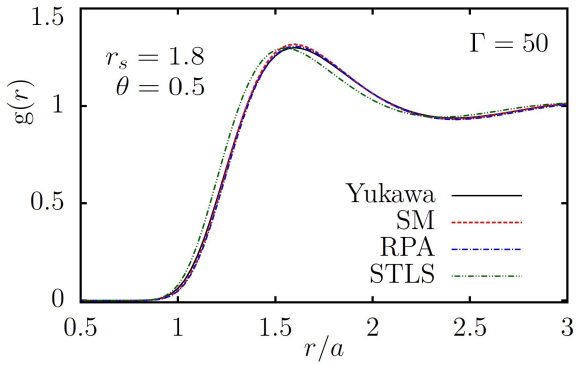

Figure 4.22: Radial pair distribution function of ions. From reference [Moldabekov 2018b].

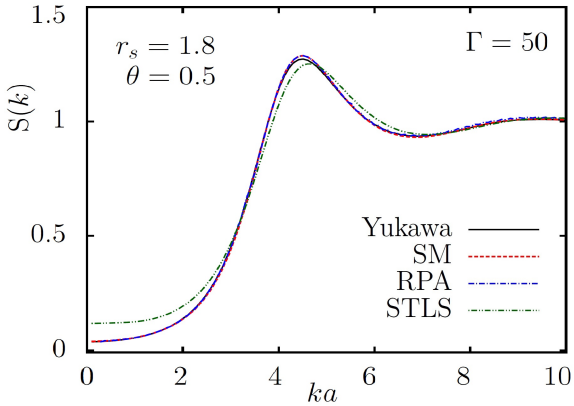

Figure 4.23: Static structure factor of ions. From reference [Moldabekov 2018b].

In the case of $r_s = 1.8$, in order to demonstrate that the strong deviation of the SSF behavior from the others at $ka < 4$ can be traced back to the discussed negative minimum in the STLS potential, in Fig. 4.21 the data obtained using the truncated STLS potential (without the part after $\Phi = 0$) are shown in comparison to the result obtained using full STLS potential. From this figure, it can be seen that the aforementioned negative minimum of the STLS potential is indeed culpable for the unphysical pattern of the SSF at $ka < 4$.

The thermal electronic excitations lead to the disappearance (damping)

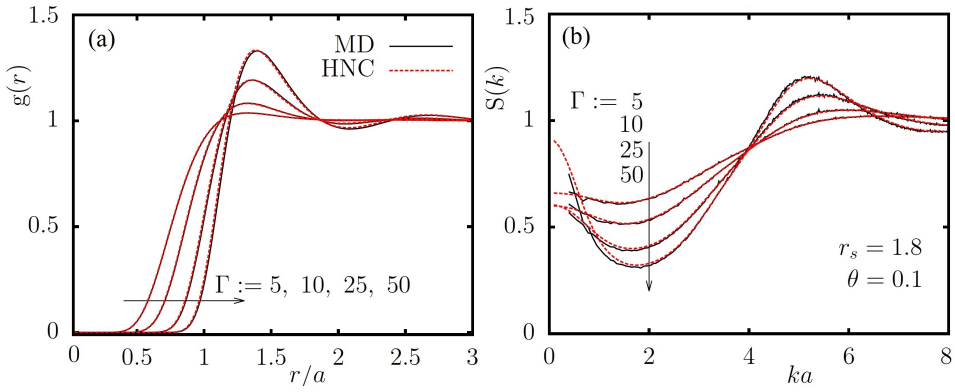

Figure 4.24: (a) Radial pair distribution function and (b) static structure factor calculated using the STLS potential by the HNC and MD simulations at $r_s = 1.8$ and $\theta = 0.1$ for different values of the coupling parameter. From reference [Moldabekov 2018b].

of the potential oscillations (i.e., the effect which we called non-locality) and, thereby, to a diminished anomal behavior of the SSF and RPDF obtained on the basis of the STLS potential. This is illustrated in Figs. 4.22 and 4.23 for $\theta = 0.5$, where the effect of the attraction cannot be seen.

4.4.4. Verification of the HNC results by MD simulations

The MD simulation of the ions interacting via the STLS potential is an important check of the revealed features of the structural properties of the ions using the HNC. In subchapter 4.3.2, it was found that the HNC calculations provide accurate data on the ionic structural properties up to $\Gamma_{\text{eff}} = 10$. It was mentioned that, in the case of the strong screening, with $\kappa > 2$, the HNC is expected to be accurate even at $\Gamma > 25$. This, and the aforementioned features of the RPDF and SSF obtained using the STLS potential were confirmed by performing MD simulations with the number of ions set equal to $N = 1000$. The results are shown in Figs. 4.24 and 4.25. In Fig. 4.24, the RPDF and SSF are computed at $\theta = 0.1$ and $r_s = 1.8$, for $\Gamma = 5,\ 10,\ 25$ and 50. In Fig. 4.25, RPDF and SSF are computed at $\Gamma = 20$, for two different combinations of the density and degeneracy parameters ($r_s = 1.4, \theta = 0.5$, and $r_s = 2.0, \theta = 0.01$). Indeed, we find excellent agreement between the MD and the HNC results.

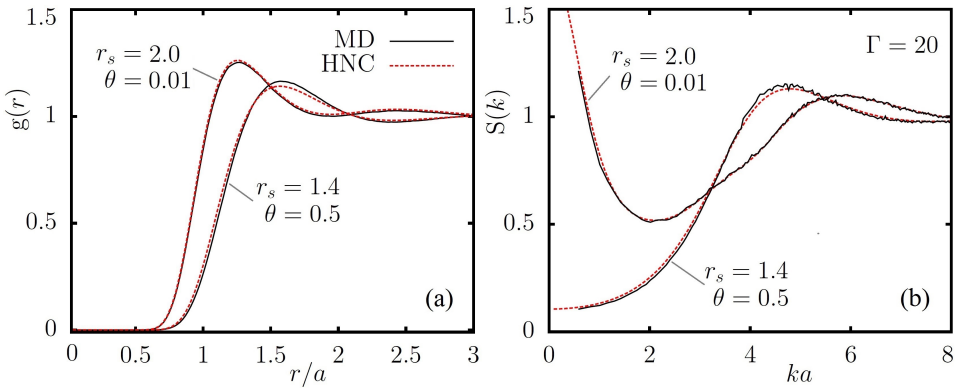

Figure 4.25: (a) Radial pair distribution function and (b) static structure factor calculated using the STLS potential by HNC and MD simulations at $\Gamma = 20$ for different values of the density and degeneracy parameters.

4.5 Applicability of the STLS approximation

We are now in a position to determine the applicability of the STLS approximation to dense plasmas with strongly coupled ions. For this purpose, the absence of the pronounced impact of the attraction in the ion-ion interaction on $S(k)$ is used as a necessary criterion. For example, in the Fig. 4.26, the STLS potential is shown at $\theta = 0.01,\ 0.1,\ 0.2,\ 0.3$ and 0.4. With increasing degeneracy parameter, the absolute value of the negative minimum reduces and its position shifts to a larger distance. Corresponding SSFs and RPDFs at $\Gamma = 50$ are shown in Fig. 4.27. As discussed earlier, the suppression of the manifestation of the ion-ion attraction takes place due to thermal electronic effects. To be specific, at $\theta = 0.4$, the value of the SSF at the minimum—which located in the range $0 < ka < 2$—is less than 5% of the SSF value at $k = 0$. Further, the SSF minimum at $0 < ka < 2$, due the negative minimum in the STLS potential, rapidly vanishes with increasing θ, as it is can be seen from Fig. 4.22 where the aforementioned minimum does not exist at $\theta = 0.5$. Apart from that, from Fig. 4.27(b), we see that the value of the first peak of the RPDF decreases with increasing θ due to the deterioration of the attractive part of the potential, while the correlation-hole increases due to the stronger repulsion between ions.

In a similar way, a large scale study of the SSF on the basis of the STLS potential has been carried out. Different values of the degeneracy and

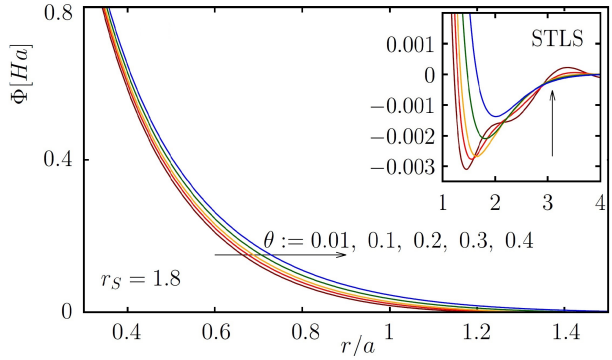

Figure 4.26: The STLS potential at $r_s = 1.8$ and different values of the degeneracy parameter of electrons θ. From reference [Moldabekov 2018b].

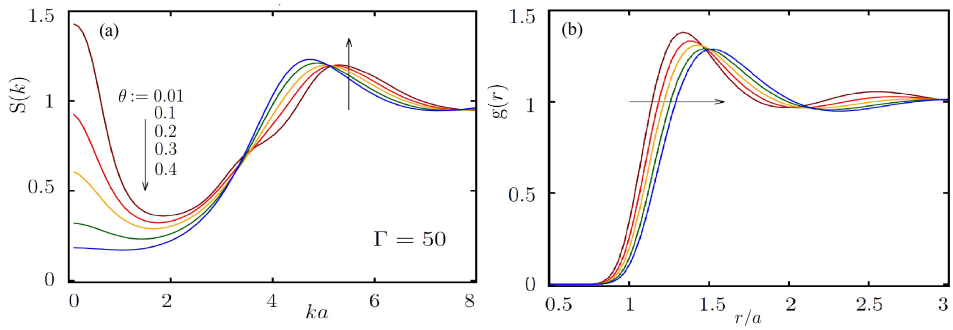

Figure 4.27: The static structure factor (a) and radial pair distribution function (b) at $\Gamma = 50$ computed using the STLS potential at $r_s = 1.8$ and different values of the degeneracy parameter of electrons. From reference [Moldabekov 2018b].

density parameters have been considered in the range $0.01 \leq \theta \leq 1$ and at the densities $r_s \leq 2$. The results are summarized in Fig. 4.28. In region I, the artificial minimum of the SSF due to the negative minimum of the STLS potential does not appear. In contrast, in region II (dashed) the unphysical absolute minimum in the SSF at $k > 0$ appears at $\Gamma \geq 1$ and amplifies with the departure from the line delineating the two areas. Therefore, in region II, the *ab initio* finite temperature QMC data for local field corrections with sufficiently high k-resolution is needed.

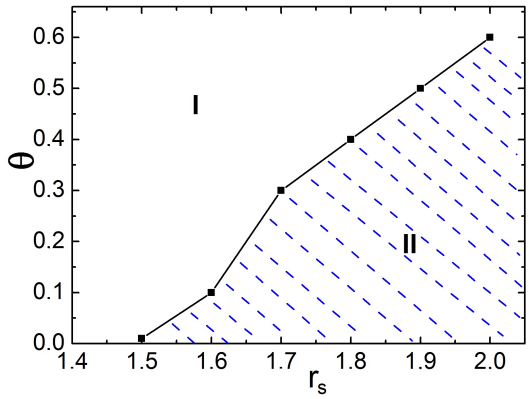

Figure 4.28: The result of analysis of the SSF at the values of the degeneracy and density parameters in the range $0.01 \leq \theta \leq 1$ and $r_s \leq 2$, respectively, is summarized. The region corresponding to the applicability parameters of the STLS potential is denoted as I. At these parameters the unphysical feature of $S(k)$ due to the pronounced negative minimum in the STLS potential is absent. In contrast, in the region denoted as II (dashed area), the artificial absolute minimum in $S(k)$ at $0 < k < 4$ appears at $\Gamma \geq 1$. From reference [Moldabekov 2018b].

4.6 Summary

The detailed analysis of the structural properties of strongly coupled ions in dense quantum plasmas has revealed the following results:

(i) The structural properties of strongly coupled ions in a quantum plasma are highly sensitive to the shape of the ion-ion pair interaction potential. Hence, a relatively small discrepancy to the true pair interaction potential due to an approximate treatment of the electronic subsystem can lead to unphysical predictions. Consequently, the self-consistent study of a two component quantum plasma requires a more involved theoretical consideration of the electrons in the case of strong ionic coupling, $\Gamma > 1$, in comparison to the case $\Gamma < 1$.

(ii) The Yukawa potential, which often has been used for the study of strongly coupled ions, is not capable to provide an adequate description of the ionic dynamics at $\theta \sim 0.1$ and $r_s \geq 1$. The same applies to the SM potential, which had been proclaimed as providing a unified

description of the linear screening in dense plasmas [Stanton 2015].

(iii) The parameters where the STLS approximation is applicable have been identified.

(iv) The HNC provides an accurate description for $\Gamma_{\text{eff}} \lesssim 10$.

Chapter 5

Conclusions and Outlook

Conclusions

The first paper on the quantum fluid model for a quantum electron gas by Manfredi and Haas in 2001 and experiments relevant to quantum plasmas have sparked an unprecedented interest in the QHD. Despite a large number of publications on this topic, the QHD approach suffered from the lack of a reliable foundation [Khan 2014], especially for the finite temperature case. This circumstance has impaired the development of the QHD description and, in fact, made the QHD unsuitable for high-energy-density plasma science. The main achievement of the work presented in the thesis at hand is the establishment of the theoretical foundations of finite temperature quantum hydrodynamics for plasmas [Moldabekov 2018a]. Now, the agreement of the QHD with the linear response theory in the limit of weak electronic density perturbation is guaranteed. Moreover, in the static limit the QHD reduces to the OF-DFT. These properties make the QHD a promising tool for the large scale simulation of dense quantum plasmas. Another important point is that the QHD has also started being popular for large scale simulations in plasmonics [Toscano 2015, Yan 2015, Ciracì 2016]. Thereby, the results presented in this thesis constitute a "timely contribution" [Manfredi 2018] for plasmonics as well. In this regard, among other results, I would like to stress the importance of a consistent inclusion of the dynamical exchange-correlation potential into the QHD for plasmonics, since a static exchange-correlation potential was used previously even for the description of high frequency phenomena [Crouseilles 2008, Yan 2015, Fernández-Domínguez 2012]. Additionally, in chapter 3, the LDA with the first order density gradient correction at finite temperature has been analyzed extensively in a whole range of frequencies and wavenumbers for the fist time. This ansatz is very important for both dense plasmas [Abdourahmane 2017, Sjostrom 2018], and plasmonics [Toscano 2015,

Krasavin 2018, Ding 2018].

Furthermore, considering the quantum plasma with strongly coupled ions and with weak electron-ion coupling—typical for dense plasmas—the impact of the electronic quantum degeneracy and correlation effects on the structural characteristics of the ions has been studied quantitatively and qualitatively. As a result, it was found that when the ionic component of the plasma is non-ideal ($\Gamma > 1$) the electronic correlations are crucial and cannot be neglected at $T < 6 \times 10^5$ K and $n < 1.6 \times 10^{24}$ cm^{-3} (or $\theta < 1$ and $r_s > 1$). In addition, the electronic quantum non-locality is strongly pronounced at $T \lesssim 6 \times 10^4$ K ($\theta \lesssim 0.1$). The importance of the findings from chapter 4 is that they undeniably indicate the need of a more involved description of the dense plasma electrons due to the stronger ionic non-ideality than in the case with $\Gamma < 1$. A case in point is given by the discussed failure of the STLS treatment of the electronic properties at the parameters which were previously considered to be well suited for this approximation [Reinholz 1995, Bennadji 2009]. In fact, the foregoing result together with the defined applicability limits of the STLS (for the quantum plasma with strongly coupled ions) is significant by itself because the STLS ansatz is often used for the self-consistent description of electron-ion plasmas [Graziani 2014b, Bennadji 2011]. Obviously, all findings mentioned here are relevant and important for the quantum fluid description of quantum non-ideal electrons on the basis of the QHD, where information about a static ionic structure is needed to compute an effective external field.

Finally, by bringing together the preceding three chapters we have a full picture of the quantum fluid approach for dense plasmas within the framework of the multi-scale description. In this approach, the electronic subsystem is described by the QHD equations presented in chapter 3 and the ions are treated as classical particles interacting with each other by the effective potential introduced in chapter 4. The examples of the parameters of experimentally generated plasmas that are relevant to this work are illustrated on the θ–r_s plane in Fig. 5.1. The discussed applicability range of the STLS scheme is also given in this figure. It can be seen that the quantum fluid approach with electronic correlations included by the STLS scheme can be used for the description of ICF plasmas starting from the initial stage with non-ideal quantum electrons all the way to the final regime with ideal electrons.

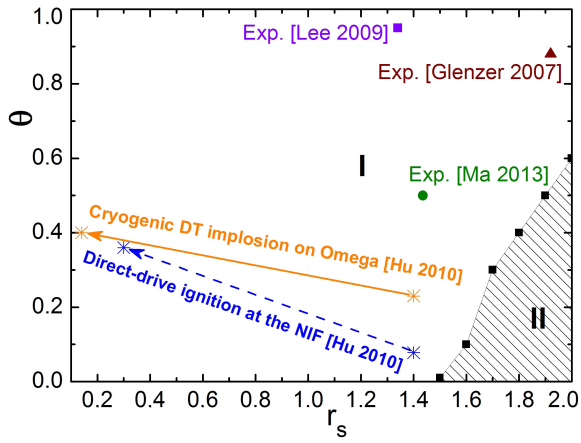

Figure 5.1: Examples of the experimental plasma parameters with $\Gamma > 1$. The data for ICF experiments were extracted from Ref. [Hu 2010]. In the experiments related to the ICF, the change in the plasma parameters during compression is sketched by an arrow. The dashed area (II) corresponds to the parameters at which the STLS scheme cannot be used for the description of the electronic correlations.

Outlook

An obvious first extension of the presented analysis of the structural characteristics of the ions in dense quantum plasmas is the investigation of the effects related to the non-linear response of the electrons. Important steps in this direction have already been done for systems where screening can be described within the multi-scale approach [Porter 2010, Gravel 2007], but not for the description of dense plasmas. On the one hand, for the electronic subsystem with the characteristic energy E_F, the inclusion of higher order effects due to non-linear response cannot lead to a significant change in the induced electronic density perturbation as far as a weak electron-ion coupling is considered. On the other hand, for the non-ideal ions—with the characteristic energy $k_B T_i \ll E_F$—this modification due to non-linear electronic response terms can yield a dramatic change in the structural characteristics since the properties of the strongly coupled ions in the quantum plasma are very sensitive to the peculiarities of the screened pair interaction potential (see the discussion in chapter 4).

The next question worth considering is an investigation of the properties

of streaming quantum plasmas. Often, an experimentally generated plasma is in a non-equilibrium condition with a non-zero mean streaming velocity of the electrons relative to the ions. Examples are experiments on an ion or electron beam driven dense plasma [Hoffmann 2005, Sharkov 2016, Kawata 2016]. In this case, plasma properties can be studied considering a stationary non-equilibrium system with a constant streaming velocity of the electrons relative to the ions. A dynamically screened ion potential can be used for the study of various physical properties of such a plasma. In comparison with the equilibrium case, the appearance of a significant ion-ion attraction and a strong wakefield can lead to a number of new and interesting features (see the figures in appendix C). A screened ion potential in dense streaming quantum plasmas has been carefully studied in Refs. [Moldabekov 2015a, Moldabekov 2015c, Moldabekov 2016].

Concerning the description of the electrons at a finite temperature by the QHD developed in chapter 3, the most interesting application in my eyes is the simulation of ICF plasmas. Previous considerations mainly used a hybrid particle-in-cell method* for a large scale simulation, where the electrons were treated as a classical fluid (i.e., neglecting the electronic quantum non-locality). Therefore, the QHD can be implemented into existing codes, as the one described in Refs. [Vu 1997, Harte 1996, Marinak 2001]. Indeed, this would be the first time that a large-scale simulation of the dense quantum plasma of ICF is performed taking into account the electronic quantum non-locality. Previously, this was not possible due to the lack of a consistent finite temperature QHD theory taking into account both the quantum non-locality and correlations.

*Besides, hydrodynamics simulations are also often used [Vold 2015, Ohnishi 2006]. In addition, it should be noted that the kinetic theory molecular dynamics [Graziani 2014b, Haack 2017] can be used to simulate certain stages of a target compression.

Appendix A

Functionals and functional differentiation

In this Appendix the functional derivatives needed to follow the derivations in chapter 3 are given. For an extended and mathematically rigorous discussion the interested reader is referred to Refs. [Giaquinta 2004a, Giaquinta 2004b, Hansen 2013].

A functional $F[f_1, f_2, ..., f_N]$ is given by an operation (procedure), which takes as an input (argument) a function or a set of functions and gives a number as an output. In the context of this thesis, this operation is defined by the integration over the variables of a function (or functions). The functional derivative $\frac{\delta F}{\delta f_1(\mathbf{r}_1)}$ is defined as

$$\int \frac{\delta F[f_1(\mathbf{r}_1), ..., f_N(\mathbf{r}_N)]}{\delta f_1(\mathbf{r}_1)} \xi(\mathbf{r}_1)\, \mathrm{d}\mathbf{r}_1 = \lim_{\varepsilon \to 0} \frac{F[f_1 + \varepsilon\xi_1, ..., f_N] - F[f_1, ..., f_N]}{\varepsilon},$$

where $\xi_1(\mathbf{r}_1)$ is an arbitrary function.

The second order functional derivative is computed as:

$$\frac{\delta^2 F}{\delta f_1(\mathbf{r}_1)\delta f_1(\mathbf{r}_1')} = \frac{\delta}{\delta f_1(\mathbf{r}_1')}\left(\frac{\delta F}{\delta f_1(\mathbf{r}_1)}\right).$$

In this work the following functionals and their derivatives are used:

$$\begin{aligned} F[f] &= \int J[f(\mathbf{r})]\mathrm{d}\mathbf{r}, \\ \frac{\delta F[f]}{\delta f(\mathbf{r})} &= \frac{\partial J[f]}{\partial f}, \\ \frac{\delta^2 F[f]}{\delta f(\mathbf{r})\delta f(\mathbf{r}')} &= \frac{\partial^2 J[f]}{\partial f^2}\delta(\mathbf{r} - \mathbf{r}'), \end{aligned} \tag{A.1}$$

where $J[f]$ denotes an ordinary function of f.

$$\begin{aligned} F[f] &= \int J[f(\mathbf{r}), \nabla f(\mathbf{r})]\, \mathrm{d}\mathbf{r}, \\ \frac{\delta F[f]}{\delta f(\mathbf{r})} &= \frac{\partial J[f(\mathbf{r}), \nabla f(\mathbf{r})]}{\partial f} - \nabla \frac{\partial J[f(\mathbf{r}), \nabla f(\mathbf{r})]}{\partial \nabla f}. \end{aligned} \tag{A.2}$$

where $J[f, \nabla f]$ is an ordinary function of f and ∇f.

$$\begin{aligned} F[f] &= \int W(|\mathbf{r} - \mathbf{r}'|) f(\mathbf{r}) f(\mathbf{r}')\, \mathrm{d}\mathbf{r}\mathrm{d}\mathbf{r}', \\ \frac{\delta F[f]}{\delta f(\mathbf{r})} &= 2 \int W(|\mathbf{r} - \mathbf{r}'|) f(\mathbf{r}')\, \mathrm{d}\mathbf{r}', \\ \frac{\delta^2 F[f]}{\delta f(\mathbf{r}) \delta f(\mathbf{r}')} &= 2W(|\mathbf{r} - \mathbf{r}'|). \end{aligned} \tag{A.3}$$

where $W(|\mathbf{r} - \mathbf{r}'|)$ is a function of $|\mathbf{r} - \mathbf{r}'|$.

$$\begin{aligned} F[f] &= \int [f(\mathbf{r})]^a W\left(\mathbf{r} - \mathbf{r}'\right) \left[f(\mathbf{r}')\right]^b \mathrm{d}\mathbf{r}\mathrm{d}\mathbf{r}' \\ \frac{\delta F[f]}{\delta f(\mathbf{r})} &= a f^{(a-1)}(\mathbf{r}) \int W\left(\mathbf{r} - \mathbf{r}'\right) f^b(\mathbf{r}')\, \mathrm{d}\mathbf{r}' \\ &\quad + b f^{(b-1)}(\mathbf{r}) \int W\left(\mathbf{r} - \mathbf{r}'\right) f^a(\mathbf{r}')\, \mathrm{d}\mathbf{r}', \\ \frac{\delta^2 F[f]}{\delta f(\mathbf{r}) \delta f(\mathbf{r}')} &= ab \left(f(\mathbf{r})^{(a-1)} f(\mathbf{r}')^{(b-1)} + f(\mathbf{r})^{(b-1)} f(\mathbf{r}')^{(a-1)} \right) W\left(\mathbf{r} - \mathbf{r}'\right), \end{aligned} \tag{A.4}$$

where a and b are constant numbers.

Appendix B

Functional derivative of a Hamiltonian in the grand canonical ensemble

In Ref. [Zubarev 1971] it was shown that for the partial derivative of a Hamiltonian with respect to a parameter a it holds

$$\left\langle \frac{\partial \mathcal{H}}{\partial a} \right\rangle = \frac{\partial \Omega}{\partial a}, \tag{B.1}$$

where $\langle \dots \rangle$ denotes averaging over the grand canonical ensemble, and $\mathcal{H}$ is a Hamiltonian of the system at rest and in the absence of an external field, i.e $w = 0$ and $V_{\text{ext}} = 0$.

In order to extend the relation (B.1) to the case of the functional derivative, i.e. $\left\langle \frac{\delta \mathcal{H}}{\delta n} \right\rangle = \frac{\delta E}{\delta n}$, we consider the density perturbation $n_1(\mathbf{r})$ around the mean density $n_0 = \text{const}$, where $\int n_1(\mathbf{r}) \mathrm{d}\mathbf{r} = 0$. In this case we have the following expansion of the semi-classical Hamiltonian around n_0:

$$\begin{aligned} \mathcal{H}[n] = \mathcal{H}[n_0] + \int \mathrm{d}\mathbf{r} \left. \frac{\delta \mathcal{H}[n]}{\delta n(\mathbf{r})} \right|_{\mathrm{n=n_0}} n_1(\mathbf{r}) \\ + \frac{1}{2} \int \int \mathrm{d}\mathbf{r} \mathrm{d}\mathbf{r}' \left. \frac{\delta^2 \mathcal{H}[n]}{\delta n(\mathbf{r}) \delta n(\mathbf{r}')} \right|_{\mathrm{n=n_0}} n_1(\mathbf{r}) n_1(\mathbf{r}') + \dots, \end{aligned} \tag{B.2}$$

where n_0 is understood as the smoothed (coarse-grained) density distribution with respect to microscopic density fluctuations.

From Eq. (B.2), we immediately see that

$$\frac{\delta \mathcal{H}[n]}{\delta n(\mathbf{r})} = \left. \frac{\delta \mathcal{H}[n]}{\delta n(\mathbf{r})} \right|_{\mathrm{n=n_0}} + \int \mathrm{d}\mathbf{r}' \left. \frac{\delta^2 \mathcal{H}[n]}{\delta n(\mathbf{r}) \delta n(\mathbf{r}')} \right|_{\mathrm{n=n_0}} n_1(\mathbf{r}') + \dots, \tag{B.3}$$

where $\delta n = \delta n_1$.

Further, we need the following formula for the functional derivative of the functional $F[f] = \exp\left[\int f(x)g(x)\mathrm{d}x\right]$:

$$\frac{\delta F[f]}{\delta f} = g(x)\exp\left[\int f(x)g(x)\mathrm{d}x\right]. \tag{B.4}$$

Using Eqs. (B.2), (B.3), and (B.4) we arrive at

$$\frac{\delta}{\delta n}\left[e^{-(\mathcal{H}[n]-\mu_0 N)/T}\right] = -\frac{1}{T}\frac{\delta\mathcal{H}[n]}{\delta n}e^{-(\mathcal{H}[n]-\mu_0 N)/T}, \tag{B.5}$$

where T is in energy units ($k_B = 1$).

Eq. B.5 allows us to deduce the desired result:

$$\begin{aligned}\frac{\delta E}{\delta n} &= \left\langle\frac{\delta\mathcal{H}}{\delta n}\right\rangle = e^{\Omega/T}\mathrm{Tr}\left(e^{-(\mathcal{H}[n]-\mu_0 N)/T}\frac{\delta\mathcal{H}}{\delta n}\right)\\ &= -Te^{\Omega/T}\frac{\delta}{\delta n}\mathrm{Tr}\left(e^{-(\mathcal{H}[n]-\mu_0 N)/T}\right) = -Te^{\Omega/T}\frac{\delta}{\delta n}e^{-\Omega/T}\\ &= -Te^{\Omega/T}\left(-\frac{1}{T}\frac{\delta\Omega}{\delta n}\right)e^{-\Omega/T} = \frac{\delta\Omega}{\delta n}.\end{aligned}$$

Appendix C

Wake effect in quantum plasmas

The effects of quantum non-locality and correlations are more pronounced in the case of a streaming plasma. This demonstrated here by considering the dynamically screened ion potential* [Ludwig 2010],

$$\Phi(\mathbf{r}) = \int \frac{\mathrm{d}^3k}{2\pi^2} \frac{Q}{k^2\epsilon(\mathbf{k}, \omega = \mathbf{k}\cdot\mathbf{v}_s)}\, e^{i\mathbf{k}\cdot\mathbf{r}} \quad , \tag{C.1}$$

where v_s is the streaming velocity of the electrons relative to an ion and $\epsilon(\mathbf{k}, \omega)$ is computed using the polarization function in relaxation-time approximation, Eq. (3.87), with the following dynamical collision frequency [Reinholz 2000, Wierling 2001]:

$$\nu_{ei}^{\mathrm{LB}}(\omega) = -i\frac{\epsilon_0 n_i \Omega_0^2}{6\pi^2 e^2 n_e m_e} \int_0^\infty dk\, k^6 \tilde{\phi}_{ei}^2(k) \times \frac{1}{\omega}\left[\epsilon_{\mathrm{RPA}}^{-1}(k,\omega) - \epsilon_{\mathrm{RPA}}^{-1}(k,0)\right], \tag{C.2}$$

where Ω_0 is a normalization volume, and $\tilde{\phi}_{ei}$ is the bare Coulomb interaction potential between an electron and an ion. Note that here the dynamical collision frequency is given in the SI units. Eq. (C.2) represents the dynamical collision frequency due to electron-ion correlations in the second order Born approximation and, in the case $\theta \ll 1$, can be used at $n \geq 1.6 \times 10^{24}\mathrm{cm}^{-3}$ ($r_s \leq 1$). Eq. (C.2) is referred to as the Lenard-Balescu (LB) dynamical collision frequency. Clearly, it takes into account the screening and related electronic quantum non-locality effects.

As a computationally easier way to incorporate the frequency dependent collision frequency, the following form of the dynamical collision frequency

* 3D Fourier transformation was performed using the modified version of KIELSTREAM [Ludwig 2014]. The latter was originally designed for the calculation of the screened potential in a streaming classical complex plasma. Therefore, for the considered case, the code has been modified by implementing the dynamic dielectric function for quantum electrons.

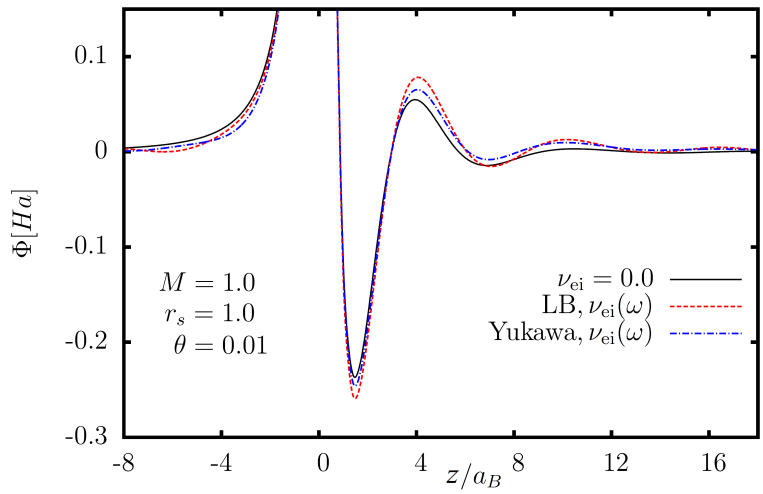

Figure C.1: The dynamically screened ion potential $\Phi(z, r = 0)$ for collisional and collisionless systems. The potential is presented along the streaming direction z. The ion is positioned at $(r = 0, z = 0)$.

is often used instead of Eq. (C.2) [Wierling 2001, Fortmann 2010]:

$$\nu_{ei}^{\rm Y}(\omega) = -i\frac{\epsilon_0 n_i \Omega_0^2}{6\pi^2 e^2 n_e m_e}\frac{1}{\omega}\int_0^\infty dk\, k^6 \tilde{\Phi}_Y^2(k) \times \left[\epsilon_{\rm RPA}(k,\omega) - \epsilon_{\rm RPA}(k,0)\right], \tag{C.3}$$

where $\tilde{\Phi}_Y(k) = \tilde{\phi}_{ei}(k)/\epsilon_{\rm RPA}(k \to 0, \omega = 0)$ is the electron-ion interaction taking into account the static screening in the long wavelength approximation (cf., Eq. (4.17)).

The main difference between $\nu_{ei}^{\rm LB}(\omega)$ and $\nu_{ei}^{\rm Y}(\omega)$ is that the former takes into account a plasmons excitation while the latter does not. In addition, $\nu_{ei}^{\rm Y}$ obviously provides a somewhat less accurate description of the electronic non-locality, as the long wavelength approximation is involved. Eq. (C.3) was derived from Eq. (C.2) assuming that $\mathrm{Im}\left[\epsilon_{\rm RPA}\right]/\mathrm{Re}\left[\epsilon_{\rm RPA}\right] \ll 1$ [Wierling 2001].

The importance of the effects of correlations and non-locality can be gauged by comparing the dynamically screened potentials computed using $\nu_{ei} = 0$ (i.e., neglecting collisions), $\nu_{ei}^{\rm LB}(\omega)$, and $\nu_{ei}^{\rm Y}(\omega)$. The results of these calculations are presented in Figs. C.1 and C.2 for $r_s = 1$, $\theta = 0.01$, $Z = 1$, with the streaming velocity defined by the parameter $M = v_s/v_F$. In this

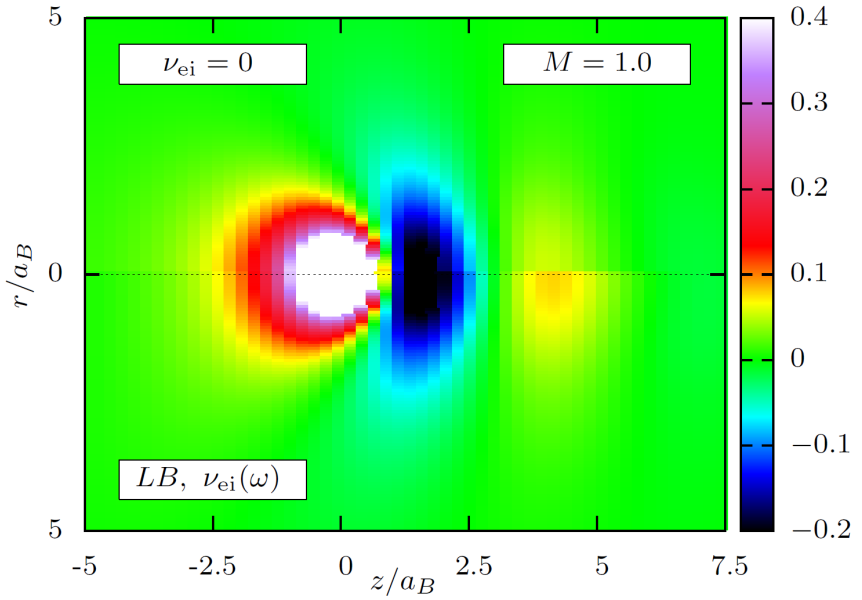

Figure C.2: The dynamically screened ion potentials for collisional (the lower part of the figure) and collisionless (the upper part of the figure) plasmas. The dynamical collision frequency is computed using Eq. (C.2).

figure, the ion is located at $(r = 0, z = 0)$ and the streaming of the electrons is directed from left to right (in the direction opposite to the z axis). In Fig. C.1, the dynamically screened ion potential along the z axis at $r = 0$ is shown. From this figure we see that (i) the effect of collisions (correlations) is significant, and (ii) the $\nu_{ei}^{\rm Y}(\omega)$ based result is not able to provide an accurate approximation to the one calculated using $\nu_{ei}^{\rm LB}(\omega)$. Thus, a fully non-local treatment is crucial. In Fig. C.2, the upper part represents the collisionless case and the lower part the case with $\nu_{ei}^{\rm LB}(\omega)$. From Figs. C.2 and C.1 it is clearly seen that the collisions lead to a stronger repulsive region (the areas around the positive maximums at $(z > 0, r = 0)$) and a stronger attractive part (the area around the first negative minimum of the potential). This is the illustration of the collision-induced wake amplification [Moldabekov 2016]. Apart from that, the wakefield in quantum plasmas has the inverse V shape at $z > 0$, in contrast to that of in a classical plasma [Moldabekov 2015c]. Therefore, both quantum and correlation effects are

highly important in the case of streaming quantum plasmas.

It should be remarked that, for dense plasmas, *the results for the dynamically screened ion potential with the self-consistently computed dynamical collision frequency are presented here for the first time.* In previous works electron-ion collisions were neglected or treated as a constant that is independent of plasma parameters [Moldabekov 2015a, Moldabekov 2015c, Moldabekov 2016, Ludwig 2018, Else 2010].

Appendix D

The stiffness theorem at finite temperature

The relation between the static inverse density response function and a change in the free energy due to a density perturbation by an external field reads [Gravel 2007]

$$F[n] - F_0[n_0] = \frac{1}{\Omega}\sum_{\mathbf{k}} \frac{\chi(\mathbf{k})|e\tilde{V}_{\text{ext}}(\mathbf{k})|^2}{2} = \frac{1}{\Omega}\sum_{\mathbf{k}} \frac{|\tilde{n}(\mathbf{k})|^2}{2\chi(\mathbf{k})}, \tag{D.1}$$

where $\chi = -\tilde{n}(\mathbf{k})/[e\tilde{V}_{\text{ext}}(\mathbf{k})]$ is the density-density response function (related to the polarization function via Eq. (4.9)).

Eq. (D.1) is a special case of the so-called *stiffness theorem* at finite temperature [Giuliani 2008]. Indeed, Eq. (D.1) resembles a *"stiffness energy"* proportional to the square of the variable (density) deviation from an equilibrium value, $|\tilde{n}|^2$, and to the *stiffness* of the system, which is given by χ^{-1}.

Herein I would like to provide a derivation of Eq. (D.1) that is based on the fact that the density distribution of a system at equilibrium minimizes the free energy of the system. The derivation presented here has the advantage of being rather simple, although it cannot be called rigorous in a mathematical sense.

Eq. (D.1) can be derived starting from the total *intrinsic free energy* of the perturbed system,

$$\begin{aligned} F[n] - \left(\frac{e^2}{2}\int \frac{\tilde{n}(\mathbf{r})\tilde{n}(\mathbf{r}')}{|\mathbf{r}-\mathbf{r}'|}\mathrm{d}\mathbf{r}\mathrm{d}\mathbf{r}' - \int e\tilde{n}(\mathbf{r})V_{\text{ext}}(\mathbf{r})\mathrm{d}\mathbf{r}\right) \\ = F_0[n_0] + \int K(\mathbf{r}-\mathbf{r}')\tilde{n}(\mathbf{r})\tilde{n}(\mathbf{r}')\,\mathrm{d}\mathbf{r}\mathrm{d}\mathbf{r}' + \\ + \int L(\mathbf{r},\mathbf{r}',\mathbf{r}'')\tilde{n}(\mathbf{r})\tilde{n}(\mathbf{r}')\tilde{n}(\mathbf{r}'')\,\mathrm{d}\mathbf{r}\mathrm{d}\mathbf{r}'\mathrm{d}\mathbf{r}'' + ..., \end{aligned} \tag{D.2}$$

where $F_0[n_0]$ is the unperturbed free energy, n_0 the mean density, V_{ext} a weak external field, and $n = n_0 + \tilde{n}$, with $|\tilde{n}|/n_0 \ll 1$, is the electron density after perturbation. In Eq. (D.1), the expansion of the *intrinsic free energy* in terms of the density perturbation $\tilde{n}$ is used [cf., Eq. (B.2)]. The contribution in Eq. (D.2) due to the term linear in $\tilde{n}$ vanishes as a result of the conditions $\int \tilde{n}(\mathbf{r})\mathrm{d}\mathbf{r} = 0$ and $\frac{\delta F[n]}{\delta n}|_{n_0} = \text{const}$. Further, we neglect the terms related to nonlinear response features, i.e., the terms with the kernel L and higher order terms.

The minimization condition of $F[n]$, applied in Eq. (D.2), yields

$$-e\varphi_{\text{eff}}(\mathbf{r}) = 2\int K(\mathbf{r}-\mathbf{r}')\tilde{n}(\mathbf{r}')\,\mathrm{d}\mathbf{r}', \tag{D.3}$$

where $\varphi_{\text{eff}}(\mathbf{r})$ is the effective potential defined by Eq. (3.9).

Using Eq. (D.3), the Fourier expansion of $K(\mathbf{r}-\mathbf{r}')$, and the convolution theorem we arrive at

$$\tilde{K}(\mathbf{k}) = -\frac{e\tilde{\varphi}_{\text{eff}}(\mathbf{k})}{2\tilde{n}(\mathbf{k})} = -\frac{1}{2\Pi(\mathbf{k})}. \tag{D.4}$$

Finally, substituting Eqs. (D.3) and (D.4) into Eq. (D.2) we deduce Eq. (D.1).

Considering non-interacting electrons, we see that in the static case Eq. (3.81) agrees with Eq. (D.4) except for the constant summand. The latter appears because $F_0[n]$ in Eqs. (3.32) and (3.78) is the free energy of the perturbed system, in contrast to $F_0[n_0]$ in Eq. (D.2). Therefore, the results represented by Eqs. (3.81) and (D.4) are consistent with each other.

Appendix E

Convergence of the long wavelength expansion of $\Pi^{-1}_{\mathrm{RPA}}(k, \omega = 0)$

In this appendix the convergence of the expansion (3.38) for the static case in the limit of long wavelengths, $k \ll 2k_F$, is discussed. We consider the dimensionless inverse static polarization function for the three dimensional case, i.e.,

$$\overline{\Pi}^{-1}_{\mathrm{RPA}}(k) = \frac{\Pi^{\mathrm{D=3}}_{\mathrm{RPA}}(k=0)}{\Pi^{\mathrm{D=3}}_{\mathrm{RPA}}(k)} = 1 + \frac{\tilde{a}_2}{\tilde{a}_0}k^2 + ... + \frac{\tilde{a}_{2l}}{\tilde{a}_0}k^{2l} + ... \tag{E.1}$$

The coefficient $\tilde{a}_0$ is given by Eq. (3.46) and $\tilde{a}_2$ is defined by Eq. (3.47) (taking into account that $\tilde{a}_2 = -a_2$). Other coefficients up to $\tilde{a}_8$ are the following [Moldabekov 2015b]:

$$\begin{aligned}
\frac{\tilde{a}_4(n,T)}{\tilde{a}_0(n,T)} &= \frac{b_1^2 - b_2}{16k_F^4}, \\
\frac{\tilde{a}_6(n,T)}{\tilde{a}_0(n,T)} &= \frac{-b_1^3 + 2b_1b_2 - b_3}{64k_F^6}, \\
\frac{\tilde{a}_8(n,T)}{\tilde{a}_0(n,T)} &= \frac{b_1^4 - 3b_1^2b_2 + b_2^2 + 2b_1b_3 - b_4}{256k_F^8},
\end{aligned} \tag{E.2}$$

where b_i involve Fermi integrals $I_i(\eta)$ of different orders:

$$b_i\left([n], \theta\right) = \frac{\theta^{-i}}{2i+1}\frac{I_{-i-1/2}(\eta)}{I_{-1/2}(\eta)}.$$

The convergence of the expansion (E.1), in the case of the homogeneous electron gas, is illustrated in Fig. E.1. From this figure we see that the first term, with $l = 2$, provides an accurate description at $k/k_F < 1$, which

improves with increasing temperature, θ. For $\theta \gtrsim 1$, a very accurate interpolation of $\Pi^{-1}_{\mathrm{RPA}}(k,0)$ at $k < 2k_F$ is presented by

$$\Pi^{-1}_{\mathrm{RPA}}(k,0) = 2(\tilde{a}_0 + \tilde{a}_2 k^2 + \tilde{a}_4 k^4).$$

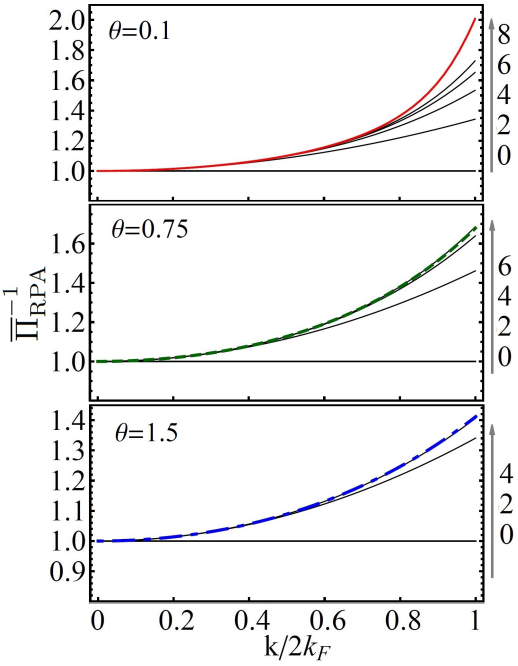

Figure E.1: The inverse static RPA polarization function is presented for the values of the degeneracy parameter 0.1, 0.75, and 1.5 (colored curves). Solid thin (black) curves represent the different maximal orders of the expansion that are included, where the maximal order is indicated on the right hand side of the arrow. The expansion coefficients $\tilde{a}_4$–$\tilde{a}_8$ are given in Eq. (E.2) and $\tilde{a}_2$ is given by a_2, Eq. (3.47), multiplied by -1. From reference [Moldabekov 2018a].

Appendix F

Complete list of publications

1. Zh. Moldabekov, M. Bonitz, and T. Ramazanov. *Theoretical foundations of quantum hydrodynamics for plasmas.* Physics of Plasmas, vol. 25, page 031903, 2018.

2. Zh. Moldabekov, S. Groth, T. Dornheim, H. Kählert, M. Bonitz and T. Ramazanov. *Structural characteristics of strongly coupled ions in dense quantum plasma.* Physical Review E, vol. 98, page 023207, 2018.

3. Zh. Moldabekov, M. Bonitz and T. Ramazanov. *Gradient correction and Bohm potential for two- and one-dimensional electron gases at a finite temperature.* Contributions to Plasma Physics, vol. 57, pages 499-505, 2017.

4. Zh. Moldabekov, S. Groth, T. Dornheim, M. Bonitz and T. Ramazanov. *Ion potential in non-ideal dense quantum plasmas.* Contributions to Plasma Physics, vol. 57, pages 532-538, 2017.

5. P. Ludwig, H. Jung, H. Kählert, J.-P. Joost, F. Greiner, Zh. Moldabekov, J. Carstensen, S. Sundar, M. Bonitz, A. Piel. *Non-Maxwellian and magnetic field effects in complex plasma wakes.* The European Physical Journal D, vol. 72, page 82, 2018.

6. Zh. Moldabekov, P. Ludwig, M. Bonitz and T. Ramazanov. *Notes on Anomalous Quantum Wake Effects.* Contributions to Plasma Physics, vol. 56, pages 442-447, 2016.

7. Zh. Moldabekov, P. Ludwig, M. Bonitz, and T. Ramazanov. *Ion potential in warm dense matter: Wake effects due to streaming degenerate electrons.* Phys. Rev. E, vol. 91, page 023102, 2015.

8. Zh. Moldabekov, P. Ludwig, J.-P. Joost, M. Bonitz and T. Ramazanov. *Dynamical Screening and Wake Effects in Classical, Quantum, and Ultrarelativistic Plasmas.* Contributions to Plasma Physics, vol. 55, pages 186-191, 2015.

9. Zh. Moldabekov, T. Schoof, P. Ludwig, M. Bonitz and T. Ramazanov. *Statically screened ion potential and Bohm potential in a quantum plasma.* Physics of Plasmas, vol. 22, page 102104, 2015.

10. V. Filinov, V. Fortov, M. Bonitz, and Zh. Moldabekov. *Fermionic path integral Monte Carlo results for the uniform electron gas at finite temperature.* Phys. Rev. E, vol. 91, page 033108, 2015.

11. N. Bastykova, S. Kodanova, T. Ramazanov, Zh. Moldabekov. *Classical ion-grain scattering in plasmas: Image force correction.* Contributions to Plasma Physics, vol. 58, pages: 198-202, 2018.

12. T. Ramazanov, S. Amirov, Zh. Moldabekov. *Impact of quantum non-locality and electronic non-ideality on e-He scattering in a dense plasma.* Contributions to Plasma Physics, vol. 58, pages: 155-163, 2018.

13. T. S. Ramazanov, Zh. A. Moldabekov, M. T. Gabdullin. *Impact of single particle oscillations on screening of a test charge.* European Physical Journal D, vol. 72 page 106, 2018.

14. A. Zh. Gabdulin, T. S. Ramazanov, Zh. A. Moldabekov. *Sound speed and diffusion in 2D Yukawa liquids: Effect of dipole-dipole interaction.* Contributions to Plasma Physics, vol. 57, pages: 458-462, 2017.

15. N. Kh. Bastykova, S. K. Kodanova, T. S. Ramazanov, Zh. A. Moldabekov. *Over the barrier electron transfer from a micron sized charged dust particle to an ion in gas discharge plasmas.* Physics of Plasmas vol. 24, page 064501, 2017.

16. T. S. Ramazanov, Zh. A. Moldabekov, M. M. Muratov. *Grain surface heating in cryogenic environment.* Physics of Plasmas, vol. 24, page 050701, 2017.

17. T. S. Ramazanov, L. G. D'yachkov, K. N. Dzhumagulova, M. T. Gabdullin, M. K. Dosbolayev, Y. A. Ussenov, Zh. A. Moldabekov, O. F.

Petrov, M. M. Vasiliev, M. I. Myasnikov, V. E. Fortov, S. F. Savin, T. A. Musabayev, Z. S. Zhantayev, A. A. Aimbetov. *Experimental investigations of strongly coupled Coulomb systems of diamagnetic dust particles in a magnetic trap under microgravity conditions.* Europhysics Letters, vol. 116, page 45001, 2016.

18. M. Issanova, S. Kodanova, T. Ramazanov, N. Bastykova, Zh. Moldabekov, C.-V. Meister. *Classical scattering and stopping power in dense plasmas: the effect of diffraction and dynamic screening.* Laser and Particle Beams, vol. 34, pages: 457-466, 2016.

19. T. Ramazanov, A. Gabdulin, Zh. Moldabekov. *Effect of Dipole-Dipole Interaction on the Compressional Oscillations in Two-Dimensional Yukawa liquids.* Contributions to Plasma Physics, vol. 56, pages: 391-396, 2016.

20. T. S. Ramazanov, S. M. Amirov, Zh. A. Moldabekov. *Effective Potentials for Charge-Helium and Charge-Singly-Ionized Helium Interactions in a Dense Plasma.* Contributions to Plasma Physics, vol. 56, pages: 411-418, 2016.

21. T. S. Ramazanov, Zh. A. Moldabekov, M. T. Gabdullin. *Multipole expansion in plasmas: Effective interaction potentials between compound particles.* Physical Review E, vol. 93, page 053204, 2016.

22. T. S. Ramazanov, Zh. A. Moldabekov, M. T. Gabdullin. *Interaction between ions in hot dense plasma via screened Cornell potential.* Physics of Plasmas, vol. 23, page 042703, 2016.

23. N. Kh. Bastykova, Z. Donko, S. K. Kodanova, T. S. Ramazanov, Z. A. Moldabekov. *Manipulation of Dusty Plasma Properties via Driving Voltage Waveform Tailoring in a Capacitive Radiofrequency Discharge.* IEEE Transactions on Plasma Science, vol. 44, pages: 545-548, 2016.

24. S. K. Kodanova, T. S. Ramazanov, N. Kh. Bastykova, Zh. A. Moldabekov. *Scattering of Dust Particles With Nonzero Dipole Moments.* IEEE Transactions on Plasma Science, vol. 44, pages: 568-570, 2016.

25. T. S. Ramazanov, A. Ah. Gabdulin, Zh. A. Moldabekov. *MD Simulation of Charged Dust Particles With Dipole Moments.* IEEE Transactions on Plasma Science, vol. 43, pages: 4187-4189, 2015.

26. T. S. Ramazanov, Zh A. Moldabekov, M. T. Gabdullin. *Effective potentials of interactions and thermodynamic properties of a nonideal two-temperature dense plasma.* Physical Review E , vol. 92, page 023104, 2015.

27. S. K. Kodanova, T. S. Ramazanov, N. Kh Bastykova, Z. A. Moldabekov. *Effect of dust particle polarization on scattering processes in complex plasmas.* Physics of Plasmas, vol. 22, page 063703, 2015.

28. S. K. Kodanova, T. S. Ramazanov, M. K. Issanova, G.N. Nigmetova, Zh. A. Moldabekov. *Investigation of Coulomb Logarithm and Relaxation Processes in Dense Plasma on the Basis of Effective Potentials.* Contributions to Plasma Physics, vol. 55, pages: 271-276, 2015.

29. T. S. Ramazanov, S. K. Kodanova, M. K. Issanova, N. K. Bastykova, Zh. A. Moldabekov. *The Modern Information Technologies and Visualization Methods for Analysis of Computer Simulation Results for Complex Plasma.* Communications in Computational Physics, vol. 15, pages: 981-995, 2014.

30. Zh. A. Moldabekov, T. S. Ramazanov. *Computer Simulation of Two Component Dense Plasma by Molecular Dynamics Method.* Communications in Computational Physics, vol. 15, pages: 1159-1166, 2014.

31. T. S. Ramazanov, Zh. A. Moldabekov, M. T. Gabdullin, T. N. Ismagambetova. *Interaction potentials and thermodynamic properties of two component semiclassical plasma.* Physics of Plasmas, vol. 21, page 012706, 2014.

32. T. S. Ramazanov, S. K. Kodanova, Zh A. Moldabekov. M. K. Issanova. *Dynamical properties of non-ideal plasma on the basis of effective potentials.* Physics of Plasmas, vol. 20, page 112702, 2013.

33. Zh. A. Moldabekov, T. S. Ramazanov, K. N. Dzhumagulova. *Pair Interaction Potential of Particles for Two-Component Plasma.* Contributions to Plasma Physics, vol. 52, pages: 207-210, 2012.

34. T. S. Ramazanov, Zh. A. Moldabekov, K. N. Dzhumagulova, M. M. Muratov. *Pseudopotentials of the particles interactions in complex plasmas.* Physics of Plasmas, vol. 18, page 103705, 2011.

35. T. S. Ramazanov, S. K. Kodanova, T. T. Daniyarov, Zh. A. Moldabekov. *Investigation an Effective Interaction Potential of Dust Particles in Nonideal Dusty Plasma.* Contributions to Plasma Physics, vol. 51, pages: 514-518, 2011.

Bibliography

[Abdourahmane 2017] D. Abdourahmane and M. Murillo. *A viscous quantum hydrodynamics model based on dynamic density functional theory.* Scientific Reports, vol. 7, page 15352, 2017. (Cited on page 111.)

[Abedi 2010] A. Abedi, N. T. Maitra and E. K. U. Gross. *Exact Factorization of the Time-Dependent Electron-Nuclear Wave Function.* Phys. Rev. Lett., vol. 105, page 123002, 2010. (Cited on pages 25, 26 and 27.)

[Akbari-Moghanjoughi 2013] M. Akbari-Moghanjoughi. *Shukla-Eliasson attractive force: Revisited.* Journal of Plasma Physics, vol. 79, no. 2, pages 189–196, 2013. (Cited on page 31.)

[Akbari-Moghanjoughi 2014] M. Akbari-Moghanjoughi. *Coupled Langmuir oscillations in 2-dimensional quantum plasmas.* Physics of Plasmas, vol. 21, no. 3, page 032110, 2014. (Cited on page 67.)

[Akbari-Moghanjoughi 2015] M. Akbari-Moghanjoughi. *Hydrodynamic limit of Wigner-Poisson kinetic theory: Revisited.* Physics of Plasmas, vol. 22, no. 2, page 022103, 2015. (Cited on pages 18 and 83.)

[Akbari-Moghanjoughi 2016] M. Akbari-Moghanjoughi. *Comment on "Surface waves on quantum plasma half-space with electron exchange-correlation effects" [Phys. Plasmas 22, 122112 (2015)].* Physics of Plasmas, vol. 23, no. 3, page 034701, 2016. (Cited on page 31.)

[Arista 1984] N. R. Arista and W. Brandt. *Dielectric response of quantum plasmas in thermal equilibrium.* Phys. Rev. A, vol. 29, page 1471, 1984. (Cited on pages 43, 44, 49, 51, 61 and 62.)

[Arkhipov 2010] Y. V. Arkhipov, A. Askaruly, D. Ballester, A. E. Davletov, I. M. Tkachenko and G. Zwicknagel. *Dynamic properties of one-component strongly coupled plasmas: The sum-rule approach.* Phys. Rev. E, vol. 81, page 026402, 2010. (Cited on page 42.)

[Banerjee 2000] A. Banerjee and M. K. Harbola. *Hydrodynamic approach to time-dependent density functional theory; Response properties of*

metal clusters. J. Chem. Phys., vol. 113, page 5614, 2000. (Cited on page 35.)

[Bao 2016] G. Bao, D. Liu and S. Luo. *Multiscale modeling and computation of optically manipulated nano devices.* Journal of Computational Physics, vol. 316, pages 558 – 572, 2016. (Cited on pages 26 and 27.)

[Barriga-Carrasco 2006] M. D. Barriga-Carrasco and A. Y. Potekhin. *Proton stopping in plasmas considering e^- – e^- collisions.* Laser Part. Beams, vol. 24, page 553, 2006. (Cited on page 58.)

[Barriga-Carrasco 2009] M. D. Barriga-Carrasco. *Comparison between static LFC and Mermin dielectric functions on proton stopping in a degenerate electron gas.* Nuclear Instruments and Methods in Physics Research Section A: Accelerators, Spectrometers, Detectors and Associated Equipment, vol. 606, no. 1, pages 215 – 217, 2009. Heavy Ion Inertial Fusion. (Cited on page 79.)

[Bates 2018] J. W. Bates, J. F. Myatt, J. G. Shaw, R. K. Follett, J. L. Weaver, R. H. Lehmberg and S. P. Obenschain. *Mitigation of cross-beam energy transfer in inertial-confinement-fusion plasmas with enhanced laser bandwidth.* Phys. Rev. E, vol. 97, page 061202, 2018. (Cited on page 41.)

[Benedict 2017] L. X. Benedict, M. P. Surh, G. S. Stanton, C. R. Scullard, A. A. Correa, J. I. Castor, F. R. Graziani, L. A. Collins, O. Čertík, D. J. Kress and M. S. Murillo. *Molecular dynamics studies of electron-ion temperature equilibration in hydrogen plasmas within the coupled-mode regime.* Phys. Rev. E, vol. 95, page 043202, 2017. (Cited on page 79.)

[Bennadji 2009] K. Bennadji, M.-M. Gombert and A. Bendib. *Local-field-correction effects on the electron response functions and on the electrical conductivity in a hydrogen plasma.* Phys. Rev. E, vol. 79, page 016408, 2009. (Cited on pages 79, 85 and 112.)

[Bennadji 2011] K. Bennadji. *Local Field Corrections Effect on Equation of State in Dense Hydrogen Plasma: Plasma Phase Transition.* Contributions to Plasma Physics, vol. 51, no. 7, pages 615–620, 2011. (Cited on pages 79 and 112.)

[Berry 1984] M. V. Berry. *Quantal phase-factors accompanying adiabatic changes.* Proceedings of the Royal Society of London Series A-mathematical and Physical Sciences, vol. 392, no. 1802, pages 45–57, 1984. (Cited on page 26.)

[Boehly 1997] T. R. Boehly *et al. Initial performance results of the OMEGA laser system.* Optics Communications, vol. 133, no. 1-6, pages 495–506, 1997. (Cited on page 24.)

[Bohm 1952a] D. Bohm. *A Suggested Interpretation of the Quantum Theory in Terms of "Hidden" Variables. I.* Phys. Rev., vol. 85, pages 166–179, 1952. (Cited on page 18.)

[Bohm 1952b] D. Bohm. *A Suggested Interpretation of the Quantum Theory in Terms of "Hidden" Variables. II.* Phys. Rev., vol. 85, pages 180–193, 1952. (Cited on page 18.)

[Bohm 1954] D. Bohm and J. P. Vigier. *Model of the Causal Interpretation of Quantum Theory in Terms of a Fluid with Irregular Fluctuations.* Phys. Rev., vol. 96, pages 208–216, 1954. (Cited on page 18.)

[Bonitz 2005] M. Bonitz, V. S. Filinov, V. E. Fortov, P. R. Levashov and H. Fehske. *Crystallization in Two-Component Coulomb Systems.* Phys. Rev. Lett., vol. 95, page 235006, 2005. (Cited on page 23.)

[Bonitz 2013a] M. Bonitz, E. Pehlke and T. Schoof. *Attractive forces between ions in quantum plasmas: Failure of linearized quantum hydrodynamics.* Phys. Rev. E, vol. 87, page 033105, 2013. (Cited on pages 18, 31 and 46.)

[Bonitz 2013b] M. Bonitz, E. Pehlke and T. Schoof. *Comment on "Discussion on novel attractive force between ions in quantum plasmas–failure of simulations based on a density functional approach".* Phys. Rev. E, vol. 87, page 033105, 2013. (Cited on pages 18 and 46.)

[Bonitz 2013c] M. Bonitz, E. Pehlke and T. Schoof. *Comment on "Discussion on novel attractive force between ions in quantum plasmas–failure of simulations based on a density functional approach".* Physica Scripta, vol. 88, no. 5, page 057001, 2013. (Cited on pages 31 and 46.)

[Bonitz 2016] M. Bonitz. Quantum kinetic theory, second edition. 2nd ed. Springer, Berlin, 2016. (Cited on pages 16, 30, 58, 62 and 79.)

[Bredow 2003] R. Bredow, Th. Bornath, W.-D. Kraeft and R. Redmer. *Hypernetted Chain Calculations for Multi-Component and Non-Equilibrium Plasmas.* Contributions to Plasma Physics, vol. 53, no. 4-5, pages 276–284, 2003. (Cited on page 16.)

[Bret 1993] A. Bret and C. Deutsch. *Dielectric response function and stopping power of a two-dimensional electron gas.* Phys. Rev. E, vol. 48, pages 2994–3002, 1993. (Cited on pages 61 and 62.)

[Brown 1972] Lowell S. Brown. *Classical Limit and the WKB Approximation.* American Journal of Physics, vol. 40, no. 3, pages 371–376, 1972. (Cited on page 28.)

[Bruhn 2011] H. Bruhn, H. Kählert, T. Ott, M. Bonitz, J. Wrighton and J. W. Dufty. *Theoretical description of spherically confined, strongly correlated Yukawa plasmas.* Phys. Rev. E, vol. 84, page 046407, 2011. (Cited on pages 87 and 88.)

[Caizergues 2014] C. Caizergues, T. Blenski and R. Piron. *Linear response of a variational average atom in plasma: Semi-classical model.* High Energy Density Physics, vol. 12, pages 12 – 20, 2014. (Cited on page 52.)

[Campa 2009] A. Campa, T. Dauxois and S. Ruffo. *Statistical mechanics and dynamics of solvable models with long-range interactions.* Physics Reports, vol. 480, no. 3, pages 57 – 159, 2009. (Cited on page 36.)

[Cederbaum 2008] L. S. Cederbaum. *Born–Oppenheimer approximation and beyond for time-dependent electronic processes.* The Journal of Chemical Physics, vol. 128, no. 12, page 124101, 2008. (Cited on page 27.)

[Chabrier 1990] G Chabrier. *An equation of state for fully ionized hydrogen.* Journal De Physique, vol. 51, no. 15, pages 1607–1632, 1990. (Cited on page 23.)

[Chihara 2001] J. Chihara, I. Fukumoto, M. Yamagiwa and H. Totsuji. *Pressure formulae for liquid metals and plasmas based on the density-*

functional theory. J. Phys.: Condens. Matter, vol. 13, page 7183, 2001. (Cited on page 37.)

[Ciracì 2016] C. Ciracì and F. Della Sala. *Quantum hydrodynamic theory for plasmonics: Impact of the electron density tail.* Phys. Rev. B, vol. 93, page 205405, 2016. (Cited on pages 31, 32, 49 and 111.)

[Clérouin 2015a] J. Clérouin, Ph. Arnault, G. Robert, C. Ticknor, J. D. Kress and L. A. Collins. *Self-Organization in Dense Plasmas: The Gamma-Plateau.* Contributions to Plasma Physics, vol. 55, no. 2-3, pages 159–163, 2015. (Cited on page 76.)

[Clérouin 2015b] J. Clérouin, G. Robert, P. Arnault, C. Ticknor, J. D. Kress and L. A. Collins. *Evidence for out-of-equilibrium states in warm dense matter probed by x-ray Thomson scattering.* Phys. Rev. E, vol. 91, page 011101, 2015. (Cited on pages 18 and 24.)

[Corradini 1998] M. Corradini, R. Del Sole, G. Onida and M. Palummo. *Analytical expressions for the local-field factor $G(q)$ and the exchange-correlation kernel $K_{xc}(r)$ of the homogeneous electron gas.* Phys. Rev. B, vol. 57, page 14569, 1998. (Cited on pages 41, 80, 81 and 98.)

[Crouseilles 2008] N. Crouseilles, P.-A. Hervieux and G. Manfredi. *Quantum hydrodynamic model for the nonlinear electron dynamics in thin metal films.* Phys. Rev. B, vol. 78, page 155412, 2008. (Cited on pages 18, 31, 32, 39 and 111.)

[Cuneo 2012] M. E. Cuneo *et al. Magnetically driven implosions for inertial confinement fusion at Sandia National Laboratories.* IEEE Trans. Plasma Sci., vol. 40, page 3222, 2012. (Cited on page 15.)

[Dabrowski 1986] B. Dabrowski. *Dynamical local-field factor in the response function of an electron gas.* Phys. Rev. B, vol. 34, page 4989, 1986. (Cited on page 41.)

[D'Adamo 2013] G. D'Adamo, A. Pelissetto and C. Pierleoni. *Predicting the thermodynamics by using state-dependent interactions.* The Journal of Chemical Physics, vol. 138, no. 23, page 234107, 2013. (Cited on page 89.)

[Daligault 2017] J. Daligault. *Crossover from classical to Fermi liquid behavior in dense plasmas.* Phys. Rev. Lett., vol. 119, page 045002, 2017. (Cited on page 58.)

[Dandrea 1986] R. G. Dandrea, N. W. Ashcroft and A. E. Carlsson. *Electron liquid at any degeneracy.* Phys. Rev. B, vol. 34, page 2097, 1986. (Cited on page 42.)

[Das Sarma 2015] S. Das Sarma and E. H. Hwang. *Screening and transport in 2D semiconductor systems at low temperatures.* Scientific Reports, vol. 5, page 16655, 2015. (Cited on page 60.)

[Das 1976] A. K. Das. *Some properties of an electron gas in a quantizing magnetic field.* Physica A: Statistical Mechanics and its Applications, vol. 85, no. 3, pages 575 – 588, 1976. (Cited on page 70.)

[Daughton 2000] W. Daughton, M. Michael and T. Lester. *Empirical bridge function for strongly coupled Yukawa systems.* Phys. Rev. E, vol. 61, pages 2129–2132, 2000. (Cited on pages 87 and 90.)

[Dharma-wardana 2000] M. W. C. Dharma-wardana and F. Perrot. *Simple Classical Mapping of the Spin-Polarized Quantum Electron Gas: Distribution Functions and Local-Field Corrections.* Phys. Rev. Lett., vol. 84, pages 959–962, 2000. (Cited on page 16.)

[Ding 2018] K. Ding, H. Hu, T. C. Leung and C. T. Chan. *Nanocorrugation-Induced Forces between Electrically Neutral Metallic Objects.* ACS Nano, vol. 12, no. 1, pages 804–812, 2018. PMID: 29257875. (Cited on page 112.)

[Dornheim 2016] T. Dornheim, S. Groth, T. Sjostrom, F. D. Malone, W. M. C. Foulkes and M. Bonitz. *Ab initio quantum Monte Carlo simulation of the warm dense electron gas in the thermodynamic limit.* Phys. Rev. Lett., vol. 117, page 156403, 2016. (Cited on page 41.)

[Dornheim 2017a] T. Dornheim, S. Groth and M. Bonitz. *Ab initio results for the static structure factor of the warm dense electron gas.* Contrib. Plasma Phys., vol. 57, page 468, 2017. (Cited on pages 42 and 80.)

[Dornheim 2017b] T. Dornheim, S. Groth, J. Vorberger and M. Bonitz. *Permutation blocking path integral Monte Carlo approach to the static density response of the warm dense electron gas.* Phys. Rev. E, vol. 96, page 023203, 2017. (Cited on page 42.)

[Dornheim 2018] T. Dornheim, S. Groth and M. Bonitz. *The uniform electron gas at warm dense matter conditions.* Physics Reports, vol. 744, pages 1 – 86, 2018. (Cited on pages 16 and 81.)

[Dufty 2013] J. Dufty and S. Dutta. *Classical representation of a quantum system at equilibrium: Theory.* Phys. Rev. E, vol. 87, page 032101, 2013. (Cited on page 16.)

[Dutta 2013] S. Dutta and J. Dufty. *Classical representation of a quantum system at equilibrium: Applications.* Phys. Rev. E, vol. 87, page 032102, 2013. (Cited on page 16.)

[Eguiluz 1975] A. Eguiluz, S. C. Ying and J. J. Quinn. *Influence of the electron density profile on surface plasmons in a hydrodynamic model.* Phys. Rev. B, vol. 11, pages 2118–2121, 1975. (Cited on page 30.)

[Eguiluz 1976] A. Eguiluz and J. J. Quinn. *Hydrodynamic model for surface plasmons in metals and degenerate semiconductors.* Phys. Rev. B, vol. 14, pages 1347–1361, 1976. (Cited on page 69.)

[Eliasson 2008] B. Eliasson and P. Shukla. *Nonlinear quantum fluid equations for a finite temperature Fermi plasma.* Physica Scripta, vol. 78, no. 2, page 025503, 2008. (Cited on page 31.)

[Else 2010] D. Else, R. Kompaneets and S. V. Vladimirov. *Shielding of a moving test charge in a quantum plasma.* Phys. Rev. E, vol. 82, page 026410, 2010. (Cited on page 122.)

[Englert 1992] B.-G. Englert. *Energy functionals and the Thomas-Fermi model in momentum space.* Phys. Rev. A, vol. 45, pages 127–134, 1992. (Cited on page 68.)

[Eschrig 1996] H. Eschrig. The fundamentals of density functional theory. Teubner, Stuttgart, 1996. (Cited on page 59.)

[Eschrig 2010] H. Eschrig. *T>0 ensemble-state density functional theory via Legendre transform.* Phys. Rev. B, vol. 82, page 205120, 2010. (Cited on page 16.)

[Fernández-Domínguez 2012] A. I. Fernández-Domínguez, A. Wiener, F. J. García-Vidal, S. A. Maier and J. B. Pendry. *Transformation-optics description of nonlocal effects in plasmonic nanostructures.* Phys. Rev. Lett., vol. 108, page 106802, 2012. (Cited on pages 59 and 111.)

[Filinov 2003] A. V. Filinov, M. Bonitz and W. Ebeling. *Improved Kelbg potential for correlated Coulomb systems.* Journal of Physics A: Mathematical and General, vol. 36, no. 22, page 5957, 2003. (Cited on page 16.)

[Filinov 2004] A. V. Filinov, V. O. Golubnychiy, M. Bonitz, W. Ebeling and J. W. Dufty. *Temperature-dependent quantum pair potentials and their application to dense partially ionized hydrogen plasmas.* Phys. Rev. E, vol. 70, page 046411, 2004. (Cited on page 16.)

[Fortmann 2010] C. Fortmann, A. Wierling and G. Röpke. *Influence of local-field corrections on Thomson scattering in collision-dominated two-component plasmas.* Phys. Rev. E, vol. 81, page 026405, 2010. (Cited on pages 79 and 120.)

[Fortov 2016] V. E. Fortov. Extreme states of matter (high energy density physics, second edition). Springer, Heidelberg, 2016. (Cited on pages 15 and 23.)

[Friedel 1952] J. Friedel. *XIV. The distribution of electrons round impurities in monovalent metals.* The London, Edinburgh, and Dublin Philosophical Magazine and Journal of Science, vol. 43, no. 337, pages 153–189, 1952. (Cited on page 81.)

[Gao 2010] X. Gao, J. Tao, G. Vignale and I. V. Tokatly. *Continuum mechanics for quantum many-body systems: Linear response regime.* Phys. Rev. B, vol. 81, page 195106, 2010. (Cited on page 28.)

[Garcia-Aldea 2012] D. Garcia-Aldea and J. E. Alvarellos. *Generalized nonlocal kinetic energy density functionals based on the von Weizsacker functional.* Phys. Chem. Chem. Phys., vol. 14, pages 1756–1767, 2012. (Cited on pages 41 and 43.)

[Gauthier 2013] M. Gauthier, C. Blancard, S. N. Chen, B. Siberchicot, M. Torrent, G. Faussurier and J. Fuchs. *Stopping power modeling in warm and hot dense matter*. High Energy Density Physics, vol. 9, no. 3, pages 488 – 495, 2013. (Cited on page 79.)

[Giaquinta 2004a] Mariano Giaquinta and Stefan Hildebrandt. Calculus of variations I. Springer Berlin Heidelberg, Berlin, Heidelberg, 2004. (Cited on page 115.)

[Giaquinta 2004b] Mariano Giaquinta and Stefan Hildebrandt. Calculus of variations II. Springer Berlin Heidelberg, Berlin, Heidelberg, 2004. (Cited on page 115.)

[Giuliani 2008] G. Giuliani and G. Vignale. Quantum Theory of the Electron Liquid. Cambridge, UK: Cambridge University Press, 2008. (Cited on pages 28, 40, 44, 55, 79, 80 and 123.)

[Glenzer 2007] S. H. Glenzer *et al.* *Observations of Plasmons in Warm Dense Matter*. Phys. Rev. Lett., vol. 98, page 065002, 2007. (Cited on pages 18 and 24.)

[Glenzer 2009] S. H. Glenzer and R. Redmer. *X-ray Thomson scattering in high energy density plasmas*. Rev. Mod. Phys., vol. 81, pages 1625–1663, 2009. (Cited on page 84.)

[Gomez 2014] M. R. Gomez *et al.* *Experimental demonstration of fusion-relevant conditions in magnetized liner inertial fusion*. Phys. Rev. Lett., vol. 113, page 155003, 2014. (Cited on page 15.)

[Grassme 1993] R. Grassme and P. Bussemer. *Friedel oscillations for temperatures $T \neq 0$*. Physics Letters A, vol. 175, no. 6, pages 441–444, 1993. (Cited on page 81.)

[Gravel 2007] S. Gravel and N. W. Ashcroft. *Nonlinear response theories and effective pair potentials*. Phys. Rev. B, vol. 76, page 144103, 2007. (Cited on pages 113 and 123.)

[Graziani 2012] F. R. Graziani *et al.* *Large-scale molecular dynamics simulations of dense plasmas: The Cimarron Project*. High Energy Density Physics, vol. 8, no. 1, pages 105–131, 2012. (Cited on pages 16 and 17.)

[Graziani 2014a] F. Graziani, M. P. Desjarlais, R. Redmer and S. B. Trickey. Frontiers and challenges in warm dense matter. Springer, 2014. (Cited on page 15.)

[Graziani 2014b] F. R. Graziani, J. D. Bauer and M. S. Murillo. *Kinetic theory molecular dynamics and hot dense matter: Theoretical foundations.* Phys. Rev. E, vol. 90, page 033104, 2014. (Cited on pages 112 and 114.)

[Greene 1969] M. P. Greene, H. J. Lee, J. J. Quinn and S. Rodriguez. *Linear Response Theory for a Degenerate Electron Gas in a Strong Magnetic Field.* Phys. Rev., vol. 177, pages 1019–1036, 1969. (Cited on page 70.)

[Gregori 2007] G. Gregori, A. Ravasio and A. H˙ *Derivation of the static structure factor in strongly coupled non-equilibrium plasmas for X-ray scattering studies.* High Energy Density Physics, vol. 3, no. 1, pages 99 – 108, 2007. Radiative Properties of Hot Dense Matter. (Cited on page 79.)

[Groth 2017a] S. Groth, T. Dornheim and M. Bonitz. *Configuration path integral Monte Carlo approach to the static density response of the warm dense electron gas.* J. Chem. Phys., vol. 147, page 164108, 2017. (Cited on pages 42 and 80.)

[Groth 2017b] S. Groth, T. Dornheim, T. Sjostrom, F. D. Malone, W. M. C. Foulkes and M. Bonitz. *Ab initio exchange-correlation free energy of the uniform electron gas at warm dense matter conditions.* Phys. Rev. Lett., vol. 119, page 135001, 2017. (Cited on page 42.)

[Haack 2017] J. R. Haack, C. D. Hauck and M. S. Murillo. *Interfacial mixing in high-energy-density matter with a multiphysics kinetic model.* Phys. Rev. E, vol. 96, page 063310, 2017. (Cited on page 114.)

[Haas 2000] F. Haas, G. Manfredi and M. Feix. *Multistream model for quantum plasmas.* Phys. Rev. E, vol. 62, pages 2763–2772, 2000. (Cited on page 49.)

[Haas 2011] F. Haas. *Introduction.* In Quantum Plasmas: An Hydrodynamic Approach, pages 1–14. Springer New York, New York, NY, 2011. (Cited on page 18.)

[Haas 2015] F. Haas and S. Mahmood. *Linear and nonlinear ion-acoustic waves in nonrelativistic quantum plasmas with arbitrary degeneracy.* Phys. Rev. E, vol. 92, page 053112, 2015. (Cited on pages 31 and 48.)

[Halevi 1995] P. Halevi. *Hydrodynamic model for the degenerate free-electron gas: Generalization to arbitrary frequencies.* Phys. Rev. B, vol. 51, pages 7497–7499, 1995. (Cited on pages 18, 52 and 59.)

[Hansen 2013] J.-P. Hansen and I. R. McDonald. Theory of simple liquids. Academic Press, Oxford, 2013. (Cited on pages 77, 84 and 115.)

[Harbola 1998] M. K. Harbola. *Differential virial theorem and quantum fluid dynamics.* Phys. Rev. A, vol. 58, page 1779, 1998. (Cited on page 55.)

[Harbour 2016] L. Harbour, M. W. C. Dharma-wardana, D. D. Klug and L. J. Lewis. *Pair potentials for warm dense matter and their application to x-ray Thomson scattering in aluminum and beryllium.* Phys. Rev. E, vol. 94, page 053211, 2016. (Cited on pages 18 and 24.)

[Harte 1996] J. A. Harte, W. E. Alley, D. S. Bailey, J. L. Eddleman and G. B. Zimmerman. *LASNEX–A 2-D physics code for modeling ICF.* Report No. UCRL-LR-105821-96-4 , Lawrence Livermore National Laboratory, 1996. (Cited on page 114.)

[Higginson 2017] D. P. Higginson *et al. Enhancement of Quasistationary Shocks and Heating via Temporal Staging in a Magnetized Laser-Plasma Jet.* Phys. Rev. Lett., vol. 119, page 255002, 2017. (Cited on pages 68 and 72.)

[Hoffmann 2005] D. H. H. Hoffmann *et al. Present and future perspectives for high energy density physics with intense heavy ion and laser beams.* Laser and Particle beams, vol. 23, page 47, 2005. (Cited on page 114.)

[Hohenberg 1964] P. Hohenberg and W. Kohn. *Inhomogeneous Electron Gas.* Phys. Rev., vol. 136, pages B864–B871, 1964. (Cited on page 28.)

[Holas 1991] A. Holas, P. M. Kozlowski and N. H. March. *Kinetic energy density and Pauli potential: dimensionality dependence, gradient expansions and non-locality.* Journal of Physics A: Mathematical and

General, vol. 24, no. 18, page 4249, 1991. (Cited on pages 60, 67 and 81.)

[Horing 1965] N. J. Horing. *Quantum theory of electron gas plasma oscillations in a magnetic field.* Annals of Physics, vol. 31, no. 1, pages 1–63, 1965. (Cited on page 70.)

[Hu 2010] S. X. Hu, B. Militzer, V. N. Goncharov and S. Skupsky. *Strong Coupling and Degeneracy Effects in Inertial Confinement Fusion Implosions.* Phys. Rev. Lett., vol. 104, page 235003, 2010. (Cited on pages 15, 24 and 113.)

[Huang 2010] C. Huang and E. A. Carter. *Nonlocal orbital-free kinetic energy density functional for semiconductors.* Phys. Rev. B, vol. 81, page 045206, 2010. (Cited on page 41.)

[Hurricane 2014] O. Hurricane *et al. Fuel gain exceeding unity in an inertially confined fusion implosion.* Nature, vol. 506, page 343, 2014. (Cited on page 15.)

[Ichimaru 1982] S. Ichimaru. *Strongly coupled plasmas: High-density classical plasmas and degenerate electron liquids.* Rev. Mod. Phys., vol. 54, page 1017, 1982. (Cited on pages 40 and 81.)

[Jérome 1982] D. Jérome and H. J. Schulz. *Organic conductors and superconductors.* Advances in Physics, vol. 31, no. 4, pages 299–490, 1982. (Cited on pages 61 and 67.)

[Jones 1971] W. Jones and W. H. Young. *Density functional theory and the von Weizsacker method.* J. Phys. C: Solid State Phys., vol. 4, page 1322, 1971. (Cited on pages 49 and 50.)

[Kählert 2014] H. Kählert, G.J. Kalmanr and M. Bonitz. *Dynamics of strongly correlated and strongly inhomogeneous plasmas.* Phys. Rev. E, vol. 90, page 011101, 2014. (Cited on page 80.)

[Kählert 2015] H. Kählert, G.J. Kalman and M. Bonitz. *Linear Fluid Theory for Weakly Inhomogeneous Plasmas with Strong Correlations.* Contributions to Plasma Physics, vol. 55, pages 352–359, 2015. (Cited on page 80.)

[Karasiev 2012] V. V. Karasiev, T. Sjostrom and S. B. Trickey. *Generalized-gradient-approximation noninteracting free-energy functionals for orbital-free density functional calculations*. Phys. Rev. B, vol. 86, page 115101, 2012. (Cited on pages 17 and 49.)

[Karasiev 2014] V. V. Karasiev, T. Sjostrom, D. Chakraborty, J. W. Dufty, K. Runge, F. E. Harris and S. B. Trickey. *Innovations in Finite-Temperature Density Functionals*. In F. Graziani, M. P. Desjarlais, R. Redmer and S. B. Tricke, editors, Frontiers and Challenges in Warm Dense Matter, pages 61–85. Springer, 2014. (Cited on pages 16 and 17.)

[Kato 1957] T. Kato. *On the eigenfunctions of many-particle systems in quantum mechanics*. Communications on Pure and Applied Mathematics, vol. 10, no. 2, pages 151–177, 1957. (Cited on page 49.)

[Kawata 2016] S. Kawata, T. Karino and A. I. Ogoyski. *Review of heavy-ion inertial fusion physics*. Matter and Radiation at Extremes, vol. 1, page 89, 2016. (Cited on pages 15 and 114.)

[Khalilpour 2015] H. Khalilpour. *Surface waves on quantum plasma half-space with electron exchange-correlation effects*. Physics of Plasmas, vol. 22, no. 12, page 122112, 2015. (Cited on page 31.)

[Khan 2014] S. Khan and M.Bonitz. *Quantum Hydrodynamics*. In M. Bonitz, J. Lopez, K. Becker and H. Thomsen, editors, Complex Plasmas: Scientific Challenges and Technological Opportunities, pages 103–152. Springer International Publishing, 2014. (Cited on pages 18, 29 and 111.)

[Kirzhnitz 1957] D. A. Kirzhnitz. *Quantum corrections to the Thomas-Fermi equation*. Zh. Eksp. Teor. Fiz., vol. 32, page 115, 1957. (Cited on page 46.)

[Kohn 1959] W. Kohn. *Image of the Fermi Surface in the Vibration Spectrum of a Metal*. Phys. Rev. Lett., vol. 2, pages 393–394, 1959. (Cited on page 102.)

[Kohn 1965] W. Kohn and L. J. Sham. *Self-Consistent Equations Including Exchange and Correlation Effects*. Phys. Rev., vol. 140, pages A1133–A1138, 1965. (Cited on page 28.)

[Koivisto 2008] M. Koivisto and M. J. Stott. *Kinetic energy functional for a two-dimensional electron system.* Phys. Rev. B, vol. 76, page 195103, 2007; errata vol. 77, page. 199902(E), May 2008. (Cited on page 59.)

[Krasavin 2018] A. V. Krasavin, P. Ginzburg and A. V. Zayats. *Free-electron Optical Nonlinearities in Plasmonic Nanostructures: A Review of the Hydrodynamic Description.* Laser & Photonics Reviews, vol. 12, no. 1, page 1700082, 2018. (Cited on page 112.)

[Krishnaswami 2015] G. S. Krishnaswami, R. Nityananda, A. Sen and A. Thyagaraja. *A Critique of Recent Semi-Classical Spin-Half Quantum Plasma Theories.* Contributions to Plasma Physics, vol. 55, no. 1, pages 3–11, 2015. (Cited on page 18.)

[Kugler 1975] A. A. Kugler. *Theory of the local field correction in an electron gas.* J. Stat. Phys., vol. 12, page 35, 1975. (Cited on page 41.)

[Kumar 2009] K. Kumar, V. Garg and R. K. Moudgil. *Spin-resolved correlations and ground state of a three-dimensional electron gas: Spin-polarization effects.* Phys. Rev. B, vol. 79, page 115304, 2009. (Cited on page 42.)

[Ladányi 1992] K. Ladányi, I. Nagy and B. Apagyi. *Partially linearized Thomas-Fermi-Weizsäcker theory for screening and stopping of charged particles in jellium.* Phys. Rev. A, vol. 45, pages 2989–2997, 1992; errata vol. 46, page. 1704, 1992. (Cited on page 49.)

[Landau 1965] L. D. Landau and E. M. Lifshitz. Quantum Mechanics (Volume 3 of A Course of Theoretical Physics). Pergamon Press, 1965. (Cited on page 28.)

[Landen 2001] O. L. Landen *et al. Dense matter characterization by X-ray Thomson scattering.* Journal Of Quantitative Spectroscopy & Radiative Transfer, vol. 71, no. 2-6, pages 465–478, 2001. (Cited on page 24.)

[Lee 2009] H. J. Lee *et al. X-Ray Thomson-Scattering Measurements of Density and Temperature in Shock-Compressed Beryllium.* Phys. Rev. Lett., vol. 102, page 115001, 2009. (Cited on pages 18 and 24.)

[Lieb 2013] E. H. Lieb and R. Schrader. *Current densities in density-functional theory.* Phys. Rev. A, vol. 88, page 032516, 2013. (Cited on page 34.)

[Liu 2014] Y. Liu and J. Wu. *An improved classical mapping method for homogeneous electron gases at finite temperature.* The Journal of Chemical Physics, vol. 141, no. 6, page 064115, 2014. (Cited on page 16.)

[Ludwig 2010] P. Ludwig, M. Bonitz, H. Kählert and J. W. Dufty. *Dynamics of strongly correlated ions in a partially ionized quantum plasma.* Journal of Physics: Conference Series, vol. 220, no. 1, page 012003, 2010. (Cited on pages 17, 25, 32, 58 and 119.)

[Ludwig 2014] P. Ludwig, C. Arran and M. Bonitz. *Introduction to Streaming Complex Plasmas B: Theoretical Description of Wake Effects.* In M. Bonitz, J. Lopez, K. Becker and H. Thomsen, editors, Complex Plasmas: Scientific Challenges and Technological Opportunities, pages 73–99. Springer International Publishing, Cham, 2014. (Cited on page 119.)

[Ludwig 2018] P. Ludwig, H. Jung, H. Kählert, J.-P. Joost, F. Greiner, Z. Moldabekov, J. Carstensen, S. Sundar, M. Bonitz and A. Piel. *Non-Maxwellian and magnetic field effects in complex plasma wakes.* The European Physical Journal D, vol. 72, no. 5, page 82, 2018. (Cited on page 122.)

[Lurie 1968] D. Lurie. *Particle and Fields.* Interscience Publishers, New York, NY, 1968. (Cited on page 34.)

[Ma 2013] T. Ma *et al. X-Ray Scattering Measurements of Strong Ion-Ion Correlations in Shock-Compressed Aluminum.* Phys. Rev. Lett., vol. 110, page 065001, 2013. (Cited on pages 18 and 24.)

[Madelung 1926] E. Madelung. *Eine anschauliche Deutung der Gleichung von Schrödinger.* Naturwissenschaften, vol. 14, no. 45, pages 1004–1004, 1926. (Cited on page 51.)

[Madelung 1927] E. Madelung. *Quantentheorie in hydrodynamischer Form.* Zeitschrift für Physik, vol. 40, no. 3, pages 322–326, 1927. (Cited on page 51.)

[Manfredi 2001] G. Manfredi and F. Haas. *Self-consistent fluid model for a quantum electron gas.* Phys. Rev. B, vol. 64, page 075316, 2001. (Cited on pages 18, 29 and 30.)

[Manfredi 2005] G. Manfredi. *How to model quantum plasmas.* Fields Inst. Commun., vol. 46, page 263, 2005. (Cited on page 31.)

[Manfredi 2018] G. Manfredi. *Preface to Special Topic: Plasmonics and solid state plasmas.* Physics of Plasmas, vol. 25, no. 3, page 031701, 2018. (Cited on page 111.)

[March 2002] N. H. March and M. P. Tosi. Introduction to liquid state physics. 2002. (Cited on pages 85 and 95.)

[Marinak 2001] M. M. Marinak, G. D. Kerbel, N. A. Gentile, O. Jones, D. Munro, S. Pollaine, T. R. Dittrich and S. W. Haan. *Three-dimensional HYDRA simulations of National Ignition Facility targets.* Physics of Plasmas, vol. 8, no. 5, pages 2275–2280, 2001. (Cited on page 114.)

[McMahon 2012] J. McMahon, M. Morales, C. Pierleoni and D. M. Ceperley. *The properties of hydrogen and helium under extreme conditions.* Rev. Mod. Phys., vol. 84, page 1607, 2012. (Cited on page 16.)

[Mermin 1964] N. D. Mermin and E. Canel. *Long wavelength oscillations of a quantum plasma in a uniform magnetic field.* Annals of Physics, vol. 26, no. 2, pages 247 – 273, 1964. (Cited on page 70.)

[Mermin 1965] N. D. Mermin. *Thermal Properties of the Inhomogeneous Electron Gas.* Phys. Rev., vol. 137, pages A1441–A1443, 1965. (Cited on page 28.)

[Mermin 1970] N. D. Mermin. *Lindhard dielectric function in the relaxation-time approximation.* Phys. Rev. B, vol. 1, page 2362, 1970. (Cited on page 58.)

[Michta 2015] D. Michta, F. Graziani and M. Bonitz. *Quantum Hydrodynamics for Plasmas - a Thomas-Fermi Theory Perspective.* Contributions to Plasma Physics, vol. 55, no. 6, pages 437–443, 2015. (Cited on pages 32, 35 and 47.)

[Moldabekov 2015a] Z. Moldabekov, P. Ludwig, M. Bonitz and T. Ramazanov. *Ion potential in warm dense matter: Wake effects due to streaming degenerate electrons.* Phys. Rev. E, vol. 91, page 023102, 2015. (Cited on pages 114 and 122.)

[Moldabekov 2015b] Z. Moldabekov, T. Schoof, P. Ludwig, M. Bonitz and T. Ramazanov. *Statically screened ion potential and Bohm potential in a quantum plasma.* Physics of Plasmas, vol. 22, no. 10, page 102104, 2015. (Cited on pages 31, 32, 46 and 125.)

[Moldabekov 2015c] Zh. Moldabekov, P. Ludwig, J.-P. Joost, M. Bonitz and T. Ramazanov. *Dynamical Screening and Wake Effects in Classical, Quantum, and Ultrarelativistic Plasmas.* Contributions to Plasma Physics, vol. 55, no. 2-3, pages 186–191, 2015. (Cited on pages 114, 121 and 122.)

[Moldabekov 2016] Zh. Moldabekov, P. Ludwig, M. Bonitz and T. Ramazanov. *Notes on Anomalous Quantum Wake Effects.* Contributions to Plasma Physics, vol. 56, no. 5, pages 442–447, 2016. (Cited on pages 114, 121 and 122.)

[Moldabekov 2017a] Zh. Moldabekov, M. Bonitz and T. Ramazanov. *Gradient correction and Bohm potential for two- and one-dimensional electron gases at a finite temperature.* Contributions to Plasma Physics, vol. 57, no. 10, pages 499–505, 2017. (Cited on pages 34, 64, 65 and 66.)

[Moldabekov 2017b] Zh. Moldabekov, S. Groth, T. Dornheim, M. Bonitz and T. Ramazanov. *Ion potential in non-ideal dense quantum plasmas.* Contributions to Plasma Physics, vol. 57, no. 10, pages 532–538, 2017. (Cited on pages 76 and 98.)

[Moldabekov 2018a] Zh. Moldabekov, M. Bonitz and T. Ramazanov. *Theoretical foundations of quantum hydrodynamics for plasmas.* Physics of Plasmas, vol. 25, no. 3, page 031903, 2018. (Cited on pages 34, 48, 50, 54, 111 and 126.)

[Moldabekov 2018b] Zh. Moldabekov, S. Groth, T. Dornheim, H. Kählert, M. Bonitz and T. Ramazanov. *Structural characteristics of strongly coupled ions in a dense quantum plasma.* submitted for publication,

arXiv:1804.11201, 2018. (Cited on pages 24, 76, 88, 89, 90, 91, 92, 93, 94, 95, 96, 97, 99, 100, 101, 103, 104, 105, 106, 108 and 109.)

[Montanari 2017] C. C. Montanari and J. E. Miraglia. *Low- and intermediate-energy stopping power of protons and antiprotons in solid targets.* Phys. Rev. A, vol. 96, page 012707, 2017. (Cited on page 79.)

[More 1986] R. M. More. *Atoms in dense plasmas.* Technical Report UCRL-93926, Lawrence Livermore National Laboratory, 1986. (Cited on page 76.)

[Moroni 1995] S. Moroni, D. M. Ceperley and G. Senatore. *Static response and local field factor of the electron gas.* Phys. Rev. Lett., vol. 75, page 689, 1995. (Cited on pages 42, 80 and 81.)

[Morozov 2005] I. Morozov, H. Reinholz, G. Röpke, A. Wierling and G. Zwicknagel. *Molecular dynamics simulations of optical conductivity of dense plasmas.* Phys. Rev. E, vol. 71, page 066408, 2005. (Cited on page 59.)

[Moses 2010a] E. I. Moses. *The National Ignition Facility and the National Ignition Campaign.* IEEE Transactions On Plasma Science, vol. 38, no. 4, 2, SI, pages 684–689, 2010. 36th IEEE International Conference on Plasma Science, San Diego, CA, MAY 31-JUN 05, 2009. (Cited on page 23.)

[Moses 2010b] E.I. Moses. *Ignition and inertial confinement fusion at the National Ignition Facility.* Journal of Physics: Conference Series, vol. 244, no. 1, page 012006, 2010. (Cited on page 23.)

[Mulser 2010] P. Mulser and D. Bauer. The laser plasma: Basic phenomena and laws, pages 5–89. Springer Berlin Heidelberg, Berlin, Heidelberg, 2010. (Cited on page 29.)

[Nersisyan 2007] H. Nersisyan, C. Toepffer and G. Zwicknagel. Interactions between charged particles in a magnetic field: a theoretical approach to ion stopping in magnetized plasmas. Springer, Berlin, 2007. (Cited on pages 69 and 70.)

[Neumayer 2010] P. Neumayer *et al.* *Plasmons in strongly coupled shock-compressed matter.* Phys. Rev. Lett., vol. 105, page 075003, 2010. (Cited on page 59.)

[Ng 1974] K.-C. Ng. *Hypernetted chain solutions for the classical one-component plasma up to* Γ*=7000.* The Journal of Chemical Physics, vol. 61, no. 7, pages 2680–2689, 1974. (Cited on pages 86, 87 and 90.)

[Niklasson 1974] G. Niklasson. *Dielectric function of the uniform electron gas for large frequencies or wave vectors.* Phys. Rev. B, vol. 10, pages 3052–3061, 1974. (Cited on page 81.)

[Ohnishi 2006] N. Ohnishi, M. Nishikino and A. Sasaki. *Numerical analysis of plasma medium of transient collisional excited X-ray laser.* J. Phys. IV France, vol. 133, pages 1193–1195, 2006. (Cited on page 114.)

[Ott 2014] T. Ott, M. Bonitz, L. G. Stanton and M. S. Murillo. *Coupling strength in Coulomb and Yukawa one-component plasmas.* Physics of Plasmas, vol. 21, no. 11, page 113704, 2014; Publisher's Note Phys. Plasmas vol. 21, page. 113704, 2014. (Cited on pages 76, 87 and 88.)

[Ott 2018] T. Ott, H. Thomsen, J.W. Abraham, T. Dornheim and M. Bonitz. *Recent progress in the theory and simulation of strongly correlated plasmas: phase transitions, transport, quantum, and magnetic field effects.* Eur. Phys. J. D, vol. 72, page 84, 2018. (Cited on page 71.)

[Paisner 1994] J. A. Paisner *et al.* *National ignition facility would boost United-states industrial competitiveness.* Laser Focus World, vol. 30, no. 5, pages 75–77, 1994. (Cited on page 24.)

[Perkins 2013] L. J. Perkins, B. G. Logan, G. B. Zimmerman and C. J. Werner. *Two-dimensional simulations of thermonuclear burn in ignition-scale inertial confinement fusion targets under compressed axial magnetic fields.* Physics of Plasmas, vol. 20, no. 7, page 072708, 2013. (Cited on pages 68 and 72.)

[Perrot 1979] F. Perrot. *Gradient correction to the statistical electronic free energy at nonzero temperatures: Application to equation-of-state calculations.* Phys. Rev. A, vol. 20, page 586, 1979. (Cited on pages 37, 46 and 47.)

[Perrot 1995] F. Perrot and A. Grimaldi. *The charge density induced by a point test charge in a magnetized electron gas.* Journal of Physics: Condensed Matter, vol. 7, no. 32, page 6545, 1995. (Cited on page 70.)

[Pines 1952] D. Pines and D. Bohm. *A Collective Description of Electron Interactions: II. Collective* vs *Individual Particle Aspects of the Interactions.* Phys. Rev., vol. 85, pages 338–353, 1952. (Cited on page 49.)

[Pitarke 2007] J. M. Pitarke, V. M. Silkin, E. V. Chulkov and P. M. Echenique. *Theory of surface plasmons and surface-plasmon polaritons.* Rep. Prog. Phys., vol. 70, page 1, 2007. (Cited on page 49.)

[Plagemann 2012] K.-U. Plagemann, P. Sperling, R. Thiele, M. P. Desjarlais, C. Fortmann, T. Döppner, H.J. Lee, S.H. Glenzer and R. Redmer. *Dynamic structure factor in warm dense beryllium.* New Journal of Physics, vol. 14, no. 5, page 055020, 2012. (Cited on page 79.)

[Plagemann 2015] K.-U. Plagemann, H. R. Rüter, T. Bornath, M. Shihab, M. P. Desjarlais, C. Fortmann, S. H. Glenzer and R. Redmer. *Ab initio calculation of the ion feature in x-ray Thomson scattering.* Phys. Rev. E, vol. 92, page 013103, 2015. (Cited on pages 18 and 24.)

[Plumper 1983] M. L. Plumper and D. J. W. Geldart. *Non-local approximation to the kinetic energy functional.* J. Phys. C: Solid State Phys., vol. 16, page 677, 1983. (Cited on pages 49 and 51.)

[Porter 2010] J. A. Porter, N. W. Ashcroft and G. V. Chester. *Pair potentials for simple metallic systems: Beyond linear response.* Phys. Rev. B, vol. 81, page 224113, 2010. (Cited on page 113.)

[Potekhin 2013] A. Y. Potekhin and G. Chabrier. *Equation of state for magnetized Coulomb plasmas.* Astronomy & Astrophysics, vol. 550, page A43, 2013. (Cited on page 70.)

[Pouget 2016] J.-P. Pouget. *The Peierls instability and charge density wave in one-dimensional electronic conductors.* Comptes Rendus Physique, vol. 17, no. 3, pages 332 – 356, 2016. (Cited on pages 60 and 67.)

[Pribram-Jones 2014] A. Pribram-Jones, S. Pittalis, E. K. U. Gross and K. Burke. *Thermal Density Functional Theory in Context.* In F. Graziani, M. P. Desjarlais, R. Redmer and S. B. Tricke, editors, Frontiers and Challenges in Warm Dense Matter, pages 25–60. Springer, 2014. (Cited on page 28.)

[Pribram-Jones 2016] A. Pribram-Jones, P. E. Grabowski and K. Burke. *Thermal Density Functional Theory: Time-Dependent Linear Response and Approximate Functionals from the Fluctuation-Dissipation Theorem.* Phys. Rev. Lett., vol. 116, page 233001, 2016. (Cited on pages 16 and 28.)

[Putaja 2012] A. Putaja, E. Räsänen, R. van Leeuwen, J. G. Vilhena and M. A. L. Marques. *Kirzhnits gradient expansion in two dimensions.* Phys. Rev. B, vol. 85, page 165101, 2012. (Cited on page 60.)

[Reinholz 1995] H. Reinholz, R. Redmer and S. Nagel. *Thermodynamic and transport properties of dense hydrogen plasmas.* Phys. Rev. E, vol. 52, pages 5368–5386, 1995. (Cited on pages 79, 81 and 112.)

[Reinholz 2000] H. Reinholz, R. Redmer, G. Röpke and A. Wierling. *Long-wavelength limit of the dynamical local-field factor and dynamical conductivity of a two-component plasma.* Phys. Rev. E, vol. 62, page 5648, 2000. (Cited on pages 42, 59 and 119.)

[Resta 2000] R. Resta. *Manifestations of Berry's phase in molecules and condensed matter.* Journal of Physics: Condensed Matter, vol. 12, no. 9, page R107, 2000. (Cited on page 26.)

[Rosenfeld 1979] Y. Rosenfeld and N. W. Ashcroft. *Theory of simple classical fluids: Universality in the short-range structure.* Phys. Rev. A, vol. 20, pages 1208–1235, 1979. (Cited on page 89.)

[Runge 1984] E. Runge and E. K. U. Gross. *Density-Functional Theory for Time-Dependent Systems.* Phys. Rev. Lett., vol. 52, pages 997–1000, 1984. (Cited on pages 28, 40 and 55.)

[Salasnich 2007] L. Salasnich. *Kirzhnits gradient expansion for a D - dimensional Fermi gas.* Journal of Physics A: Mathematical and Theoretical, vol. 40, no. 33, page 9987, 2007. (Cited on pages 60 and 67.)

[Saumon 2012] D. Saumon, C. E. Starrett, J. D. Kress and J. Clérouin. *The quantum hypernetted chain model of warm dense matter.* High Energy Density Physics, vol. 8, no. 2, pages 150 – 153, 2012. (Cited on page 79.)

[Schweng 1991] H. K. Schweng, H. M. Böhm, A. Schinner and W. Macke. *Temperature dependence of short-range correlations in the homogeneous electron gas.* Phys. Rev. B, vol. 44, pages 13291–13297, 1991. (Cited on page 79.)

[Seuferling 1989] P. Seuferling, J. Vogel and C. Toepffer. *Correlations in a two-temperature plasma.* Phys. Rev. A, vol. 40, pages 323–329, 1989. (Cited on page 16.)

[Shaffer 2017] N. R. Shaffer, S. K. Tiwari and S. D. Baalrud. *Pair correlation functions of strongly coupled two-temperature plasma.* Physics of Plasmas, vol. 24, no. 9, page 092703, 2017. (Cited on page 16.)

[Sharkov 2016] B. Yu. Sharkov, D. H. H. Hoffmann, A. A. Golubev and Y. Zhao. *High energy density physics with intense ion beams.* Matter and Radiation at Extremes, vol. 1, page 28, 2016. (Cited on pages 15 and 114.)

[Shaw 1970] R. W. Shaw. *Exchange and correlation in the theory of simple metals.* Journal of Physics C: Solid State Physics, vol. 3, no. 5, page 1140, 1970. (Cited on page 81.)

[Shukla 2008] P. K. Shukla and B. Eliasson. *Screening and wake potentials of a test charge in quantum plasmas.* Physics Letters A, vol. 372, no. 16, pages 2897 – 2899, 2008. (Cited on page 46.)

[Shukla 2011] P. K. Shukla and B. Eliasson. *Colloquium: Nonlinear collective interactions in quantum plasmas with degenerate electron fluids.* Rev. Mod. Phys., vol. 83, pages 885–906, 2011. (Cited on pages 30 and 53.)

[Shukla 2012] P. K. Shukla and B. Eliasson. *Novel Attractive Force between Ions in Quantum Plasmas.* Phys. Rev. Lett., vol. 108, page 165007, 2012. (Cited on pages 31 and 46.)

[Singwi 1968] K. S. Singwi, M. P. Tosi, R. H. Land and A. Sjölander. *Electron Correlations at Metallic Densities.* Phys. Rev., vol. 176, pages 589–599, 1968. (Cited on page 79.)

[Sjostrom 2013a] T. Sjostrom and J. Daligault. *Nonlocal orbital-free noninteracting free-energy functional for warm dense matter.* Phys. Rev. B, vol. 88, page 195103, 2013. (Cited on pages 17, 39, 41 and 57.)

[Sjostrom 2013b] T. Sjostrom and J. Dufty. *Uniform electron gas at finite temperatures.* Phys. Rev. B, vol. 88, page 115123, 2013. (Cited on page 41.)

[Sjostrom 2014a] T. Sjostrom and J. Daligault. *Fast and Accurate Quantum Molecular Dynamics of Dense Plasmas Across Temperature Regimes.* Phys. Rev. Lett., vol. 113, page 155006, 2014. (Cited on pages 17 and 49.)

[Sjostrom 2014b] T. Sjostrom and J. Daligault. *Gradient corrections to the exchange-correlation free energy.* Phys. Rev. B, vol. 90, page 155109, 2014. (Cited on pages 17, 40, 41, 42 and 81.)

[Sjostrom 2015] T. Sjostrom and J. Daligault. *Ionic and electronic transport properties in dense plasmas by orbital-free density functional theory.* Phys. Rev. E, vol. 92, page 063304, 2015. (Cited on page 17.)

[Sjostrom 2018] T. Sjostrom and S. Crockett. *Quantum molecular dynamics of warm dense iron and a five-phase equation of state.* Phys. Rev. E, vol. 97, page 053209, 2018. (Cited on page 111.)

[Sperling 2013] P. Sperling, T. Liseykina, D. Bauer and R. Redmer. *Time-resolved Thomson scattering on high-intensity laser-produced hot dense helium plasmas.* New J. Phys., vol. 15, page 025041, 2013. (Cited on page 59.)

[Springer 1973] J. F. Springer, M. A. Pokrant and F. A. Stevens. *Integral equation solutions for the classical electron gas.* The Journal of Chemical Physics, vol. 58, no. 11, pages 4863–4867, 1973. (Cited on page 86.)

[Stanton 2015] L. G. Stanton and M. S. Murillo. *Unified description of linear screening in dense plasmas.* Phys. Rev. E, vol. 91, page 033104, 2015. (Cited on pages 31, 46, 82, 83 and 110.)

[Starrett 2017] C. E. Starrett. *Thomas-Fermi simulations of dense plasmas without pseudopotentials.* Phys. Rev. E, vol. 96, page 013206, 2017. (Cited on page 49.)

[Steiner 1963] E. Steiner. *Charge Densities in Atoms.* The Journal of Chemical Physics, vol. 39, no. 9, pages 2365–2366, 1963. (Cited on page 49.)

[Tanaka 1986] S. Tanaka and S. Ichimaru. *Thermodynamics and Correlational Properties of Finite-Temperature Electron Liquids in the Singwi-Tosi-Land-Sjölander Approximation.* Journal of the Physical Society of Japan, vol. 55, pages 2278–2289, 1986. (Cited on pages 41 and 79.)

[Tanaka 1987] S. Tanaka and S. Ichimaru. *Dynamic theory of correlations in strongly coupled, classical one-component plasmas: Glass transition in the generalized viscoelastic formalism.* Phys. Rev. A, vol. 35, page 4743, 1987. (Cited on page 41.)

[Tanaka 2017] S. Tanaka. *Improved equation of state for finite-temperature spin-polarized electron liquids on the basis of Singwi–Tosi–Land–Sjölander approximation.* Contrib. Plasma Phys., vol. 57, page 126, 2017. (Cited on pages 41 and 79.)

[Tejero 2009] C. F. Tejero and E. Lomba. *Density-dependent interactions and thermodynamic consistency in integral equation theories.* Molecular Physics, vol. 107, no. 4-6, pages 349–355, 2009. (Cited on page 89.)

[Teng 2017] D. Teng, Q. Cao and K. Wang. *An extension of the generalized nonlocal theory for the mode analysis of plasmonic waveguides at telecommunication frequency.* J. Opt., vol. 19, page 055003, 2017. (Cited on page 59.)

[Thiele 2008] R. Thiele *et al. Plasmon resonance in warm dense matter.* Phys. Rev. E, vol. 78, page 026411, 2008. (Cited on page 59.)

[Tokatly 2007] I. V. Tokatly. *Time-dependent deformation functional theory.* Phys. Rev. B, vol. 75, page 125105, 2007. (Cited on page 28.)

[Toscano 2015] G. Toscano, J. Straubel, A. Kwiatkowski, C. Rockstuhl, F. Evers, H. Xu, N. A. Mortensen and M. Wubs. *Resonance shifts*

and spill-out effects in self-consistent hydrodynamic nanoplasmonics. Nat. Commun., vol. 6, page 7132, 2015. (Cited on pages 111 and 112.)

[Trappe 2016a] M. Trappe, P. Grochowski, M. Brewczyk and K. Rzążewski. *Ground-state densities of repulsive two-component Fermi gases.* Phys. Rev. A, vol. 93, page 023612, 2016. (Cited on page 59.)

[Trappe 2016b] M. Trappe, Y. L. Len, H. K. Ng, C. A. Müller and B.-G. Englert. *Leading gradient correction to the kinetic energy for two-dimensional fermion gases.* Phys. Rev. A, vol. 93, page 042510, 2016. (Cited on page 68.)

[Ullrich 2014] C. A. Ullrich. *Time-Dependent Density-Functional Theory: Features and Challenges, with a Special View on Matter Under Extreme Conditions.* In F. Graziani, M. P. Desjarlais, R. Redmer and S. B. Tricke, editors, Frontiers and Challenges in Warm Dense Matter, pages 1–23. Springer, 2014. (Cited on page 28.)

[van Zyl 2011] B. P. van Zyl, K. Berkane, K. Bencheikh and A. Farrell. *Gradient corrections to the kinetic energy density functional of a two-dimensional Fermi gas at finite temperature.* Phys. Rev. B, vol. 83, page 195136, 2011. (Cited on pages 60 and 63.)

[van Zyl 2014] B. P. van Zyl, A. Farrell, E. Zaremba, J. Towers, P. Pisarski and D. A. W. Hutchinson. *Nonlocal kinetic energy functional for an inhomogeneous two-dimensional Fermi gas.* Phys. Rev. A, vol. 89, page 022503, 2014. (Cited on page 68.)

[Vashista 1972] P. Vashista and K. S. Singwi. *Electron correlations at metallic densities. V.* Phys. Rev. B, vol. 6, page 875, 1972. (Cited on page 42.)

[Veysman 2016] M. Veysman, G. Röpke, M. Winkel and H. Reinholz. *Optical conductivity of warm dense matter within a wide frequency range using quantum statistical and kinetic approaches.* Phys. Rev. E, vol. 94, page 013203, 2016. (Cited on pages 42 and 85.)

[Vold 2015] E. L. Vold, A. S. Joglekar, M. I. Ortega, R. Moll, D. Fenn and K. Molvig. *Plasma viscosity with mass transport in spherical iner-*

tial confinement fusion implosion simulations. Physics of Plasmas, vol. 22, no. 11, page 112708, 2015. (Cited on page 114.)

[Vu 1997] H. X. Vu. *Three-dimensional particle-in-cell simulations of ion-driven parametric instabilities.* Physics of Plasmas, vol. 4, no. 5, pages 1841–1848, 1997. (Cited on page 114.)

[Wang 1992] L.-W. Wang and M. Teter. *Kinetic-energy functional of the electron density.* Phys. Rev. B, vol. 45, pages 13196–13220, 1992. (Cited on pages 41 and 57.)

[Wang 1997] N. Wang and I. Nagy. *Electronic energy loss of helium ions in aluminum.* Phys. Rev. A, vol. 55, pages 2083–2086, 1997. (Cited on page 79.)

[Wang 2000] Y. Wang and E. A. Carter. *Orbital-free kinetic energy density functional theory.* In S. Schwartz, editor, Progress in Theoretical Chemistry and Physics, page 117. Kluwer, Dordrecht, 2000. (Cited on page 44.)

[Weizsäcker 1935] C. F. v. Weizsäcker. *Zur Theorie der Kernmassen.* Zeitschrift für Physik, vol. 96, no. 7, pages 431–458, 1935. (Cited on page 49.)

[White 2013] T. G. White, S. Richardson, B. J. B. Crowley, L. K. Pattison, J. W. O. Harris and G. Gregori. *Orbital-Free Density-Functional Theory Simulations of the Dynamic Structure Factor of Warm Dense Aluminum.* Phys. Rev. Lett., vol. 111, page 175002, 2013. (Cited on page 17.)

[Wierling 2001] A. Wierling, Th. Millat, G. Röpke, R. Redmer and H. Reinholz. *Inverse bremsstrahlung of hot, weakly coupled plasmas.* Physics of Plasmas, vol. 8, no. 8, pages 3810–3819, 2001. (Cited on pages 119 and 120.)

[Wigner 1932] E. Wigner. *On the Quantum Correction For Thermodynamic Equilibrium.* Phys. Rev., vol. 40, pages 749–759, 1932. (Cited on page 30.)

[Witt 2018] W. C. Witt, B. G. del Rio, J. M. Dieterich and E. A. Carter. *Orbital-free density functional theory for materials research.* Journal of Materials Research, pages 1–19, 2018. (Cited on page 41.)

[Xiao 2010] D. Xiao, M.-C. Chang and Q. Niu. *Berry phase effects on electronic properties.* Rev. Mod. Phys., vol. 82, pages 1959–2007, 2010. (Cited on page 26.)

[Yan 2015] W. Yan. *Hydrodynamic theory for quantum plasmonics: Linear-response dynamics of the inhomogeneous electron gas.* Phys. Rev. B, vol. 91, page 115416, 2015. (Cited on pages 18, 31, 32, 35, 52, 59 and 111.)

[Yan 2016] W. Yan and N. A. Mortensen. *Nonclassical effects in plasmonics: An energy perspective to quantify nonclassical effects.* Phys. Rev. B, vol. 93, page 115439, 2016. (Cited on page 31.)

[Ying 1974] S. C. Ying. *Hydrodynamic response of inhomogeneous metallic systems.* Il Nuovo Cimento B (1971-1996), vol. 23, no. 1, pages 270–281, 1974. (Cited on pages 30 and 35.)

[Zastrau 2014] U. Zastrau *et al. Resolving ultrafast heating of dense cryogenic hydrogen.* Phys. Rev. Lett., vol. 112, page 105002, 2014. (Cited on page 15.)

[Zhang 2017] Y. Zhang, M. X. Gao and B. Guo. *Surface plasmon dispersion relation at an interface between thin metal film and dielectric using a quantum hydrodynamic model.* Optics Communications, vol. 402, pages 326 – 329, 2017. (Cited on page 67.)

[Zubarev 1971] D. N. Zubarev. *Nonequilibrium Statical Thermodynamics.* Nauka, Moscow, 1971. [English translation (Consultant Bureau, New York, 1974)]. (Cited on pages 36 and 117.)

[Zwicknagel 1999] G. Zwicknagel, C. Toepffer and P.-G. Reinhard. *Stopping of heavy ions in plasmas at strong coupling.* Physics Reports, vol. 309, no. 3, pages 117 – 208, 1999. (Cited on page 79.)

[Zyryanov 1961] P. S. Zyryanov. *Quantum theory of acoustic oscillations of an electron-ion plasma in a magnetic field.* J. Exptl. Theoret. Phys., vol. 40, pages 1353–1359, 1961. (Cited on page 70.)

[Zyryanov 1962] P. S. Zyryanov and V. P. Kalashnikov. *Quantum-Mechanical Dielectric Tensor for an Electron Plasma in a Magnetic Field.* J. Exptl. Theoret. Phys., vol. 41, pages 1119–1124, 1962. (Cited on page 70.)

Acknowledgment

Firstly, I would like to express my sincere gratitude to my advisor Prof. Michael Bonitz for support, motivation, pedagogical wisdom, and immense knowledge. I am grateful to Dr. S. Groth and Dr. T. Dornheim for the stimulating discussions, sharing with me the data on the local field correction in the STLS approximation, and for thoroughly proofreading this thesis. My sincere thanks go to Dr. H. Kählert in collaboration with whom the part of the research described in subchapter 4.4.4 has been completed. Besides, I would like to thank Dr. P. Ludwig, his help during my move to Kiel cannot be overestimated. I should like to express my sincere gratitude to Prof. T. Ramazanov, who has given me kind encouragement over the years. In addition, I give my gratitude to the financial support of DAAD, the scholarship of which made possible this work to be done. Last but not the least, I would like to thank my family for supporting me spiritually throughout working on this thesis.

Selbständigkeitserklärung

Ich erkläre, dass die vorliegende Dissertation nach Inhalt und Form meine eigene Arbeit darstellt und unter Einhaltung der Regeln guter wissenschaftlicher Praxis der Deutschen Forschungsgemeinschaft entstanden ist. Ausgewählte Ergebnisse wurden in den auf Seite 4 angegebenen Fachartikeln publiziert, was an entsprechender Stelle in dieser Arbeit gekennzeichnet wurde. Weiterhin bestätige ich, dass diese Arbeit weder ganz noch in Teilen in einem anderen Prüfungsverfahren zur Begutachtung vorgelegen hat.

Kiel,

Zhandos Moldabekov